Dissertation zur Erlangung des Doktorgrades
der Fakultät für Chemie und Pharmazie
der Ludwig-Maximilians-Universität München

Intracellular protein delivery by defined polycations or combining a targeting ligand with an endosomolytic peptide

Xiaowen Liu

aus

Gaoan, Jiangxi, China

2016

Erklärung

Diese Dissertation wurde im Sinne von § 7 der Promotionsordnung vom 28. November 2011 von Herrn Prof. Dr. Ernst Wagner betreut.

Eidesstattliche Versicherung

Diese Dissertation wurde eigenständig und ohne unerlaubte Hilfe erarbeitet.

München, 07.10.2016

…….....

Xiaowen Liu

Dissertation eingereicht am: 07.10.2016

1. Gutachter: Prof. Dr. Ernst Wagner

2. Gutachter: Prof. Dr. Wolfgang Frieß

Mündliche Prüfung am 17.11.2016

To my family

TABLE OF CONTENTS

1 INTRODUCTION

1.1 Protein therapeutics

Two major breakthroughs in the history of biochemistry are particularly notable, i) the elucidation of nucleic acids as carrying information molecular, which have been drawn significant attention by scientist of the time in the area of bio-related domain[1] [2]; ii) the presentation of proteins as many biogenic activities. Proteins, commonly range in length from 100 to 1000 amino acids, are synthesized on ribosomes as linear chains of amino acids forming polypeptides in a specific order dictated from information encoded in the cellular DNA and then fold into tertiary structure to achieve their full function. Proteins are responsible for nearly every task of cellular life, including shaping cells, transporting essential nutrients, catalyzing biochemical reactions, and inner organization, product manufacture and waste cleanup, and routine maintenance, representing biomolecules with most functional and diverse character within living organisms[3] [4] [5] [6] [7]. By the most conservative calculation, human body synthesizes at least 30,000 different kinds of proteins to maintain the daily function of body and proteins hold 20% of a cell weight[8] [9] [10] [11]. Viewed from the perspective of pathogenesis, these estimates are provided with enormous challenge to human being healthy, as diseases may arise from when any of these proteins perform misfolding, aggregation, or other kinds of abnormalities, or present in a relative high or low active concentration[4] [12] [11] [13] [14].

Protein therapeutics in general have gained dramatically attention and widely used in almost every field of medicine since the milestone protein therapeutics, clinical recombinant human insulin, was approved by the US Food and Drug Administration (FDA) in 1982[4]. Since then, more than 130 proteins or peptides have been approved by FDA for clinical applications, such as cancer therapy, diabetes mellitus, hemophilia, and AIDS, and many more are in development[4 15 16] . Compared to small molecular and nucleic acid drug, due to the amino-acid-based secondary and tertiary structure, protein therapy represents an innovative approach with higher specificity than many simple small molecular drugs and lower risk for potential genetic adverse effects in contrast to gene therapy. In addition to pharmaceuticals, direct protein delivery into the intracellular space provides a wide range of biological applications including specific interaction with metabolic processes or signaling pathways. Based on pharmacological activity of active protein, the function of active protein can be basically divided into five groups: (a) Replacing a particular activity in case of protein deficient or abnormal; such as insulin-based drugs for treatment of diabetes[17 18 19 20]; Factor VIII in Haemophilia A and Factor III Haemophilia A could replace the deficient clotting factor[21 22 23], and so on. (b) Augmenting an existing pathway; the most significant example is that the recombinant erythropoietin used to increase erythrocyte production when patients suffer from anaemia or myelodysplastic syndrome caused by chemotherapy[24 25 26]. (c) Providing a novel function or activity; in this case, the endogenous proteins extracted from other organisms are

used to function as novel activity in the human body. For example, L-Asparaginase, purified from E.coli, can be applied to reduce the concentration of asparagine in serum, which is needed for acute lymphoblastic leukaemia, thus inhibiting proliferation of cancer cells[27 28]. (d) Interfering with a molecule or organism; many protein therapeutics in this group use the antigen recognition sites of immunoglobulin (Ig) molecules or the receptor binding-domains of native protein ligands to guide the immune system to destroy the aimed targeted molecules or cells. Such as, the immunoadhesin etanercept, a fusion between two human proteins: tumor necrosis factor TNF) receptor and the Fc region of the human antibody protein IgG1 was used to treat inflammatory arthritis and psoriasis[29 30 31]. The most attractive one is PD-1, a cell surface receptor expressed on T cells and pro-B cells, which could down regulate the immune system by preventing the activation of T cells. When PD-1 inhibitors (approved by FDA) are used to block the PD-1, which then active the immune system to attack tumors and are successfully treated with some types of cancer cell[32 33 34]. (e) Working as the vaccines or drugs. Though there are currently no clinical approved therapeutics in this area, many scientists are turning their effort in this new promising discipline. For example, transgenic tobacco plants (Nicotiana benthamiana) are used for diagnosis and therapy to some special kinds of disease[35 36 37 38]. Protein therapeutics show their promising prospect and are still in their fancy, many kinds of protein therapeutics will become realization along with the thorough research from biochemistry scientists.

Therapeutic protein approaches are well established for the extracellular replacement of deficient proteins, immune-modulating cytokines and vaccines, the application of therapeutic antibodies, or antibody-drug conjugates [4]. Effective delivery of functional proteins to intracellular target sites would enormously expand the repertoire of therapeutic protein applications; thus creating a strong demand of robust intracellular transfer technologies[39 40 41]. A major bottleneck to expand protein therapy is to obtain efficient delivery to the target sites without affecting their natural function. Hence, many strategies have been followed to enable controlled intracellular delivery of therapeutic proteins, such as polymeric nanoparticles[42 43], hydrogels and nanocapsules[44 45], liposomes[46 47], cell penetrating peptides (CPP)[48 49] and protein–transduction domains (PTD)[50 51 52]. One particular challenge is the versatile production of stable protein complexes with full bioactivity. Irreversible covalent modifications may affect protein activity, and non-covalent ionic or hydrophobic interactions with carriers do not always provide sufficient stability due to the diverse nature of different cargo proteins. An elegant solution to this problem has been developed by Kataoka and colleagues[53 54]. Lysine amino groups were covalently modified with citraconic anhydride, resulting in charge-converted negatively charged proteins suitable for polyion complex micelle formation with cationic polymers. Upon cellular uptake of the protein micelles, the pH-sensitive citraconic amide bonds are reversed within the acidic endosomal compartments, recovering the free bioactive form of the proteins.

1.2 Barriers and strategies for transduction protein to the desired destination

Protein therapy represents an innovative approach with higher specificity and complex set of functions and superior biocompatibility than many simple small molecular drugs, protein therapeutics also exhibit lower risk for potential genetic of permanent adverse effects comparing to gene therapy[4]. Although past few decades have witnessed considerable progress of protein-based therapeutics, a major bottleneck to expand protein therapy is their efficient delivery to the target sites without affecting their natural functions. Oral route would be preferred to any other administration form of a drug because of its high levels of patient acceptance and long term compliance[55 56 57 58], but for now it is a huge challenge to protect the therapeutics protein from degrading by high proteolytic activity and harsh conditions in the gastro intestinal tract because of its unfavorable low pH physiochemical environment and abundant of enzyme[59 60]. Till recent, injections (i.e. intravenous, intramuscular or subcutaneous route) of therapeutics are the most common route for administrating the protein drugs or peptides in vivo[60-61], it is an passive diffusion process for intramuscular and subcutaneous route which restrict their use for inner organs. To date, most therapeutics proteins are taken by the intravenous injection, when the protein therapeutics applied in this route, proteins suffer from poor stability in the serum because of most proteins are negative charged at neutral pH, unfolding and aggregation resulting in transformational three-dimensional structure[62]. Protein also surround by a

complicated environment with proteolytic and chemical degradation, or eliminating by the immune system of the organism[63]. It is also very necessary to prolong the in vivo half-life of therapeutics protein in order to enhance the activity time of proteins to the focal of the target.

Besides these, after a long journey, intracellular proteins therapeutics arriving at the target destination then should overcome the natural barrier of bilayer phospholipid structure to enter into the cells. Uptakes usually proceed through the endocytosis mechanism into endosomes and subsequently lysosomes, which present an acidic and enzyme-rich environment[64 65 66]. It is a very tricky problem to avoid degrading by enzymes and maintain protein bioactivity release to the cytoplasm. Hence, the mentioned obstacles represent a reality to restrict the widespread applications of proteins as therapeutic strategies, but also maintain a tremendous opportunity for the drug delivery domain[4]. Many strategies have been followed to enable extension of circulation time and masking immunogenicity of protein drugs by conjugation of the protein with macromolecules like poly(ethylene glycol) (PEG) and injectable controlled delivery of therapeutic proteins, such as thermal[67 68], light redox[69 70], and magnetic stimuli-triggered functional units combined with a number of synthetic materials, including liposomes[71 72], and polymers[73]. Dai and colleagues have developed single-walled carbon nanotubes (SWNTs) as the bovine serum albumin (BSA) and streptavidin (SA) vector, and presented evidence that the uptake mechanism of protein-SWNT is through clathrin-dependent endocytosis as the pathway[74 75]. Other kinds of

inorganic nanomaterials were also studied as the protein carrier, such as gold nanomaterial[76 77], mesoporous silica nanoparticles[78 79] and upconversion nanoparticles[80]. The main drawback of these nanomaterial protein systems comes from the difficult metabolism of the inorganic carriers, and the inorganic nanomaterials staying in vivo for long time could possible result in other kinds of aside effects to the organism. Many more biocompatibility delivery systems have been developed. Intracellular transduction of proteins can also be achieved by attachment of cell-penetrating peptides (CPPs)[49 81 82] and protein-transduction domains (PTDs)[50 83] or genetic engineering of supercharged proteins[84 85] or by anchored targeting units[86].

1.3 Aim of this thesis

Protein therapeutics represent burgeoning biopharmaceuticals in clinical applications, and many strategies have been developed for delivery of protein into focus. The efficiency transduction of proteins without denaturing its activity into the targeting sites is still an important ongoing task. Herein, based on some work in our group, current thesis is to focus on the intracellular delivery of protein without loss of function.

The first aim of this thesis was the development of a high efficiency protein transduction system by synthetic sequence defined polymers. CPPs as carriers are widely used strategies for protein delivery, but major limitations of their

application are low efficiency of intracellular delivery and possible reduction of protein activity during derivatization[49, 81-82]. So an alternative option, via cationic polymers, has been developed to enhance the efficiency of protein delivery. Much effort has been put to form a formulation by electrostatic absorption between polymer and charged protein, which is not stable exposed in the organisms or blood, so a high efficiency carrier that could transduce protein into cells and put to good use of its biological activity is needed to be exploited. pH-sensitive covalent modification of proteins with a structure defined histidine-rich cationic oligomer (689)[87] for efficient intracellular transduction and traceless release of functional proteins was to be developed. Enhanced Green fluorescent protein (EGFP)[88], as model for the visualization of protein transduction, and RNase A[89], as therapeutic protein with antitumoral effect, were to be modified with the pH-sensitive bifunctional azidomethyl-methylmaleic anhydride AzMMMan linker[90 91]. And sequence defined oligomer 689 was to be coupled with DBCO and used to modify EGFP-AzMMMan and RNase A-AzMMMan by copper free click chemistry. The impact of modification degree was to evaluate on the internalization and cellular distribution of EGFP as well as the biological effect of RNase A conjugates at various ratios.

The second aim of this thesis was to evaluate intracellular delivery of protein conjugates by covalent combination with targeting ligand and an endosomal escape lytic peptide. Natural evolution has already presented very potent polycation-free protein delivery in the form of bacterial cytotoxins[92 93 94 95]. These

protein toxins internalize by endocytosis, followed by subsequent translocation of a toxin subunit across the endosomal membrane. For example, Diphtheria toxin consists of a toxic protein unit A, which is disulfide-linked with a delivery protein unit B. The delivery unit B contains two subdomains, which are required to facilitate the distinct delivery steps of cellular uptake and endosomal escape separately. One subunit mediates cell surface receptor binding (to heparin-binding epidermal growth factor precursor) triggering receptor-mediated endocytosis. The other represents a translocation domain, which at endosomal low pH undergoes a conformational change and inserts into the endosomal membrane, facilitating release of the toxic subunit A (inhibitor of cellular protein translation) into the cytosol after disulfide bond cleavage from unit B[96 97]. The potency of cytotoxins has already been translated into the generation of therapeutic immunotoxins, where researchers replaced the receptor-binding subunit with a target-specific antibody fragment or receptor ligands[98 99 100 101 102 103 104].

Folate receptor (FR) proteins are selectively overexpressed on the surface of brain, kidney, lung, and breast cancer cells compared to normal cells, folate ligand exhibits high affinity to the FR highly expressed on these tumors cells. Imitating the immunotoxin strategy in an artificial context, polycation-free multifunctional conjugates were to be developed, RNase A[89] as cargo protein, polyethylene glycol-folate (PEG-folate) for folic acid receptor (FR) mediated cellular uptake[105 106 107 108], and INF7, an influenza hemagglutinin derived synthetic endosomal pH-responsive peptide for endosomal escape[109 110]. These functional units were to be

attached to RNase A by the aforementioned AzMMMan/DBCO traceless-linker system. The biological activity of RNase A was to be tested when modified with both PEG-folate and INF7 units, or modified with PEG-folate and INF7 units alone. Meanwhile, EGFP as a probe protein was to be modified as the mentioned strategy, and the cytoplasmic intracellular of EGFP should be visualized when modified with both functional units.

2 MATERIALS

2.1 Chemicals

Dimethylmaleic anhydride, N-bromosuccinimide, benzoyl peroxide, sodium azide, Sodium bicarbonate, FITC, and RNase A (from bovine pancreas), RNA (Mr 5000-8000, Torula utilis) were purchased from Sigma-Aldrich (Munich, Germany). 2,4,6-Trinitrobenzenesulfonic (TNBS) acid solution 1M in water was purchased from Fluka (Germany). Dibenzylcyclooctyne-PEG_4-maleimide (DBCO-PEG_4-maleimide) and DBCO-NHS ester were purchased from Jena Bioscience (Jena, Germany). INF7 peptide (GLFE AIEG FIEN GWEG MIDG WYGC-amide) was purchased from Biosyntan (Berlin, German). Cyanine5 dye NHS ester (Cy5-NHS) was obtained from Lumiprobe (Hannover, Germany). Sephadex G-25 and Sephadex G-10 material were supplied by GE Healthcare (Freiburg, Germany). Isopropyl-β-D-thiogalactopyran oside (IPTG) was purchased from Biomol (Hamburg, Germany).

2.2 Materials for solid-phase synthesis

2-Chlorotrityl chloride resin, Fmoc-PEG_{28}-OH, tBu-Glu(OH)-Fmoc, N-(trifluoroacetyl) pteroic acid, peptide grade dimethylformamide (DMF), N,N-diisopropylethylamine (DIPEA), piperidine, and trifluoroacetic acid (TFA), 1-hydroxy-benzotriazole (HOBt), triisopropylsilane (TIS), tris(2-carboxyethyl) phosphine (TCEP), 1,8-diazabicyc [5.4.0] undec-7-ene (DBU), 3,6-dioxa-1,8-

octanedithiol (DODT), were purchased from Iris Biotech (Marktredwitz, Germany). Benzotriazol-1-yl-oxy-tris-pyrrolidino-phosphonium hexafluorophosphate (Pybop) and syringe microreactors were obtained from Multisyntech GmbH (Witten, Germany).

2.3 Solvents

Dichloromethane (DCM), Methanol (MeOH), Tetrahydrofuran (THF) were purchased from Merck (Darmstadt, Germany). Chloroform ($CHCl_3$), n-hexane, n-heptane, Dimethyl sulfoxide (DMSO), Acetonitrile (ACN), Diethyl ether (Et_2O) were obtained from Sigma Aldrich (Munich, Germany). All solvents were purified by distillation and dried before use. Water was used after purification and deionization. Deuterated solvents were bought from Sigma Aldrich.

2.4 Cell culture material

Cell culture media, antibiotics, and fetal bovine serum (FBS) were purchased from Invitrogen (Karlsruhe, Germany). Anticoagulated human red blood cells (obtained from LMU Clinics-Campus Großhadern, Munich, Germany). All cell culture consumables (flasks, dishes, well plates) were purchased from NUNC (Langenselbold, Germany) or TPP (Trasadingen, Switzerland).

2.4 Bacteria strains

E.coli protein expression strain BL21(DE3)plysS was purchased from Novagen (Merck4biosciences, Darmstadt, Germany).

2.5 Buffers

Disodium hydrogen phosphate - citric acid buffer (pH 4.0, pH 5.0, pH 6.0), PBS buffer (pH 7.4, pH 8.0), Hepps buffer (pH 7.3, pH 8.0, pH 8.5, pH 9.0). TNBS buffer.

2.6 Cell lines

Name	**Description**	**ATCC number**
KB	human nasopharyngeal epidermoid carcinoma cell line	CCL-17
HeLa	human cervix adenocarcinoma cell line	CCL-2
Neuro2A	murine neuroblastoma cell line	CCL-131

3 METHODS AND CHARACTERIZATIONS

3.1 Synthesis of 3-(bromomethyl)-4-methyl-2, 5-furandione (BrMMMan)

The compound was synthesized following a previous protocol with slight modifications[90]. Briefly, dimethylmaleic anhydride (5.04 g, 40 mmol), N-bromosuccinimide (14.24 g, 80 mmol), and benzoyl peroxide (200 mg, 0.83 mmol) were dissolved in carbon tetrachloride (CCl_4, 300 mL) in a 500 mL round-bottom flask. The mixture was gently refluxed for 5 h. Then the reaction mixture was allowed to cool to room temperature, afterwards a second portion of benzoyl peroxide (200 mg, 0.83 mmol) was added. The mixture was refluxed for another 5 h and then left overnight at room temperature. The solids were removed by filtration and washed 2 times with CCl_4 (25 mL). The combined organic solutions were washed 2 times with water (100 mL) and one time with brine (100 mL), then dried over Na_2SO_4 and concentrated in vacuo to result in thick yellow oil. The oil was first purified by chromatography on a silica gel column (elution with petroleum ether/ethyl acetate 8:2) to obtain a crude product and then further purified by distilling twice using a miniature high vacuum distillation system. Three fractions were observed, the second fraction was collected (purity, about 90 %) and distilled again. A yield of the product (BrMMMan) of 1.30 g (purity,

about 97%) was obtained. ^{1}H-NMR (500 MHz, $CDCl_3$) δ(ppm) = 2.17 (s, 3H, -C$\underline{H}_3$), 4.17 (s, 2H, -C$\underline{H}_2$-Br), 7.25 (C$\underline{H}Cl_3$) **(**Figure 4.1-2**).**

3.2 Synthesis of 3-(azidomethyl)-4-methyl-2, 5-furandione (AzMMMan)

Synthesis was performed analogously as described in Maier´s paper with minor modifications[90]. 3-(bromomethyl)-4-methyl-2,5-furandione (BrMMMan, 310.5 mg, 1.5 mmol) was dissolved in dry acetone (10 mL), afterwards sodium azide (105.6 mg, 1.6 mmol) was added in one portion. The mixture was stirred over night at room temperature. After filtering, the solvent was evaporated and the crude product was purified by silica gel column using hexane/ethyl acetate (7:3) as mobile phase. After evaporating the solvent, the product (83.6 mg, yield 33.4 %) was obtained. ^{1}H-NMR (500 MHz, $CDCl_3$) δ(ppm) = 2.22 (s, 3H, -C$\underline{H}_3$), 4.27 (s, 2H, -C$\underline{H}_2$-N_3), 7.25 ($CHCl_3$) (Figure 4.1-3).

3.3 Synthesis of Fmoc- and Boc-protected building block Fmoc-Stp(Boc)$_3$-OH

The cationic building blocks Fmoc-Stp(Boc)$_3$-OH was synthesis as described before[111 112]. Briefly, the synthesis is based on first selectively protection of the primary amine groups of TEPA with ethyl trifluoroacetate (Et-TFA), subsequently, the three remain secondary amine groups were Boc-protected by reaction with di-tert-butyl dicarbonate (Boc_2O). The mixture was then work-up, filtered and dried at the high vaccum, which resulted in (TFA)$_2$-(Boc)$_3$-TEPA.

The primary groups were deprotected by incubating $(TFA)_2$-$(Boc)_3$-TEPA with aqueous NaOH containing 45 % EtOH, after alkaline hydrolysis step, $(Boc)_3$-TEPA is obtained. Then the two primary amines of $(Boc)_3$-TEPA were asymmetrically reacted with succinic anhydride and Fmoc-OSu. The product was finally purified by dry column vacuum chromatography (DCVC)[112].

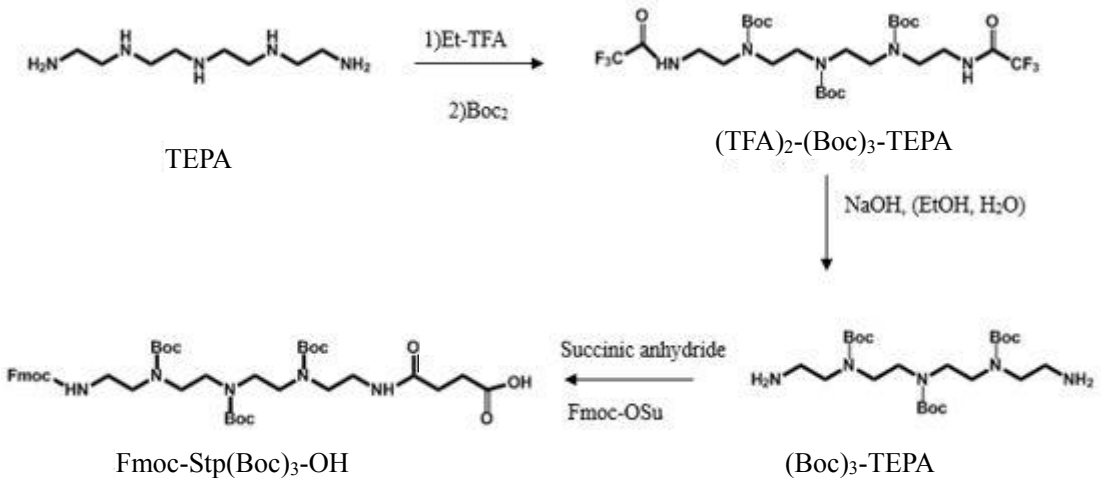

Figure 3-1. The scheme of synthesis of Fmoc-Stp$(Boc)_3$-OH.

3.4 Loading of a 2-chlorotrityl chloride resin with Fmoc-Lys(Boc)-OH

0.8 mmol of a chlorotrityl chloride resin (500 mg) were pre-swollen in DCM (5 mL) for 10 min. Fmoc-Lys(Boc)-OH (0.4 mmol) and DIPEA (1.2mmol) dissolved in DCM (dried over $CaCl_2$) were added to the resin for 1 h. After removing the solvents, a mixture of 2 ml DCM, 1.5ml MeOH, and 250µl DIPEA was added twice for 10 min. After removing of the reaction mixture, the resin was washed 3 times with DCM (5 mL) and 3 times with DMF (5 mL). Some resin was separated for determination of the resin loading and the remaining resin was

treated 7 times for 5 min with 20 % piperidine in DMF for removal of the Fmoc protection group. Deprotection was checked by a positive Kaiser test. Afterwards, the resin was washed 5 times with DMF and 4 times with DCM and dried in high vacuum.

3.5 Loading of a chlorotrityl chloride resin with Fmoc-Cys-Trt-OH

Loading of a chlorotrityl chloride resin with Fmoc-Cys-Trt-OH. 0.8 mmol of a chlorotrityl chloride resin (500 mg) were pre-swollen in DCM (5 mL) for 10min. Fmoc-Cys-Trt-OH (0.4 eq) and DIPEA (0.8 eq) were dissolved in DCM (dried over $CaCl_2$) and added to the resin for 1 hour to obtain a low loaded resin of 0.1 to 0.3 mmol/g. Subsequent steps were done as described above for the loading of a chlorotrityl chloride resin with Fmoc-Lys(Boc)-OH.

3.6 Kaiser test

Kaiser test was used for qualitative detection of free amino groups on the resin[113]. For this purpose a very small amount of resin beads, previously washed with DMF and DCM, were transferred to an Eppendorf tube. One drop of each 80 % (w/v) phenol in EtOH, 5 % (w/v) ninhydrin in EtOH and a solution of 0.02 mM KCN in pyridine were added to the Eppendorf tube and heated for 4 min at 99 °C. In the absence of free amino groups the beads remained colorless and the solution yellow (negative Kaiser Test). The presence of free amino groups was indicated by a blue color of the resin beads and the solution (positive Kaiser test).

3.7 Resin load determination

For determination of the resin loading, 10 mg of the resin were separated from the main batch and dried under high vacuum. The resin was then treated with 1 mL deprotection solution (20 % piperidine in DMF) for 1 h, diluted 25 µl of supernatant in 975 µl DMF and UV absorption was measured at 301 nm. The blank samples were prepared as the same procedure of the sample. Finally, the resin loading in [mmol/ g] is obtained by the following equation: resin load [mmol/g] = (A*1000) / (m [mg]*7800*D). M: resin mass. A: Absorbance. 7800: molar extinction coefficient [$L*mol^{-1}*cm^{-1}$]. D: dilution factor.

3.8 Synthesis of 386 and 689

Chlorotrityl chloride resin preloaded with Fmoc-Cys-Trt-OH was used for synthesis of oligomers of artificial oligoamino acids (386, 689) under standard Fmoc solid phase peptide synthesis conditions using syringe microreactors[87 111-112]. In case of 689, the coupling steps are the same as 386 except for followed by one more coupling with histidine after each STP coupling. Briefly, coupling steps were carried out using 4 eq. Fmoc-amino acid, 4 eq. HOBT, 4 eq. PyBop and 8 eq. DIPEA in DCM/DMF (1/1, 1.5 ml: 1.5 ml) for 1 h incubation time. Fmoc deprotection was accomplished by 7 × 5 min incubation with 20% piperidine in 2ml DMF. After each coupling and deprotection step a washing procedure comprising 3 × 1.5 ml DMF, 3 × 1.5 ml DCM incubation and a Kaiser test were performed[113]. In case of a positive result of the Kaiser test after coupling, the last

coupling step was repeated. In case of a negative result after deprotection, the last deprotection step was redone. Symmetrical branching points were introduced by using Fmoc-Lys(Fmoc)-OH. Finally, all peptides were cleaved off the resin by incubation with TFA/TIS/H_2O at the ratio of 95: 2.5:2.5 (v/v/v) for 90 min. The cleavage solution was concentrated under reduced pressure and peptides were precipitated in 50 mL precooled MTBE/n-hexane (1:1 v/v). All oligomers were purified by size exclusion chromatography using an Äkta purifier system (GE Healthcare Bio-Sciences AB, Uppsala, Sweden) based on a P-900 solvent pump module, a UV-900 spectrophotometrical detector, a pH/C-900 conductivity module, a Frac-950 automated fractionator, a Sephadex G-10 column and 10 mM hydrochloric acid solution–acetonitrile 7:3 as solvent. If necessary, additional purification was carried out by preparative RP-HPLC using a VWR LaPrep system and a Waters Symmetry Prep C18 column (7 µm, 19×150 mm). All peptides were lyophilized. The presence of the different elements of the oligomer sequences was validated by ^{1}H-NMR. The purity of the oligomers was investigated by RP-HPLC.

3.9 Synthesis of folate-PEG_{28}-lysine

2-Chlorotrityl chloride resin preloaded with Fmoc-Lys(Boc)-OH was used for the synthesis of PEGylated folate conjugates by solid phase synthesis[114 115]. The protected Fmoc-PEG_{28}-OH, Fmoc-Glu-OtBu and N-(trifluoroacetyl) pteroic acid were coupled to deprotected α-amine of the resin-bound lysine using 4 equiv amino acid, 4 equiv HOBT, 4 equiv PyBop, and 8 equiv DIPEA in DCM/DMF

and 1 h incubation time. Fmoc deprotection was carried out by 7 ×5 min incubation with 20% piperidine in DMF and twice with 20% piperidine containing 2% DBU. After each coupling and deprotection, resin was washed three times with DMF and DCM, and a Kaiser test[113] was performed. After completion of the coupling, the resin was washed with DMF, DCM, n-hexane and then dried in vacuo. Afterwards, the conjugate was cleaved from the resin by incubation with TFA/TIS/H_2O at the ratio of 95: 2.5:2.5 (v/v/v) for 90 min. Concentration of the filtered solution under reduced pressure and precipitation of the conjugate in 50 mL precooled MTBE/n-hexane (1:1 v/v) followed. After centrifugation, the supernatant was discarded and the precipitated conjugate was purified by size exclusion chromatography using an ÄKTA purifier system (GE Healthcare Bio-Sciences AB, Uppsala, Sweden) based on a P-900 solvent pump module, a UV-900 spectrophotometric detector, a pH/C-900 conductivity module, a Frac-950 automated fractionator, a Sephadex G10 column (diameter 10 mm, length 60 mm), and 10 mM hydrochloric acid/acetonitrile 7:3 as solvent. The collected fractions were lyophilized and analyzed by ^{1}H NMR.

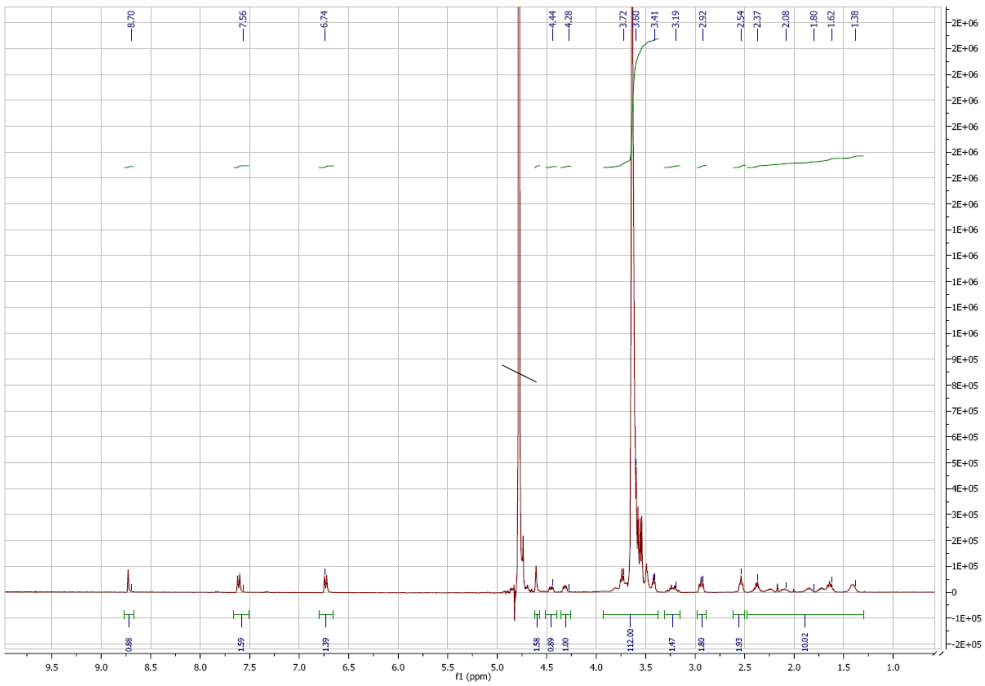

Figure 3-2. ^{1}H NMR of lysine-PEG$_{28}$-folate.

3.10 Synthesis of 689 (386)-Mal-PEG$_4$-DBCO

Oligomer 689 (HCl salt, MW = 6038.4 g/mol, 3 mg, 0.5 μmol) was dissolved in 0.9 mL of Hepps (pH = 8.5); afterward, DBCO-PEG$_4$-Mal (1 mg, 1.5 μmol) dissolved in 100 μL of DMSO was slowly added, and the mixture was reacted for 1 h under constant shaking (800 rpm) at 20 °C. Then this solution was directly used for conjugation with EGFP-AzMMMan or RNase A-AzMMMan (Figure3-3). The 386-AzMMMan was synthesized in an analog way using 2 mg of 386 (HCl salt, MW = 3955.2 g/mol, 0.5 μmol) and 1 mg of DBCO-PEG$_4$-Mal (1.5 μmol).

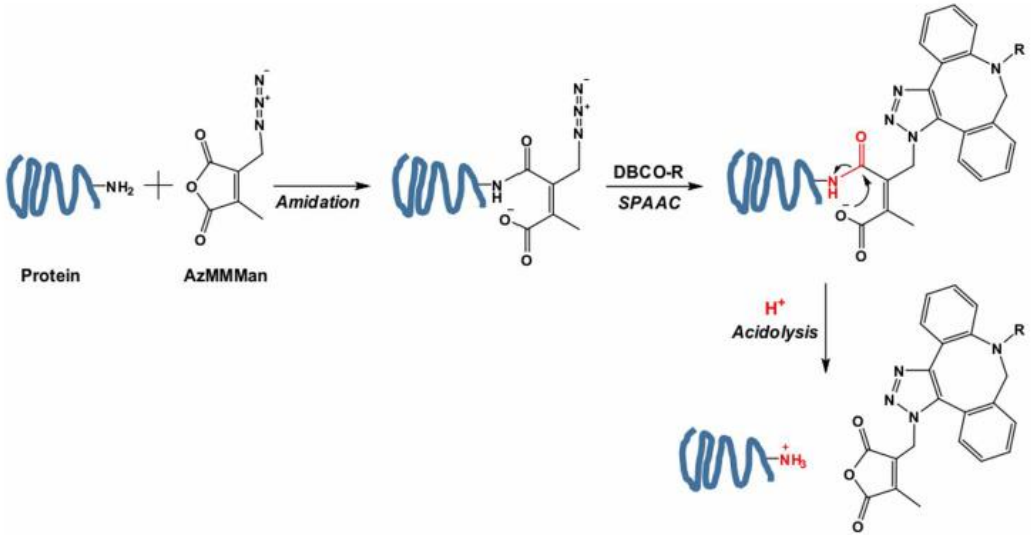

Figure 3-3. Illustration of protein modification and subsequent traceless release using the pH responsive AzMMMan linker. AzMMMan, azidomethyl-methylmaleic anhydride; DBCO,dibenzylcyclooctyne; SPAAC, strain-promoted alkyne-azide cycloaddition.

3.11 Synthesis of folate-PEG$_{28}$-lysine-DBCO

Folate-PEG$_{28}$-lysine (5 mg, 2.7 μmol) was dissolved in a 400 μL mixture of Hepps (0.5 M, pH 8.5) and DMSO (1:1 v/v). Subsequently, DBCO NHS ester (1.25 mg, 3.1 μmol) diluted in DMSO (100 μl) was added and reacted for 2 hours under constant shaking (800 rpm, 20 °C).The mixture was purified by dialysis against 5 L PBS using dialysis membrane with a MWCO of 800Da (Carl Roth, Karlsruhe, Germany) and then was harvested. The product was then adjusted to a volume of 3 ml and stored in the freezer (-80 ^{o}C) for following reactions.

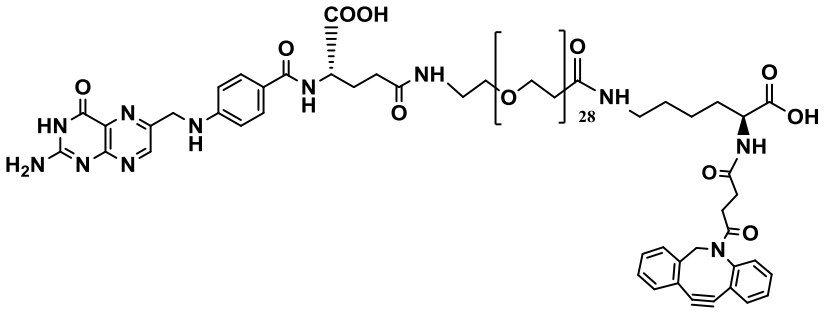

Figure 3-4. The chemical structure of folate-PEG$_{28}$-lysine-DBCO.

3.12 Synthesis of INF7-Mal-PEG$_4$-DBCO

The thiol group of INF7 peptide was used for conjugation with the maleimide group of DBCO-PEG$_4$-Mal. Briefly, INF7 (5mg, 1.78 μmol) was dissolved in PBS (pH 7.4), using NaOH (0.5M) solution to adjust the pH to 7.4. Then DBCO-PEG$_4$-maleimide (1.1mg, 1.61 μmol) was added and reacted for 1 hour under constant shaking (800 rpm, 20 °C). The solution was stored in the freezer (-80 °C) and used for following reactions. MALDI MS data are displayed in the following.

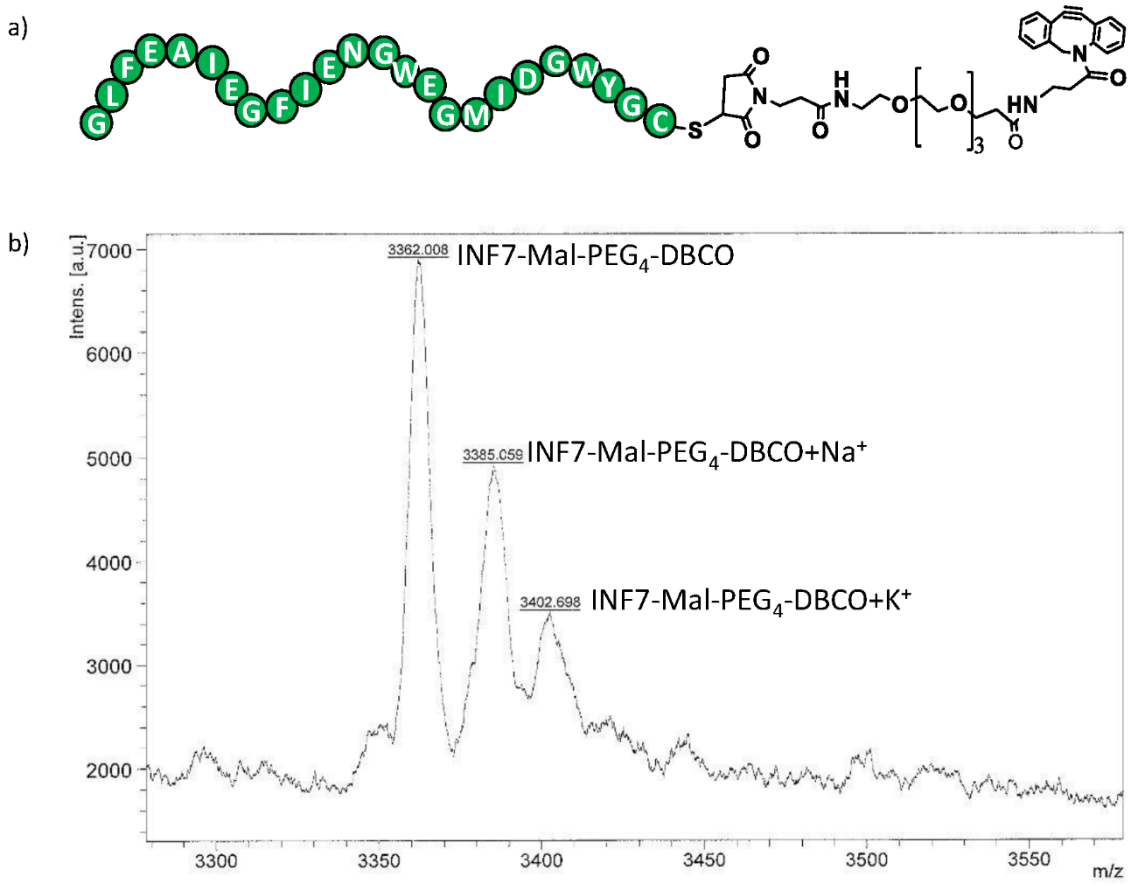

Figure 3-5. a) The chemical structure of INF7-Mal-PEG4-DBCO. b) MALDI-MS of INF7-Mal-PEG4-DBCO (3362.008). MALDI MS was carried out by Stephan Morys (PhD study, Department of Pharmacy, LMU).

3.13 Expression and purification of nlsEGFP

Recombinant nlsEGFP was produced as previously reported[90]. Briefly, E.coli bacterial strain BL21(DE3)plysS, transformed with a pET23a(+) plasmid containing the nlsEGFP gene construct were grown to an optical density of 0.75 (600 nm) under constant shaking in TB medium (37 °C). Protein expression was induced by addition of IPTG to a final concentration of 1 mM and incubation was continued for 16 hours at 32 °C. The cells were harvested at 4000 rpm by centrifugation. After ultrasonic cell lysis, the EGFP containing a polyhistidine tag was purified by nickel chromatography using a gradient from binding buffer (50 mM sodium hydrogen phosphate, 300 mM sodium chloride, 20 mM imidazole) to elution buffer (50 mM sodium hydrogen phosphate, 500 mM sodium chloride, 250 mM imidazole). The protein was dialyzed (MWCO 14000) over night at 4 °C against phosphate buffered saline (PBS) buffer (pH 7.3).

3.14 Synthesis of EGFP-AzMMMan

The modification of nlsEGFP with AzMMMan was carried out as reported before[90]. Briefly, nlsEGFP (5 mg, 0.16 μmol) was dissolved in Hepps buffer (950 μL, 0.5 M, pH=9.0). Afterwards AzMMMan (5 mg, 30 μmol) was diluted in acetonitrile (50 μL) and dropped slowly to the protein solution. Subsequently the mixture was incubated for 2 hours under constant stirring (800 rpm) at 20 °C and then purified by size exclusion chromatography (SEC) using Sephadex G25 material, PBS 8.0 as mobile phase. The concentration of EGFP-AzMMMan was

quantified photometrically (extinction coefficient of 55000 $M^{-}1cm^{-}1$ at 488 nm). AzMMMan modified EGFP was snap frozen by liquid nitrogen and stored in the freezer (-80 °C).

3.15 Synthesis of EGFP-AzMMMan-DBCO-PEG$_4$-Mal-689 and -386

Protein conjugates were synthesized by copper free click chemistry (Figure 3-3). Briefly, four parts of EGFP-AzMMMan (0.25 mg, $7.90*10^{-3}$ μmol) were separately dissolved in Hepps (pH=8.5), subsequently reacted with the cationic oligomer (DBCO-PEG$_4$-Mal-689) at various molar ratios (molar ratios of 689: EGFP=2, 4, 8, 16) for 4 h under constant shaking (800 rpm, 20 °C). Free oligomer was removed by dialysis (dialysis membrane MWCO 14000) against 5 L PBS (pH=8.0) overnight at 4 °C. The purified solution was collected and the concentration of EGFP-AzMMMan-DBCO-PEG$_4$-Mal-689 was quantified photometrically (extinction coefficient of 55000 $M^{-1}cm^{-1}$ at 488 nm). The solution was snap frozen by liquid nitrogen and stored in the freezer (-80 °C). Protein conjugates with DBCO-PEG$_4$-Mal-386 were synthesized analogously.

3.16 Synthesis of EGFP -AzMMMan-DBCO-lysine-PEG$_{28}$-folate

Four batches of EGFP-AzMMMan (0.5 mg, 1.58×10^{-2} μmol) were separately diluted in Hepps (0.5 M, pH 8.5), and individual ratios of folate-PEG$_{28}$-lysine-DBCO (folate: EGFP =1, 5, 15, 20) were added and reacted for 4 hours under constant shaking (800 rpm, 20 °C). Free DBCO-lysine-PEG$_{28}$-folate was removed

by dialysis (dialysis membrane MWCO 14000) against 5L of PBS (pH 8.0) overnight at 4 ºC. The purified solution was collected, and the concentration of EGFP-AzMMMan-DBCO-lysine-PEG_{28}-folate was quantified photometrically (extinction coefficient of 55 000 $M^{-}1$ $cm^{-}1$ at 488 nm). The solution was snap frozen by liquid nitrogen and stored in the freezer (−80 °C).

3.17 Synthesis of EGFP-AzMMMan-DBCO-PEG_4-Mal-INF7

INF7 modified EGFP was synthesized similarly to last section. Briefly, four batches of EGFP-AzMMMan (0.5mg, 1.58×10^{-2} μmol) were separately diluted in Hepps (0.5M, pH 8.5), afterwards individual ratios of INF7-Mal-PEG_4-DBCO (INF7: EGFP =1, 5, 15, 20) were added separately and reacted for 4 hours under constant shaking (800 rpm, 20 °C). Free INF7-Mal-PEG_4-DBCO was removed by dialysis (dialysis membrane MWCO 14000) against 5L of PBS (pH 8.0) overnight at 4 ºC. The purified solution was then collected, and the concentration of EGFP-AzMMMan-DBCO-PEG_4-Mal was quantified photometrically (extinction coefficient of 55 000 M^{-1} cm^{-1} at 488 nm). The solution was snap frozen by liquid nitrogen and stored in the freezer (−80 °C).

3.18 Synthesis of INF7-Mal-PEG_4-DBCO-EGFP-AzMMMan-DBCO-lysine-PEG_{28}-folate

Briefly, four batches of EGFP-AzMMMan (0.5mg, 1.58×10^{-2} μmol) were diluted in Hepps (0.5M, pH 8.5), afterwards, DBCO-lysine-PEG_{28}-folate (0.272 mg, 0.158 μmol) was added to each protein solution and reacted for 2 hours under

constant shaking (800 rpm, 20 °C). Then four individual ratios of DBCO-PEG_4-Mal-INF7 (INF7: EGFP=1, 5, 10, 15) were added and the reaction mixture was incubated for four hours under constant shaking (800 rpm, 20 °C). The four different protein conjugates were purified and quantified using the same method as described in the last section.

3.19 Synthesis of RNase A-Cy5

RNase A (5 mg, 0.37 μmol) was dissolved in 900 μL PBS (pH=8.5), then NHS-Cy5 (0.225 mg, 0.37 μmol) was dissolved in 100 μL DMSO and added to the protein solution. The mixture reacted for 2 hours under constant shaking at 20 °C. Then SEC using Sephadex G25 material and and PBS 8.0 as mobile phase was carried out to purify the mixture. The purified RNase A-Cy5 was used to react with AzMMMAn and DBCO-PEG_4-Mal-689 as described below.

3.20 Synthesis of RNase A-FITC

RNase A (5 mg, 0.37 μmol) was dissolved in 900 μl Hepps (0.5 M, pH 8.5), then FITC (0.144 mg, 0.37 μmol) was dissolved in DMSO (100 μl) and added into the protein solution. The mixture was reacted for 2 hours under constant shaking at 20 °C. After that, size exclusion chromatography (SEC) using Sephadex25 material and PBS (pH 8.0) as mobile phase was carried out to purify the product. RNase A-FITC was filed up and concentrated. Then the purified RNase A-FITC was quantified by BCA assay and stored in freezer (-80 °C) and used for the reaction with AzMMMan as described below.

3.21 Synthesis of FITC (Cy5)-RNase A-AzMMMan

RNase A-FITC (RNase A-Cy5) (3 mg) was dissolved in 500µl Hepps (0.5 M, pH 9.0) and AzMMMan (3 mg) was dissolved in 50µl DMSO was added in to the RNase A-FITC (RNase A-Cy5) solution, after reacted for 2 hours, the solution was purified by size exclusion chromatography (SEC) using Sephadex25 material and PBS (pH 8.0) as mobile phase, product was filed up and concentrated, then was quantified by BCA and stored in freezer (-80 ^{o}C). The obtained FITC (Cy5)-RNase A-AzMMMan was directly used for the further modification with oligomer (386,689) or DBCO coupled folate ligand or INF7 peptide.

3.22 Synthesis of RNase A-AzMMMan

RNase A-AzMMMan conjugate was prepared similarly to the EGFP-AzMMMan conjugate. Briefly, RNase A (5 mg, 0.37 µmol) was dissolved in 950 µL Hepps (0.5 M, pH=9.0) buffer, subsequently, AzMMMan (5 mg, 30 µmol)) dissolved in acetonitrile (50 µL) was added to the protein solution slowly, followed by 2 hours incubation under constant shaking at 20 ^{o}C. The mixture was purified by Sephadex G25 column (diameter 10 mm, length 30 mm, PBS (pH 8.0) as mobile phase). RNase A-AzMMMan was concentrated to 2 ml and finally quantified by BCA assay. Then the solution was snap frozen by liquid nitrogen and stored in the freezer (-80 ^{o}C).

For quantification of amines in RNase A, which had not reacted with excessive AzMMMan, a TNBS assay was performed. For this purpose, a 30 mM TNBS

solution in 0.1 M aqueous sodium tetra borate was prepared as working solution. A standard curve was obtained by diluting various amounts of lysine (0.05 to 2 μg) to 100 μl working solution in 96 well plates. Meanwhile, defined amounts of RNase A or RNase A-AzMMMAn were also treated with the working solution. Blanks were prepared in the same way by adding water to the working solution. After incubating at room temperature for 20 min, the absorption of samples were measured at 450 nm.

3.23 Synthesis of RNase A (Cy5)-AzMMMan-DBCO-PEG$_4$-Mal-689

Four batches of RNase A-AzMMMan (0.25 mg, $1.83*10^{-2}$ μmol) were dissolved in 900 μL Hepps (pH=8.5), afterwards various equivalents of DBCO-PEG$_4$-Mal-689 (molar ratios of 689: RNase A=6, 3, 1.5, 0.75) were added to the AzMMMan modified protein. The mixture reacted for 4 hours under constant shaking (800 rpm) at 20 ^{o}C. RNase A conjugate was snap frozen by liquid nitrogen and stored in the freezer (-80 ^{o}C). For conjugate Cy5-RNase A-AzMMMan- DBCO-PEG$_4$-Mal-689 (689: RNase A= 6), the synthesis steps are the same as RNase A-AzMMMan-DBCO-PEG4-Mal-689 except for using Cy5-RNase A-AzMMMan to replace RNase A-AzMMMan. (Cy5-)RNase A-AzMMMan-DBCO-PEG$_4$-Mal-386 conjugates were synthesized analogously.

3.24 Synthesis of RNase A-PEG$_{28}$-folate

RNase A-AzMMMan (1.83×10^{-2} μmol) was diluted in 150 μL Hepps (0.5 M, pH

8.5) and reacted with folate-PEG_{28}-lysine-DBCO (at molar ratio of 11 or 3 for conjugates **1** and **2**, respectively) for 4 hours under constant shaking (800 rpm, 20 °C). Free folate-PEG_{28}-lysine-DBCO was removed by dialysis (dialysis membrane MWCO 3500) against 5 L of PBS (pH 8.0) overnight at 4 °C. The purified solution was collected, and the concentration of RNase A conjugate was quantified by BCA. The solution was snap frozen by liquid nitrogen and stored in the freezer (−80 °C).

The completeness of the reaction of RNase A-AzMMMan with 11 equivalents of folate-PEG_{28}-lysine-DBCO in conjugate **1** synthesis was monitored by analytical HPLC (detection wavelength 280 nm) using a VWR Hitachi Chromaster HPLC system (5160 pump module, 5260 auto sampler, 5310 column oven, 5430 diode array detector). A Waters Xbridge C18 column (5 µm, 4.6 x 150 mm), a linear gradient between 0.1M TEAA buffer/acetonitrile was used for elution. The residual nonreacted folate-PEG_{28}-lysine-DBCO was monitored over an analysis time of 45 min.

3.25 Synthesis of FITC-RNase A-PEG_{28}-folate

RNase A-FITC (0.22 µmol) was dissolved in 500µl Hepps (0.5 M, pH 9.0) and AzMMMan (3 mg, 18 µmol) was dissolved in 50 µL DMSO and was added in to the RNase A-FITC solution. After incubation for 2 hours, the solution was purified by size exclusion chromatography (SEC) using Sephadex G25 material and PBS (pH 8.0) as mobile phase. The product was collected and concentrated to 1.5 ml,

then was quantified by BCA and stored in the freezer (-80 °C). Subsequently, two parts of FITC-RNase A-AzMMMan (1.83×10^{-2} μmol each) were separately diluted in 150 μL Hepps (0.5 M, pH 8.5), and 1 (for conjugate **FITC-folate-1**) or 3 (for conjugate **FITC-folate-3**) molar equivalents of folate-PEG_{28}-lysine-DBCO were added and reacted for 4 hours under constant shaking (800 rpm, 20 °C). Free folate-PEG_{28}-lysine-DBCO was removed by dialysis (dialysis membrane MWCO 3500) against 5L of PBS (pH 8.0) overnight at 4 °C. The dialyzed solution was collected, and the concentration of FITC-RNase A-PEG_{28}-folate was quantified by BCA assay. The solution was snap frozen by liquid nitrogen and stored in the freezer (−80 °C).

3.26 Synthesis of INF7-PEG_4-RNase A-PEG_{28}-folate

Briefly, RNase A-AzMMMan (7.32×10^{-2} μmol) was diluted in 600 μL Hepps (0.5M, pH 8.5). Afterwards, folate-PEG_{28}-lysine-DBCO (0.22 μmol, three molar equivalents) was added to the protein solution and reacted for 1 hour under constant shaking (800 rpm, 20 °C). The solution was divided into four equal parts. To each RNase A (1.83×10^{-2} μmol) solution, INF7-Mal-PEG_4-DBCO at 1, 2, 4, 8 molar equiv. for conjugates **3**, **4**, **5** or **6**, respectively) was added. The reaction mixtures were incubated for further three hours under constant shaking (800 rpm, 20 °C). The four different protein conjugates were purified by dialysis (dialysis membrane MWCO 3500) and quantified by BCA assay. The solutions were then snap frozen by liquid nitrogen and stored in the freezer (−80 °C) for following experiments.

3.27 Synthesis of RNase A-PEG$_4$-INF7

INF7 modified RNase A was synthesized similarly to last section. Briefly, RNase A-AzMMMan (1.83×10^{-2} μmol) was diluted in 150 μL Hepps (0.5 M, pH 8.5), afterwards INF7-Mal-PEG$_4$-DBCO (at INF7: RNase A molar ratio of 8) was added and reacted for 4 hours under constant shaking (800 rpm, 20 °C). Free INF7-Mal-PEG$_4$-DBCO was removed by dialysis (dialysis membrane MWCO 3500) against 5 L of PBS (pH 8.0) overnight at 4 °C. The purified solution was then collected, and the concentration of RNase A-conjugate (**7**) was quantified by BCA. The solution was snap frozen by liquid nitrogen and stored in the freezer (−80 °C).

3.28 Analytics and methods

3.28.1 Flash column chromatography (FCC)

Stationary phase silica gel with a mean diameter between 0.035 and 0.073 mm was used. Column height and diameter were varied according to sample size and the required resolution.

3.28.2 Thin layer chromatography (TLC)

Silica gel coated aluminium plates were used for thin layer chromatography. Detection method was UV-detection at 254 nm.

3.28.3 ^{1}H-NMR

The ^{1}H-NMR spectra was recorded at room temperature using a JNMR-GX (400 MHz, Joel) or a JNMR-GX 500 (500 MHz) with a coupling constant of 0.3 Hz. All spectra were recorded without TMS as internal standard and thus spectra were calibrated to the residual proton signal of the deuterated solvent. For the measurements 10-100 mg sample were used. Spectra were analyzed using the NMR software MestreNova (MestreLab research).

3.28.4 Size-exclusion chromatography (SEC)

All oligomers and linker modified proteins were purified by size exclusion chromatography using the ÄKTA purifier 10 system (GE Healthcare Bio-Sciences AB, Uppsala, Sweden) combined with a P-900 solvent pump module, a UV-900 UV/VIS multi-wavelength detector, a pH/C-900 conductivity module and a Frac-950 automated fraction collector. Sephadex G-10 or Sephadex G-25 was used as the gel filtration medium and PBS (pH 8.0) as elution buffer. The absorption at 214, 260 and 280 nm was monitored and the fractions were collected, snap-frozen and freeze-dried.

3.28.5 UV-Vis spectroscopy

Concentrations of EGFP, linker, and linker modified EGFP were determined by measuring UV-Vis absorbance at wavelength of 488nm or broad wavelength (200nm-800nm). For these measurements a Genesys 10 S UV-Vis spectrophotometer (Thermo Scientific, Bonn, Germany) was used.

3.28.6 High-performance liquid chromatography (HPLC)

The completeness of the reaction of RNase A-AzMMMan with 11 equivalents of folate-PEG_{28}-lysine-DBCO in conjugate **1** synthesis was monitored by analytical HPLC (detection wavelength 280 nm) using a VWR Hitachi Chromaster HPLC system (5160 pump module, 5260 auto sampler, 5310 column oven, 5430 diode array detector). A Waters Xbridge C18 column (5 μm, 4.6 x 150 mm), a linear gradient between 0.1M aqueous TEAA buffer and acetonitrile was used for elution.

3.28.7 SDS-PAGE of RNase A (EGFP) conjugates

Protein samples were loaded on a 12.5% SDS-PAGE gel. The gels ran for 2 h at 125 V. After electrophoresis, gels were stained with Coomassie solution (acetic acid/ethanol/H2O, 1:3:6, v/v/v and 0.3% Coomassie brilliant blue G250, w/v), then destained by washing with a solution of acetic acid/ethanol/H2O (1:3:6, v/v/v) and photographed.

3.28.8 Release of RNase A from conjugates detected by SDS-PAGE

Protein samples were loaded on a 12.5% SDS-PAGE gel. In case of RNase A release studies, conjugates were pre-incubated in an acidic disodium hydrogen phosphate - citric acid buffer (pH 5.0, 6.0) and PBS (pH 7.4) for 24 hours at 37 °C. Then the treated samples were loaded on a 12.5 % SDS-PAGE gel. The gel ran for 2 hours at 125V. After electrophoresis the gel was stained with coomassie solution (acetic acid/ethanol/water, 1/3/6, v/v/v and 0.3 % coomassie brilliant blue

G250, w/v). Then the gel was destained by washing with a solution of acetic acid/ethanol/H_2O (1/3/6, v/v/v).

3.28.9 Ethidium bromide assay for determination of enzymatic RNase A activity

1 μL EtBr (0.5 μg/mL) was added into 997 μL PBS buffer (pH=7.4) as blank control, then 2 μL RNA (10 mg/mL) were added, the solution was stirred and fluorescence intensity was monitored during 5 min equilibration. After addition of RNase A samples (1 μg RNase A) the solutions were incubated under stirring for additional 5 min. The EtBr fluorescence was measured at the excitation wavelength λex=510 nm and emission wavelength λem=590 nm using a Cary Eclipse spectrophotometer (Varian, Germany).

3.28.10 Erythrocyte leakage assay

Anticoagulated human red blood cells (obtained from LMU Clinics - Campus Großhadern, Munich, Germany) were washed with PBS for several times. After centrifugation, the erythrocyte pellet was resuspended, divided into three parts and each diluted to 5×10^7 erythrocytes per mL with PBS at pH 7.4, 6.5 or 5.5, respectively. Different concentrations of RNase A conjugates, free RNase A, INF7-Mal-PEG4-DBCO or free INF7 were diluted in 75 μL with the PBS at the mentioned pH values and transferred to a V-bottom 96-well plate (NUNC, Denmark). Control wells were treated with 1% Triton X-100 for 100% lysis and

PBS at the different pH values (pH 7.4, 6.5, 5.5) as negative control without lysis. Afterwards, 75 µL erythrocyte suspension was added to each well, resulting in a final concentration of 1 µM, 2 µM, 4 µM RNase A conjugates or free RNase A, and 8 µM, 16 µM, 32 µM INF7-Mal-PEG4-DBCO or free INF7. The plates were incubated under constant shaking for 1 h at 37 °C. After centrifugation, 80 µL were transferred to flat bottom 96-well plates for photometric quantification of hemoglobin release at 405 nm with a microplate reader (Tecan Spectrafluor Plus, Tecan, Switzerland). Relative hemolysis was defined according to the following formula:

$$hemolysis(\%) = \frac{A_{405}(conjugate\ treated) - A_{405}(PBS\ treated)}{A_{405}(Triton\ X\ treated) - A_{405}(PBS\ treated)} \cdot 100$$

3.28.11 MALDI-MS

One microliter of sample was spotted on a 1 µL matrix droplet consisting of SDHB Matrix dissolved at 10 mg/mL in 30 % acetonitrile / water. Samples were analyzed using an Autoflex II mass spectrometer (Bruker Daltonics, Bremen, Germany). 300 spectra of respective probes were averaged for one sample spectrum.

3.29 Biological testing

3.29.1 Cell culture for folate modified proteins

Human KB cells were cultured in folic acid free RPMI-1640 medium, supplemented with 10% FBS, 100 U mL^{-1} penicillin, 100 µg mL^{-1} streptomycin

and 4 mM stable glutamine at 37 °C in an incubator with 5% CO_2 and humidified atmosphere.

3.29.2 Cell culture for oligomer modified proteins

HeLa (human cervical adenocarcinoma cells) and Neuro 2A (mouse neuroblastoma cells) cells were grown in Dulbecco's modified Eagle's medium (DMEM), supplemented with 10% fetal bovine serum (FBS), 4 mM stable glutamine, 100 U/mL of penicillin, and 100 µg/mL of streptomycin. All cells were cultured in an incubator at 37 °C with 5% CO_2 and humidified atmosphere.

3.29.3 Flow cytometric measurement of uptake of oligomer modified EGFP or RNase A-Cy5

HeLa cells were seeded into 24-well plates at a density of 50 000 cells per well. After 24 h, the medium was replaced with fresh medium. Subsequently, the EGFP conjugates (final concentration 1µM) or the RNase A-Cy5 conjugates (final concentration 4 µM) were added into each well and incubated at 37 °C for 2 h. Then the cells were washed with 500 µL of PBS containing 1000 IU heparin per mL. After additional wash with PBS only, the cells were detached with trypsin/EDTA, diluted with PBS containing 10% FBS, harvested by centrifugation, and taken up in PBS containing 10% FBS. The cellular fluorescence was assayed by excitation of EGFP at 488 nm and detection of emission at 510 nm with a Cyan ADP flow cytometer (Dako, Hamburg, Germany).

For RNase A-Cy5 conjugates, the cellular fluorescence was assayed by excitation of Cy5 at 635 nm and detection of emission at 665 nm. Cells were appropriately gated by forward/sideward scatter and pulse width for exclusion of doublets, and counterstained with DAPI (4, 6-diamidino-2-phenylindole) to discriminate between viable and dead cells. Minimum ten thousand gated cells per sample were collected. Data were recorded with Summit software (Summit, Jamesville, NY). Analysis was done by FlowJo 7.6.5 flow cytometric analysis software. All experiments were performed in triplicates.

3.29.4 Fluorescence microscopy of oligomer modified EGFP conjugates

HeLa cells were seeded into eight-well Nunc chamber slides (Thermo Scientific, Braunschweig, Germany) at a density of 10 000 cells per well. After 24 h, the medium was replaced with fresh medium. Subsequently, the EGFP conjugates were added into each well (final concentration 1 μM) and incubated at 37 °C for 24 h. Then the cells were washed with 300 μL of PBS containing 1000 IU heparin per mL. After additional wash with PBS only, the cells were fixed with 4% paraformaldehyde. Nuclei were stained with DAPI (1 μg/mL). The cells were observed on a Zeiss Axiovert 200 fluorescence microscope (Jena, Germany). A 20×objective or a 40× objective and appropriate filter sets for analysis of EGFP and DAPI were used. Data were analyzed and processed by AxioVision Rel. 4.8 software (Zeiss, Jena, Germany).

3.29.5 Flow cytometric measurement of association of folate modified EGFP conjugates

KB cells were seeded into 24-well plates at a density of 50 000 cells per well. After 24 h, the 500 µL medium was replaced with fresh serum-containing medium. Then, various nlsEGFP conjugates (final concentration 0.5 µM) or nlsEGFP (final concentration 1.5 µM) were added into each well and incubated on ice for 45 min. For competition experiments with free folic acid, the KB cells were pre-treated with 100 µM free folic acid on ice for 30 min before adding conjugates. Then, the cells were washed with 500 µL PBS, detached with trypsin/EDTA and diluted with PBS containing 10% FBS. After centrifugation, the cells were taken up in 600 µL PBS containing 10% FBS. The cellular fluorescence was assayed by excitation of EGFP at 488 nm and detection of emission at 510 nm with a Cyan ADP flow cytometer (Dako, Hamburg, Germany). Cells were appropriately gated by forward/sideward scatter and pulse width for exclusion of doublets, and counterstained with DAPI (4′, 6-diamidino-2-phenylindole) to discriminate between viable and dead cells. Minimum ten thousand gated cells per sample were collected. Data was recorded with Summit software (Summit, Jamesville, NY). Analysis was done by FlowJo® 7.6.5 flow cytometric analysis software. All experiments were performed in triplicates.

3.29.6 Flow cytometric measurement of uptake of folate modified EGFP conjugates

KB cells were seeded into 24-well plates at a density of 50 000 cells per well. After 24 h, the 500 µL medium was replaced with fresh serum-containing medium. Then, the various nlsEGFP conjugates (final concentration 0.5 µM or 2.5 µM) or nlsEGFP (final concentration 1.5 µM) were added into each well and incubated at 37 °C for 45 min, followed by an incubation of 3 h in fresh media or incubated at 37 °C for 2 h. For free folic acid competition experiments, the KB cells were pre-treated with 100 µM free folic acid on ice for 30 min before adding conjugates. Then, the cells were washed with 500 µL PBS, detached with trypsin/EDTA and diluted with PBS containing 10% FCS. After centrifugation, the cells were taken up in 600 µL PBS (pH 4.0) containing 50 µg/ml Trypan blue to extinguish the outside fluorescence. The cellular fluorescence was assayed by excitation of nlsEGFP at 488 nm and detection of emission at 510 nm with a Cyan ADP flow cytometer (Dako, Hamburg, Germany). Cells were appropriately gated by forward/sideward scatter and pulse width for exclusion of doublets, and counterstained with DAPI (4′, 6-diamidino-2-phenylindole) to discriminate between viable and dead cells. Minimum ten thousand gated cells per sample were collected. Data was recorded with Summit software (Summit, Jamesville, NY). Analysis was done by FlowJo® 7.6.5 flow cytometric analysis software. All experiments were performed in triplicates.

3.29.7 Fluorescence microscopy of folate modified EGFP

KB cells or Neuro 2A cells were seeded into 8 well Nunc chamber slides (Thermo

Scientific, Germany) coated with collagen at a density of 10 000 cells per well. After 24 h, the 300 μL medium was replaced with fresh medium. Subsequently, nlsEGFP conjugates or nlsEGFP were added into each well (final concentration 0.5 μM) and incubated at 37 °C for 30 min, followed by a 3 h incubation in fresh media. For free folic acid competition experiments, the KB cells were pre-treated with 100 μM free folic acid on ice for 30 min before adding conjugates. Afterwards, the cell nuclei were stained by Hoechst Dye 33342 (1 μg/mL). Then, the live cells in medium or PBS (pH 4.0) to extinguish the outside fluorescence were observed on a Zeiss Axiovert 200 fluorescence microscope (Jena, Germany). A 63× magnification DIC oil immersion objective (Plan-APOCHROMAT) and appropriate filter sets for analysis of EGFP or Hoechst fluorescence were used. Data were analyzed and processed by AxioVision Rel. 4.8 software (Zeiss, Jena, Germany).

3.29.8 Cellular association of folate modified RNase A conjugates

KB cells were seeded into 24-well plates at a density of 50 000 cells per well. After 24 h, the 500 μL medium was replaced with fresh serum-containing medium. Then, FITC-RNase A-AzMMMAn or the RNase A conjugates **FITC-folate-1** and **FITC-folate-3** (all final concentration 2 μM) were added into each well and incubated on ice for 45 min. For competition experiments with free folic acid, the KB cells were pre-treated with 400 μM free folic acid on ice for 30 min before adding conjugates. Then, the cells were washed with 500 μL PBS, detached with

trypsin/EDTA and diluted with PBS containing 10% FBS. After centrifugation, the cells were taken up in 600 µL PBS containing 10% FBS. The cellular fluorescence was assayed by excitation of FITC at 488 nm and detection of emission at 510 nm with a Cyan ADP flow cytometer (Dako, Hamburg, Germany). Cells were appropriately gated by forward/sideward scatter and pulse width for exclusion of doublets, and counterstained with DAPI (4′, 6-diamidino-2-phenylindole) to discriminate between viable and dead cells. Minimum ten thousand gated cells per sample were collected. Data was recorded with Summit software (Summit, Jamesville, NY). Analysis was done by FlowJo® 7.6.5 flow cytometric analysis software. All experiments were performed in triplicates.

3.29.9 Cellular internalization of folate modified RNase A conjugates

Cellular internalization was performed as described for the cellular association experiment, with the following differences: the incubation was at 37 °C for 45 min; after centrifugation, the cells were taken up in 600 µL PBS (pH 4.0) to extinguish the outside fluorescence.

3.29.10 Fluorescence microscopy of folate modified RNase A conjugates

KB cells were seeded into 8 well Nunc chamber slides (Thermo Scientific, Germany) coated with collagen at a density of 10 000 cells per well. After 24 h, the 300 µL medium was replaced with fresh medium. Subsequently, FITC-RNase A-AzMMMan or the RNase A conjugate **FITC-folate-3** was added into each well

(final concentration 2 μM) and incubated at 37 °C for 2 h, followed by a 2 h incubation in fresh media. For free folic acid competition experiments, the KB cells were pre-treated with 400 μM free folic acid on ice for 30 min before adding conjugates. Then, the live cells were analyzed using a Zeiss Axiovert 200 fluorescence microscope (Jena, Germany). A 63× magnification DIC oil immersion objective (Plan-APOCHROMAT) and appropriate filter sets for analysis of FITC fluorescence were used. Data were analyzed and processed by AxioVision Rel. 4.8 software (Zeiss, Jena, Germany).

3.29.11 MTT assay of oligomer modified proteins

HeLa cells or Neuro 2A cells were seeded into 96-well plates at a density of 10 000 cells per well. After 24 h, the medium was replaced with 80 μL of fresh medium. Subsequently, the RNase A conjugates (final concentration 0.5; 1.0; 2.0; 4.0 μM), RNase A-AzMMMan (final concentration 0.5; 1.0; 2.0; 4.0 μM), oligomers (final concentration 3.0; 6.0; 12.0; 24.0 μM), and mixture of RNase A-AzMMMan (final concentration 0.5; 1.0; 2.0; 4.0 μM) and oligomers (final concentration 3.0; 6.0; 12.0; 24.0 μM) were diluted into 20 μL with PBS, added to each well, and incubated at 37 °C for 48 h. Afterward, MTT solution (10 μL per well, 5.0 mg/mL) was added. After incubation for 2 h, the medium was removed, and the 96-well plates were stored at −80 °C for at least 1 h. One-hundred microliters of DMSO per well was added to dissolve the purple formazan product. The optical absorbance was measured at 590 nm, with a reference

wavelength of 630 nm, by a microplate reader (Tecan Spectrafluor Plus, Tecan, Switzerland). The relative cell viability (%) related to control wells treated only with 20 μL of PBS was calculated as ([A] test/[A] control) × 100. All experiments were performed in triplicates.

3.29.12 MTT assay of folate modified proteins

KB cells were seeded into collagen coated 96-well plates at a density of 10 000 cells per well. After 24 h, the medium was replaced with 80 μL fresh medium. Subsequently, the RNase A conjugates 2 to 7 or the free RNase A (final concentrations 1 to 8 μM), the control mixture of RNase A-FolA conjugate with INF7 at a ratio of 1:8 (without or with dialysis) or the free INF7 (final concentrations 8 to 64 μM) were diluted in 20 μL of PBS, added to each well and incubated at 37 °C for 48 h. Afterwards, MTT solution (10 μL per well, 5.0 mg/mL) was added. After incubation for 2 h, the medium was removed and the 96-well plates were stored at -80 °C for at least one hour. 100 μL DMSO per well were added to dissolve the purple formazan product. The optical absorbance was measured at 590 nm, with a reference wavelength of 630 nm, by a microplate reader (Tecan Spectrafluor Plus, Tecan, Switzerland). The relative cell viability (%) related to control wells treated only with 20 μL PBS was calculated as ([A] test/[A] control) × 100%. All experiments were performed in triplicates.

Statistical Analysis.

The statistical significance of experiments were analyzed by the unpaired t test, $p < 0.05$ was considered statistically significant in all analyses (95% confidence interval).

4 RESULTS

4.1 pH-Reversible cationic RNase A conjugates for enhanced cellular delivery and tumor cell killing

The chapter has been partly adapted from:

Liu X, Zhang P, He D, Rödl W, Preiß T, Rädler JO, Wagner E, Lächelt U. pH-Reversible Cationic RNase A Conjugates for Enhanced Cellular Delivery and Tumor Cell Killing. Biomacromolecules. 2016 Jan 11;17(1):173-82.

Lysine residues are convenient anchor points in proteins for synthetic modification by acylation. However, irreversible modification can affect the activity of proteins. This work is based on the formation of covalent amide bonds between the lysines of proteins (Enhanced Green Fluorescent Protein, EGFP; RNase A, Ribonucleases A) and the pH sensitive bifunctional (amine- and azide-reactivity) linker AzMMMan (Figure 4.1-1). The pH in the endo- and lysosomes (early endosomes 6.0-6.5, late endo- and lysosomes 4.5-5.5) is lower than in any other part of the cell[64 66 116]. This unique feature can be utilized as a specific trigger for a dynamic response to the environment within the acidic vesicles.

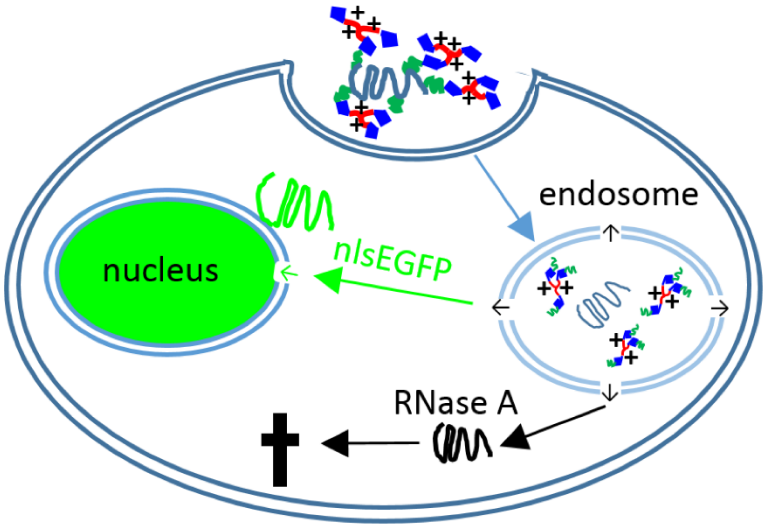

Scheme 4.1-1. Native proteins are delivered to the cytosol via cellular uptake (I) and endosomal release (II) facilitated by the conjugated cationic oligomers, which get cleaved off in the acidic environment of the endosomes.

By using the AzMMMan linker for conjugation, a protein vector can be designed, which is stably associated with the protein in the extracellular space and releases the cargo in a traceless fashion at the low endosomal pH after cellular uptake. The AzMMMan linker modified proteins (EGFP, RNase A) were conjugated with sequence defined cationic oligomers DBCO-PEG$_4$-Mal-689 and -386 by copper free click chemistry for mediation of cellular uptake and endosomal escape (Figure 4.1-1).

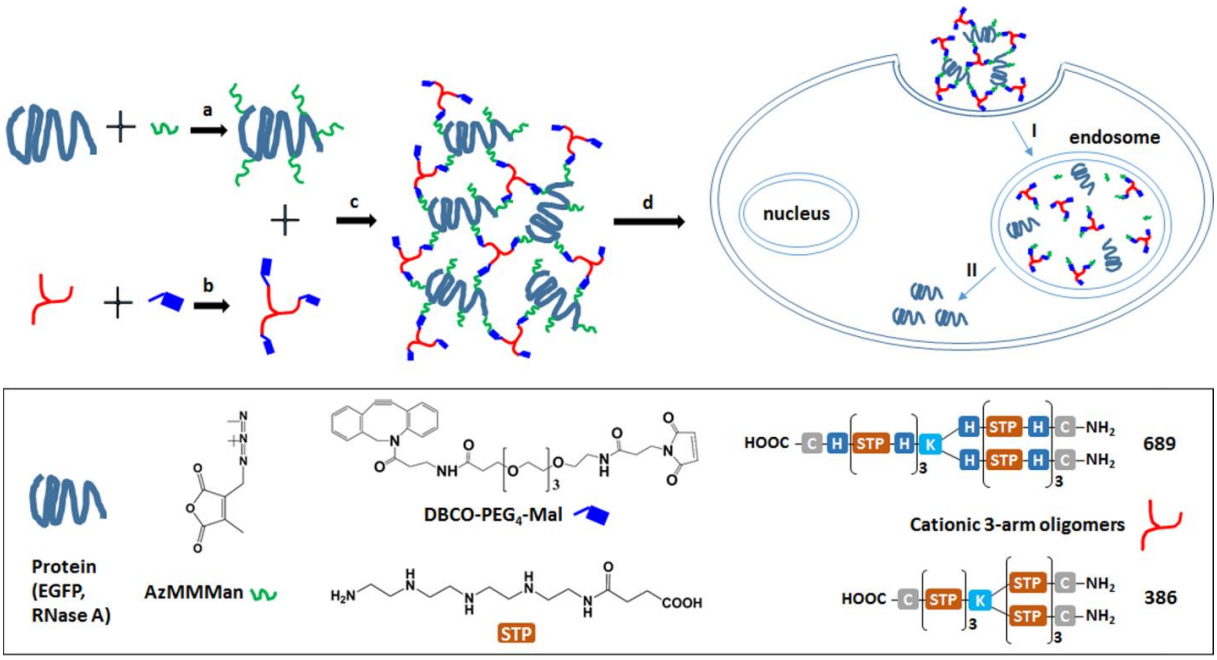

Figure 4.1-1. Schematic illustration of preparation of a pH sensitive protein conjugate. a) Amino functions of the protein (EGFP, RNase A) react with AzMMMan linker; b) 3-arm cysteine containing oligomer reacts with DBCO-PEG4-Mal via thiol-maleimide reaction; c) linker modified protein couples with 3-arm oligomer via azide alkyne cycloaddition; d) cationic protein conjugate enters the cell. C, H and K represent the corresponding α-amino acids in one-letter-code; STP stands for the used oligoamino acid succinoyl tetraethylene pentamine.

4.1.1 AzMMMan linker

Linker has been widely used to connect target macromoleculars with other kinds of active units which forms a complex formulation combines the functional parts of each constituent. But much of linkers lack characterization of traceless release from the target units or carrier, which could reduce the functional activity of the modified target units. Here a pH-labile amzide linker is synthesized[90], which could bridge the -NH_2 groups exist abundantly in almost all biological molecular, such as proteins. The synthesized linker could be obtained by two steps, the first step is from dimethylmaleic anhydride to 3-(bromomethyl)-4-methyl-2,5-furandione (BrMMMAn) by radical substitution reaction; the second step is a nucleophilic

substitution, -N_3 group substitute –Br from BrMMMAn. The NMR shows pure final AzMMMAn linker is obtained.

4.1.2 Synthesis of BrMMMan (3-(bromomethyl)-4-methyl-2, 5-furandione)

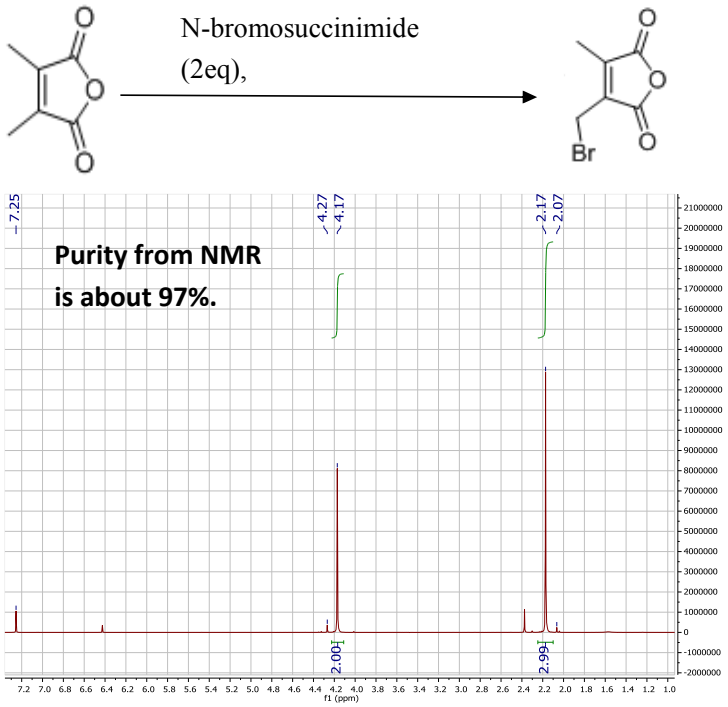

Figure 4.1-2. ^{1}H-NMR (500 MHz, $CDCl_3$) of synthesis product BrMMMan. δ(ppm) = 2.17 (s, 3H, -CH_3 BrMMMan, 4.17 (s, 2H, -CH_2 BrMMMan), 2.07 (s, 6H, -CH_3 2,3-dimethylmaleic anhydride, 4.27 (s, 4H, –CH_2 2,3-dibromomethylmaleic anhydride), 7.25 ($CHCl_3$).

4.1.3 Synthesis of 3-(azidomethyl)-4-methyl-2,5-furandione (AzMMMan)

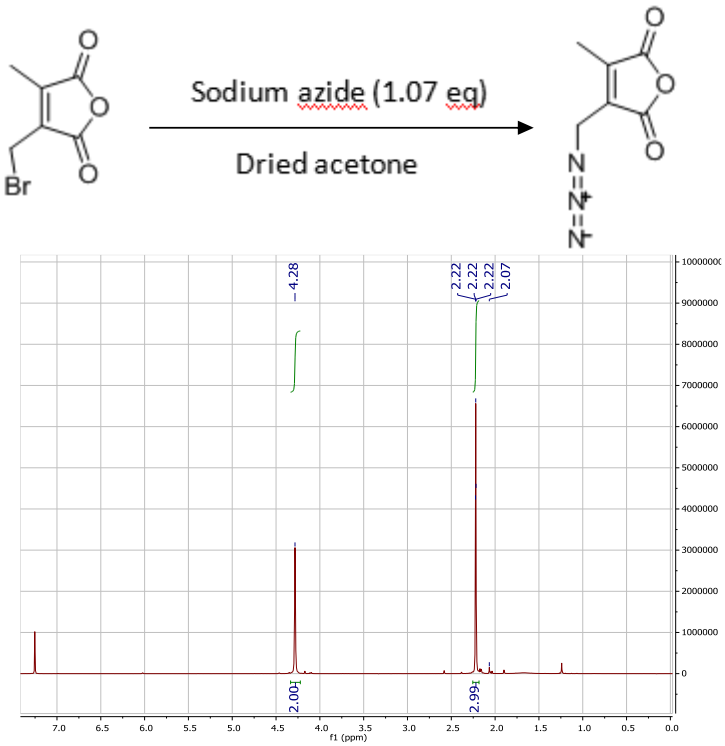

Figure 4.1-3. ^{1}H-NMR (500 MHz, $CDCl_3$) of synthesis product AzMMMan. δ(ppm) = 2.22 (s, 3H, -C<u>H</u>$_3$ AzMMMan), 4.28 (s, 2H, -C<u>H</u>$_2$-N$_3$ AzMMMan), 7.25 ($CHCl_3$).

4.1.4 Protein modifications

The lysines of the proteins EGFP, RNase A were first reacted with an excess amount of AzMMMan linker in Hepps (0.5 M, pH 9.0) for 2 hours, followed by size exclusion chromatography to remove non-coupled linker. Successful AzMMMan modification of EGFP could be confirmed by UV spectroscopy, since AzMMMan and EGFP-AzMMMan have an intensive absorbance around 240 nm comparing to non-modified EGFP (Figure 4.1-4). The sequence-defined oligoamino amides 689 and 386 were synthesized by solid phase synthesis[87 111], and the three contained cysteines were modified with DBCO-PEG$_4$-Maleimide.

The reaction of the AzMMMan functionalized proteins with DBCO-PEG$_4$-Maleimide-689 and -386 followed. The AzMMMan modified proteins bring in azide groups, which can be used for biorthogonal reaction with dibenzylcyclooctyne (DBCO) by strain promoted azide alkyne cycloaddition that enables the conjugation of two components via a stable triazole structure. By this means, linker modified proteins were incubated with various molar ratios of DBCO-PEG$_4$-Mal-689 (molar ratios of 689: EGFP=2, 4, 8, 16; 689: RNase A=0.75, 1.5, 3, 6), initiating the click reaction between the DBCO group of the cationic conjugate and the azide group of AzMMMan modified proteins (Figure 4.1-1). Since the used SV40nls-EGFP contains 26 and RNase A only 11 primary

amines, approx. 2.7-fold higher molar ratios were used during synthesis of the EGFP conjugates to compensate the multiplicity.

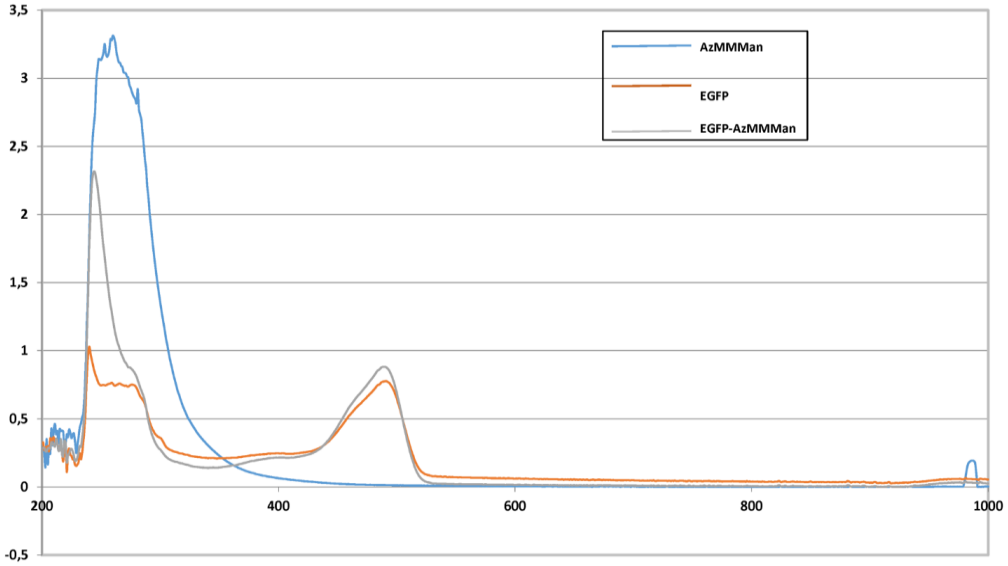

Figure 4.1-4. UV-Vis spectra of AzMMMan (incubation for 4h in Hepps pH 9.0), nlsEGFP and EGFP-AzMMMan.

The conjugates were analyzed by SDS polyacrylamide gel electrophoresis to confirm successful assembly (Figure 4.1-5 a), b), c)). The SDS-PAGE gel reveals a gradual shift of the protein band toward lower migration distance with increasing 689/386 to protein ratio. The protein conjugate with highest modification ratio (689: EGFP=16 and 689/386: RNase A=6) exhibited the shortest migration indicating the highest molecular weight, which can be explained by more extensive DBCO-PEG_4-Mal-689 attachment and crosslinking.

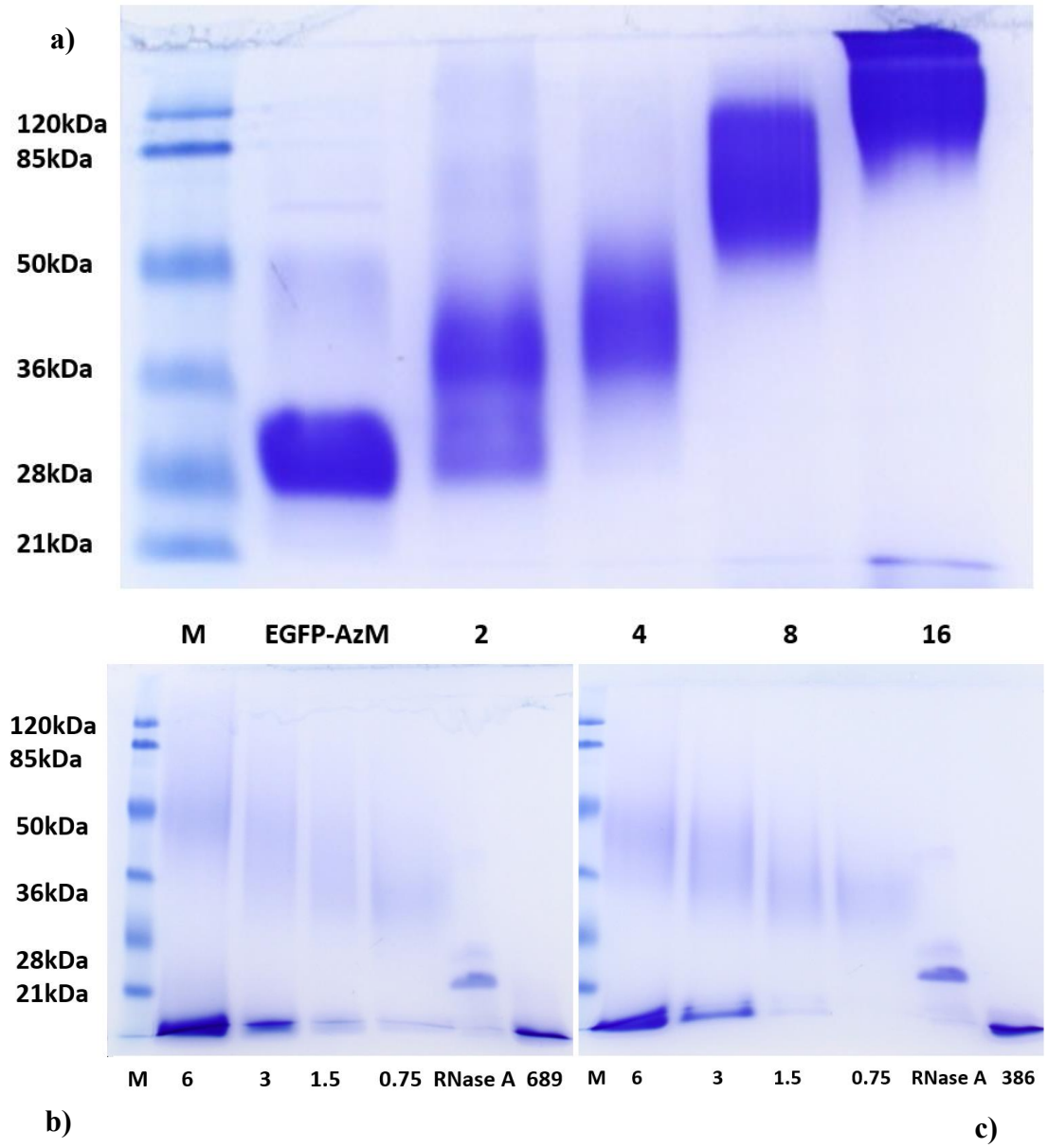

Figure 4.1-5. a) SDS-PAGE of 689-EGFP conjugates. M, molecular weight marker; numbers indicate the molar ratio of 689 to EGFP. Equal amounts (10 µg) of EGFP protein were loaded in each lane. b) SDS-PAGE of 689- (left) and c) 386- (right) modified RNase A, M, molecular weight marker, numbers indicate the molar ratio of oligomer to RNase A of the protein conjugates. Bare RNase A (RNase) and oligomers (386, 689) were used as controls. RNase A conjugate and bare RNase A samples contained 3µg of protein. Bare 689 and 386 oligomer samples contained 5 µg of oligomer.

To show the cross-linking of 689-EGFP conjugates more detailed, fluorescence correlation spectroscopy (FCS) measurements of EGFP were performed (Figure 4.1-6). FCS is a highly sensitive single-molecule technique for measuring hydrodynamic radii of fluorescent molecules or particles in highly diluted

solutions in the nanomolar concentration range[117]. EGFP and EGFP-AzMMMan, as well as the conjugates with 689 to EGFP ratios of 2 and 4, were shown to have hydrodynamic radii of 2−4 nm. In contrast, the samples with 689 to EGFP ratios of 8 and 16 showed clusters with a hydrodynamic radius above 0.1 µm. This indicates that large EGFP complexes are formed depending on the molar ratio of cross-linking three-arm oligomer. However, it has to be noted that also at the high ratios small particles were detected, which suggests that the conjugation approach results in rather heterogeneous mixtures of variably cross-linked proteins.

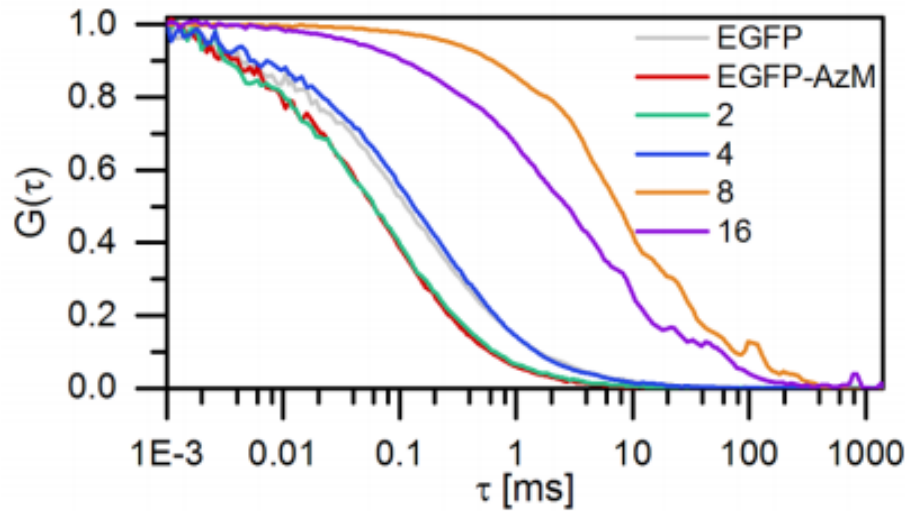

Figure 4.1-6. FCS measurements. Numbers indicate the molar ratio of 689 to EGFP. Normalized average correlation curves show clustered (RH > 0.1 µm) 689-EGFP conjugates at high 689 to EGFP ratios (8, 16), whereas particle size at low ratios (2, 4) remain in the range of EGFP and EGFP-AzM (RH =2−4 nm). FCS were carried out by Tobias Preiß (Faculty of Physical, LMU).

4.1.5 Flow cytometry of EGFP conjugates

EGFP was equipped with positive charge by modification with the cationic oligomer 689. The sequence-defined oligomer 689 contains 9 repeats of the artificial amino acid STP[112] which exhibits positive charge at neutral pH but also a buffer capacity in the endolysosomal pH range, which was intended to enable transport of the protein into cells and the escape from endosomes by the proton-sponge effect[66, 118 119]. It is hypothesized that different ratios of oligomer on the protein surface could influence the amount of intracellular protein transduction. To investigate this, the internalization of different conjugates with varied modification ratios into HeLa cells was investigated by flow cytometry. The results demonstrated that the sequence defined 3-arm cationic oligomer could deliver the protein into cells. As expected, increasing oligomer conjugation promoted the intracellular protein delivery indicated by a shift toward higher cellular fluorescence intensity in Figure 4.1-7. This illustrates the importance of an optimization of coating degree, even when the protein is modified by the same carrier.

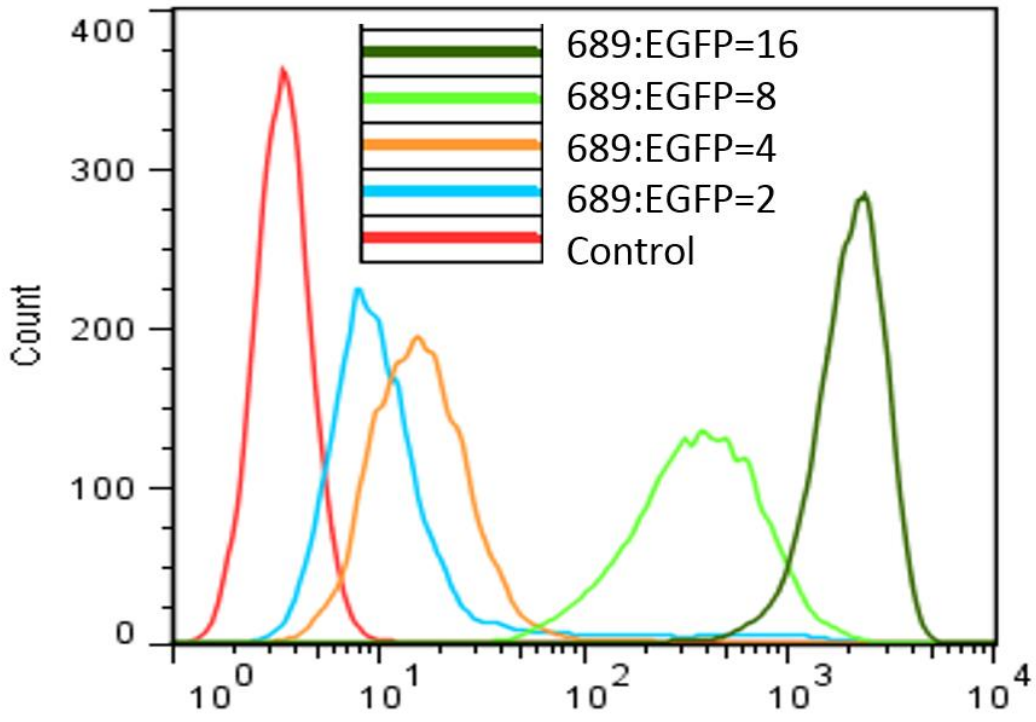

Figure 4.1-7. Cellular uptake of conjugates with different 689 to EGFP molar conjugation ratios determined by flow cytometry. Untreated control cells are shown in red. 689: EGFP=2 (blue), 689: EGFP=4 (yellow), 689: EGFP=8 (green), 689: EGFP=16 (brown). Experiments were carried out by Peng Zhang (PhD study, Department of Pharmacy, LMU).

Having successfully demonstrated efficient cellular uptake of 689 modified EGFP, a comparison study between the two similar cationic oligomers 386 and 689 has been carried out. 386 is also a 3-arm cationic STP-based oligomer, having been successfully used for siRNA, DNA and protein delivery before[111 120 121], but 689 additionally contains histidines after each STP units to enhance endosomal buffering. The flow cytometry results show 386 and 689 oligomer modified EGFP being internalized into cells to comparable extent (Figure 4.1-8). In the extracellular environment, the pH is about 7.4 and the additional histidines in 689

are not protonated. Therefore, these two oligomers mediate similar uptake of modified EGFP.

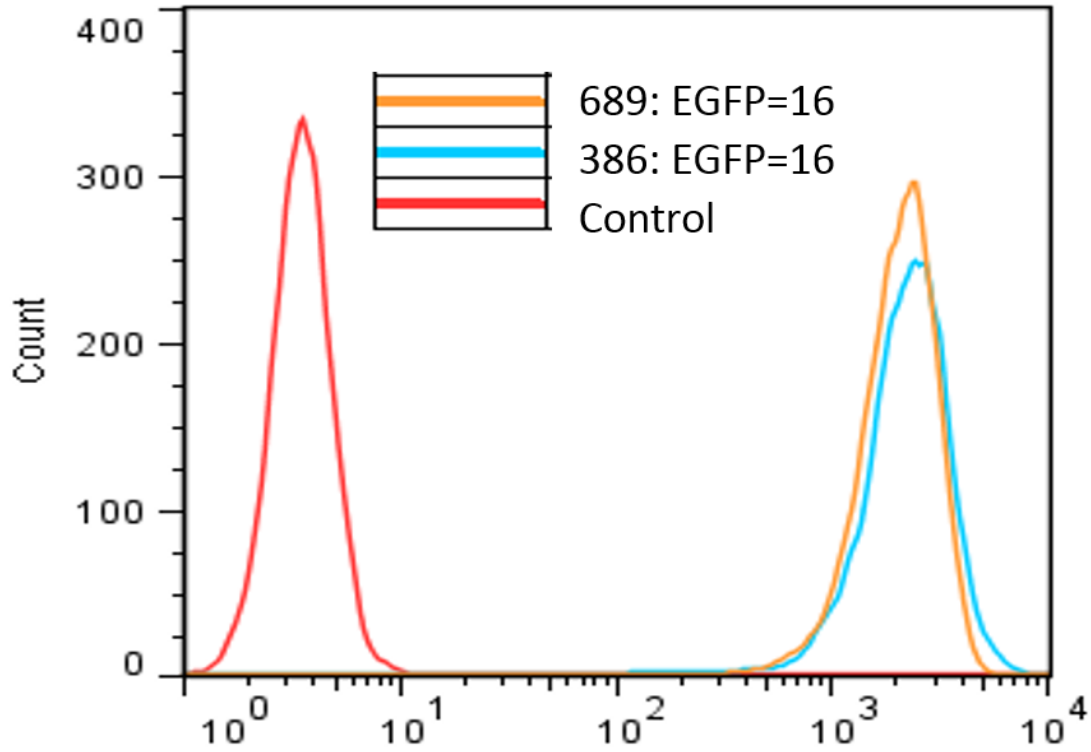

Figure 4.1-8. Flow cytometry of cells incubated with 689 or 386 modified EGFP with the same molar ratio (16). HeLa cells were incubated with samples (1 µM EGFP) at 37 °C for 2 h before flow cytometry. Experiments were carried out by Peng Zhang (PhD study, Department of Pharmacy, LMU).

4.1.6 Intracellular distribution of EGFP

The cellular uptake and intracellular distribution of the EGFP conjugates with varied modification degree was further investigated by fluorescence microscopy (Figure 4.1-9). Since the used recombinant EGFP contains a nuclear localization signal (NLS), nuclear delivery after protein conjugate internalization is investigated. The protein conjugates (689: EGFP=4 and 689: EGFP=8) show successful nuclear entry, whereas the protein conjugates (689: EGFP=2 and 689:

EGFP=16) did not show any nuclear delivery. It is hypothesized that since ratio 2 (689: EGFP) also mediates lower cellular uptake (Figure 4.1-10), the amount of accumulated conjugates with proton-sponge activity is not enough to break through the endosome. On the other hand, since the SV40 large T antigen NLS contains multiple lysines, the extensive modification in case of ratio 16, might affect intracellular trafficking. It concludes that the four EGFP conjugates have high intracellular uptake efficiency, and two optimized conjugates show successful nuclear delivery.

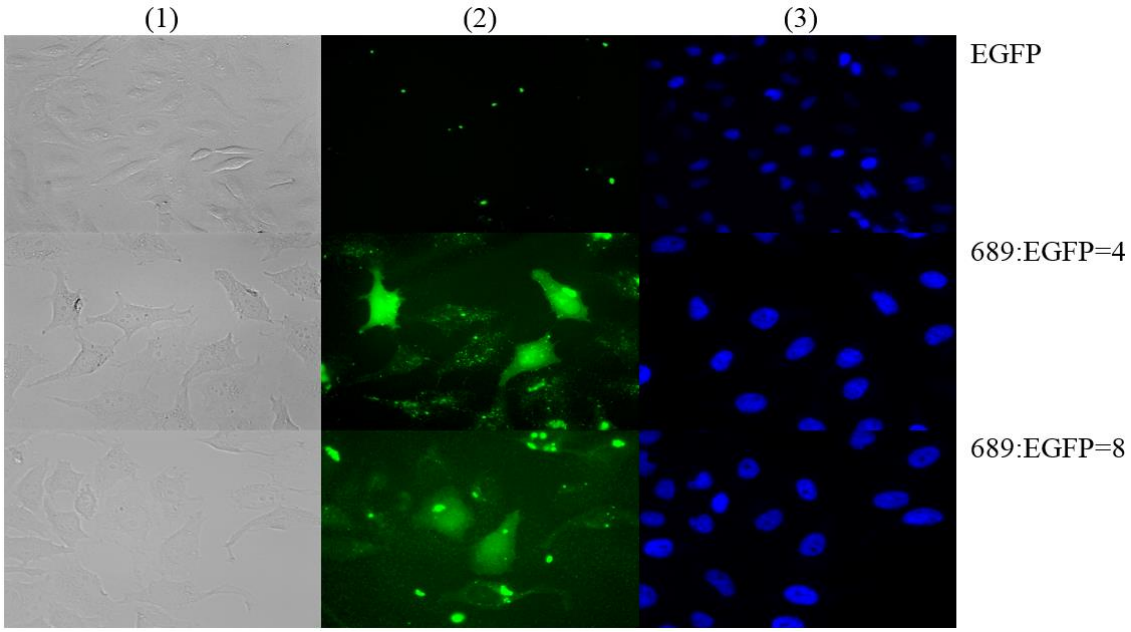

Figure 4.1-9. Microscopy images of cells treated with different EGFP samples. First row: unmodified EGFP control, second row 689: GFP=4, third row, 689: GFP=8; (1): Bright field images; (2): EGFP fluorescence; (3): DAPI fluorescence (nuclear staining). HeLa cells were incubated samples (1 µM EGFP) for 24 h at 37 °C. 40× objective was used for image acquisition. Experiments were carried out by Peng Zhang (PhD study, Department of Pharmacy, LMU).

In case of all four protein conjugates significant intracellular EGFP fluorescence could be observed (Figure 4.1-10), even the protein conjugates with negative zeta

potential (conjugation ratios 689: EGFP=2 and 689: EGFP=4) were efficiently internalized. In case of the latter protein conjugates, the cationic oligomer does not suffice to reverse all the negative charge of the protein into positive charge. Nevertheless, the attached cationic oligomer mediated transport of EGFP into cells. This accounts for the high potency of the used sequence-defined oligomer.

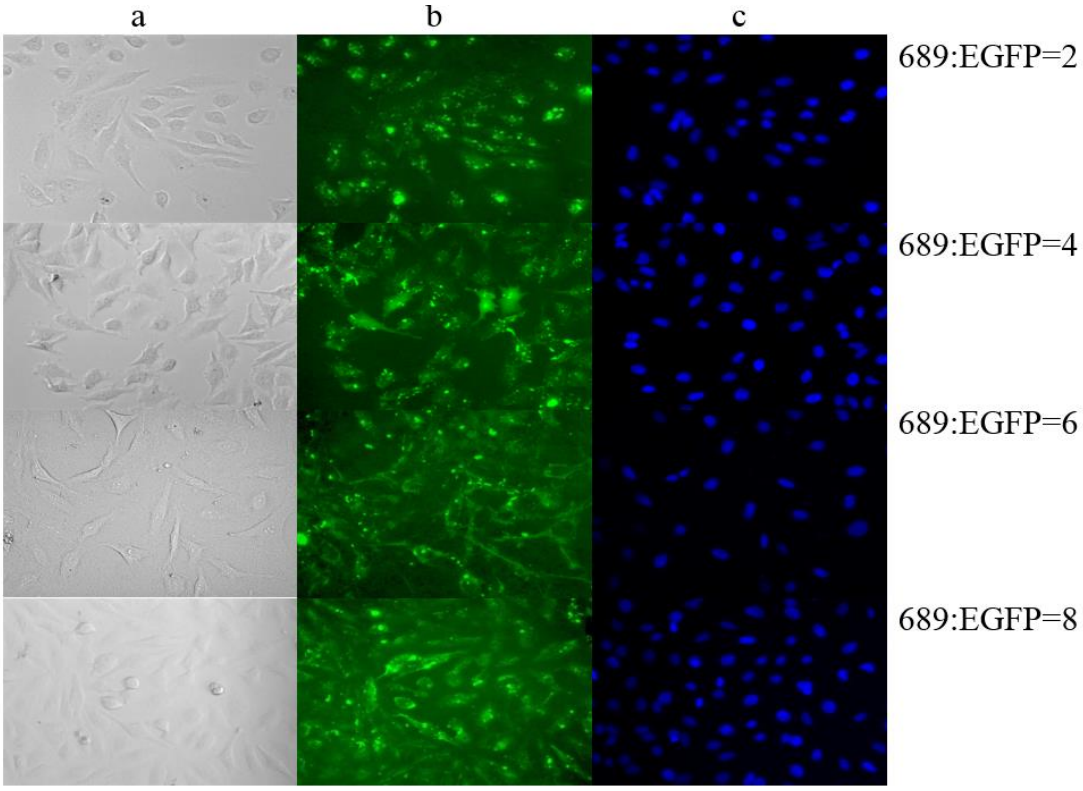

Figure 4.1-10. Fluorescence microscopy of HeLa cells treated with different EGFP conjugates of varied molar ratios. (a) Bright field, (b) EGFP fluorescence and (c) DAPI fluorescence (nuclear staining). Cells were incubated with 1 µM protein solutions for 24 h. 40× objective was used for image acquisition. Experiments were carried out by Peng Zhang (PhD study, Department of Pharmacy, LMU).

4.1.7 pH-responsive release of RNase A conjugates

RNase A was utilized to demonstrate the feasibility of covalent modification by the established method with a biologically active protein. RNase A, an endoribonuclease, catalyzes the cleavage of the phosphodiester bond between the 5'-ribose of a nucleotide and the phosphate group attached to the 3'-ribose of an adjacent pyrimidine nucleotide. The enzyme has been used as an alternative chemotherapy drug for clinical cancer treatment, since it can degrade intracellular RNA inducing apoptosis of tumor cells[89]. Wang recently used cationic lipid-like nanoparticles to coat negatively charged RNase A through electrostatic interaction, showing an intracellular delivery and cancer killing result[71]. Herein, the cationic vector to attach with pH-sensitive AzMMMan modified RNase A is utilized. The resulting protein conjugate was expected to form a more stable delivery system than the often used electrostatic noncovalent complexes. A series of 689 or 386 oligocation modified RNase A conjugates was synthesized. To investigate the pH-responsive cleavage, RNase A-AzMMMan-DBCO-PEG_4-Mal-689/386 were incubated (molar conjugation ratio of 689 or 386 to RNase A = 6) at neutral or acidic pH and the release of free RNase A was monitored by SDS-PAGE (Figure 4.1-11). The gel demonstrated that incubation for 24 hours at pH 5 resulted in significant protein release, in contrast to incubation in PBS buffer at pH 7.4 where almost no cleavage of RNase A could be observed.

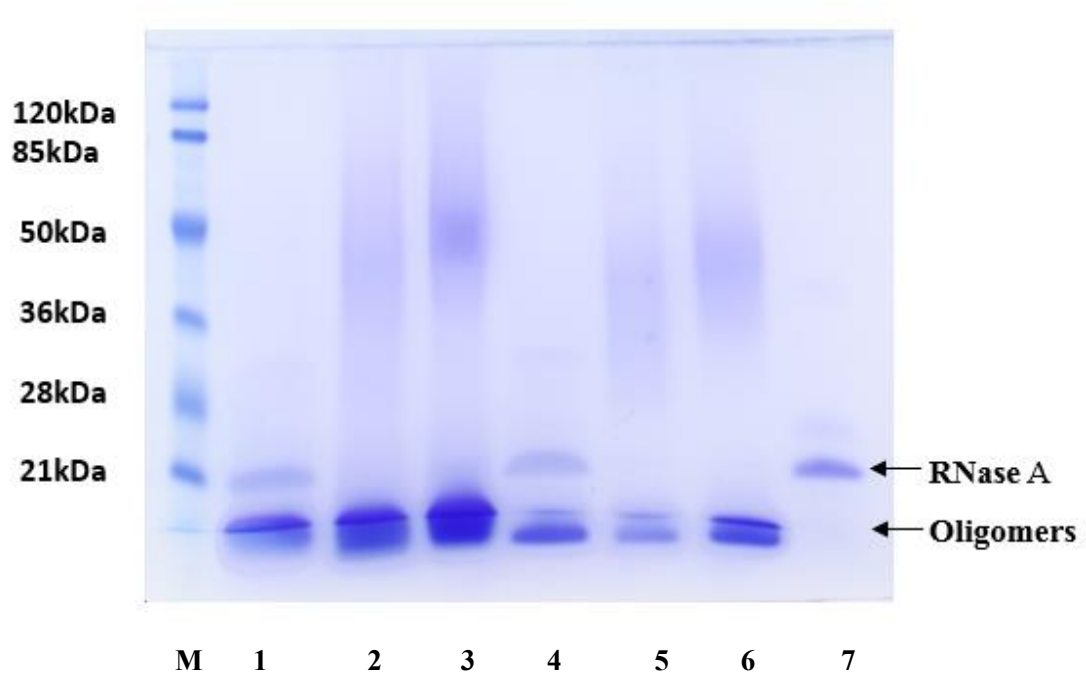

Figure 4.1-11. pH dependent traceless release of RNase A from protein conjugates (molar conjugation ratio 6). M, molecular weight marker; 1) 689 modified RNase A incubated in citrate-phosphate buffer (pH=5) for 24 h at 37 ºC; 2) 689 modified RNase A incubated in PBS (pH=7.4) for 24 h at 37 ºC ; 3) 689 modified RNase A without any treatment; 4) 386 modified RNase A incubated in citrate-phosphate buffer (pH=5) for 24 h at 37 °C; 5) 386 modified RNase A incubated in PBS (pH=7.4) for 24 h at 37 ºC ; 6) 386 modified RNase A without any treatment. Equal amounts (3 µg) of RNase A were loaded in each lane.

4.1.8 Ethidium bromide assay for determination of enzymatic RNase A activity

For detecting the enzymatic activity of RNase A and its conjugates, an ethidium bromide (EtBr) fluorescence assay (Figure 4.1-12, 4.1-13) is developed. The fluorescence intensity of a solution containing 0.5 ng EtBr and 20 µg RNA in 1 mL PBS (pH=7.4) was monitored during an equilibration time of 5 min. After addition of RNase A samples, the decrease of fluorescence intensity based on the enzymatic RNA degradation was monitored over 5 min.

While unmodified RNase A solutions which were incubated for 24 h at pH 7.4, pH 5 or freshly prepared did not exhibit remarkable differences (Figure 4.1-12, left), the enzymatic activity of RNase A-AzMMMan conjugates was strongly dependent on the pH during the pre-incubation phase. RNase A-AzMMMan-386 (Figure 4.1-12, middle), -689 (Figure 4.1-12, right) and RNase A-AzMMMan (Figure 4.1-13, left) revealed extremely low activity after a 24 h incubation phase at pH 8.5, whereas activity was restored after incubation at pH 5, indicating the pH-responsive release of unmodified RNase A. After 24 h incubation at pH 7.4, an intermediate activity was observed which obviously is caused by partial AzMMMan cleavage. In contrast, stable amidation of RNase A by bifunctional SMCC linker reduced the enzymatic activity in an irreversible, pH-independent fashion (Figure 4.1-13, right).

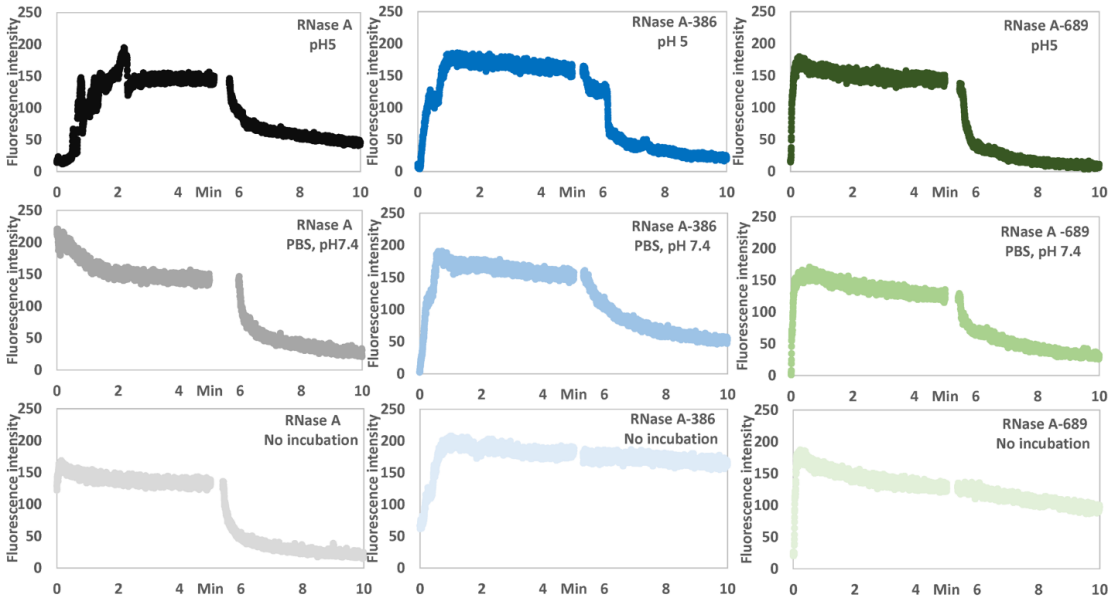

Figure 4.1-12. a) Enzymatic activity of RNase A measured by an ethidium bromide assay. Unmodified RNase A (left), RNase A-AzMMMan-DBCO-PEG$_4$-Mal-386 (molar ratio 6, middle) and RNase A-AzMMMan-DBCO-PEG$_4$-Mal-689 (molar ratio 6, right) under different conditions. First row, incubated in citrate-phosphate buffer (pH=5) for 24 hours at 37 °C;

second row, incubated in PBS (pH=7.4) for 24 hours at 37 °C; third line, fresh solutions of unmodified RNase A (left), 386 (middle) and 689 conjugates (right) without incubation.

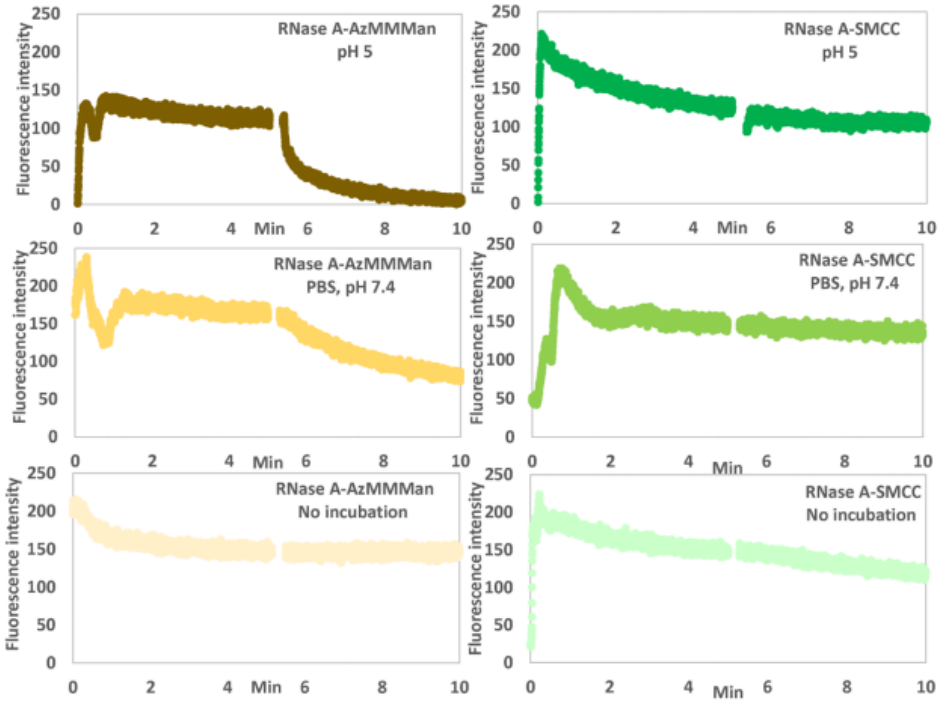

Figure 4.1-13. Enzymatic activity of RNase A conjugates determined by an ethidium bromide assay. Activity of pH-cleavable RNase A-AzMMMan (left) and irreversible conjugate RNase A-SMCC (right) were investigated after different treatments. First line, incubated in buffer (pH=5) for 24 hours at 37 °C; second line, incubated in PBS (pH=7.4) for 24 hours at 37 °C; third line, samples stored in Hepps (pH=8.5) without additional treatment. RNase A-SMCC was synthesized analogously to RNase A-AzMMMan but with use of SMCC (Thermo Scientific) instead of AzMMMan.

4.1.9 Cytotoxic potency of RNase A conjugates

To verify that the covalently modified therapeutic protein can be successfully delivered into the cytoplasm, cell viability assays (MTT) were performed with the two series of oligomer (689 and 386) modified RNase A to investigate the biological activity and effect on tumor cell viability. As shown in Figure 4.1-14a, all RNAse A conjugates revealed some cytotoxicity, while the control RNase-

AzMMMan did not induce any obvious inhibition of metabolic activity. For the same series (689 or 386) oligomer modified RNAse A, the toxicity increased with the degree of oligomer conjugation. When treated at the same ratio (0.75, 1.5, 3, 6 μM) of two covalently modified RNase A conjugate at the same concentration, oligomer 689 modified RNase A showed higher toxicity than 386 oligomer modified RNase. Considering Figure 4.1-8, which shows that 386 and 689 modified proteins possess similar cellular internalization at the same modification degree, this possibly can be explained by an enhanced endosomal escape due to the increased buffer capacity of the histidine-rich oligomer 689, which could promote an improved proton sponge effect resulting in higher toxicity of 689 modified RNase A. Flow cytometry experiments with the most toxic protein conjugates (molar ratio, 689: RNase A=6, 386: RNase A=6) have been carried out to verify their internalization. The results shown in Figure 4.1-14b confirm again that 689 and 386 show similar uptake ability, consistent with Figure 4.1-8 and our former study. Considering the cellular uptake results, the differential activity possibly can be explained by an enhanced endosomal escape due to the increased buffer capacity of the histidine-rich oligomer 689, which could promote an improved proton sponge effect resulting in higher toxicity of 689 modified RNase A[87 122].

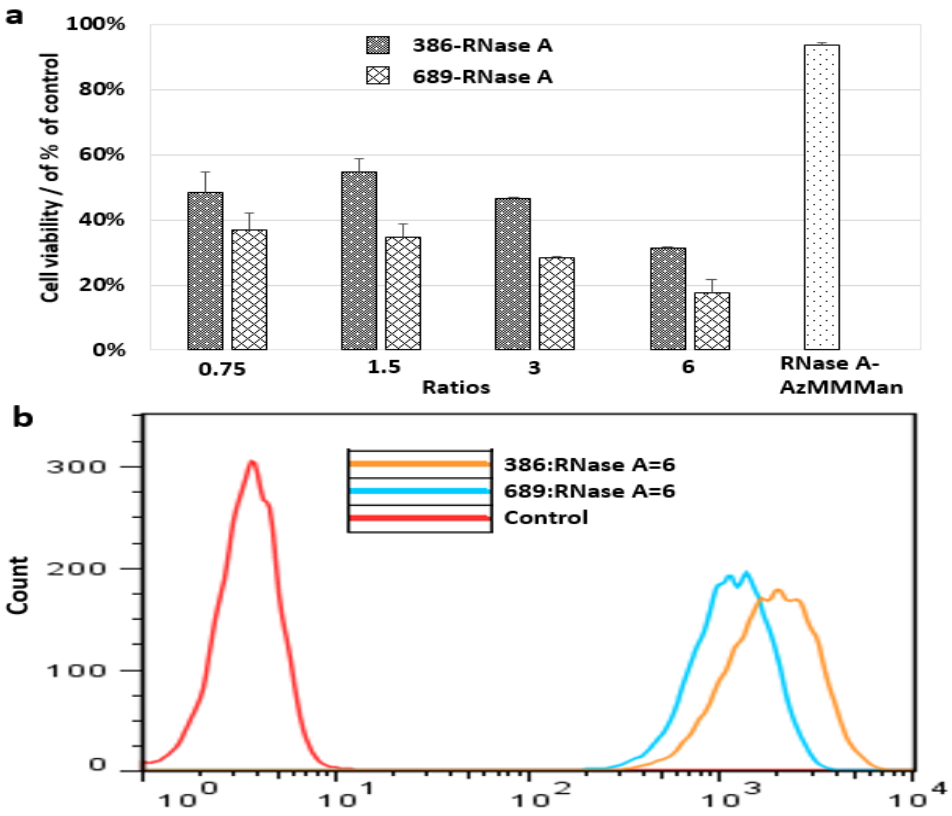

Figure 4.1-14. Cellular uptake and cytotoxic potency of RNase A conjugates. a) Viability of HeLa cells (MTT) after treatment with 4 µM of 386 RNase A conjugates (left bar) or 689 RNase A conjugates (right bars) with different oligomer. RNase A molar ratios (0.75, 1.5, 3, 6). b) Cellular uptake of 4 µM 386- or 689-modified RNase A-Cy5 (oligomer: RNase A molar ratio 6). Experiments were carried out by Peng Zhang (PhD study, Department of Pharmacy, LMU).

Finally, to demonstrate that the process of cell killing is dependent on the protein concentration, various amounts of 386 and 689 modified RNase A conjugates (0.5 µM, 1 µM, 2 µM, 4 µM) as well as control groups (oligomers 386, 689; RNase A-AzMMMan, RNase A-AzMMMan + free 689) were incubated with HeLa cells for 48 hours. Figure 4.1-15a reveals that cells treated with RNase A-AzMMMan-DBCO-PEG$_4$-Mal-689 show significantly decreased cell viability. Cells have only 19% survival rate when treated by 4.0 µM RNase A conjugate, while cells treated with 0.5 µM do not seem to be affected. This accounts for the dose-response

correlation between cytotoxicity and added concentration of the RNase A conjugate. Cells treated only with RNase A-AzMMMan, 386 or 689 oligomer alone do not show remarkable reduction of cell viability. Likewise, the mixture of RNase A-AzMMMan and oligomer 689 did not decrease cell viability below 80%, but showed slightly higher cytotoxicity than RNase A-AzMMMan alone. This could be explained by electrostatic binding between negatively charged RNase A-AzMMMan and positively charged 689 which may result in delivery of a very small amount of RNase A-AzMMMan into the cytoplasm, inducing slightly toxic effects.

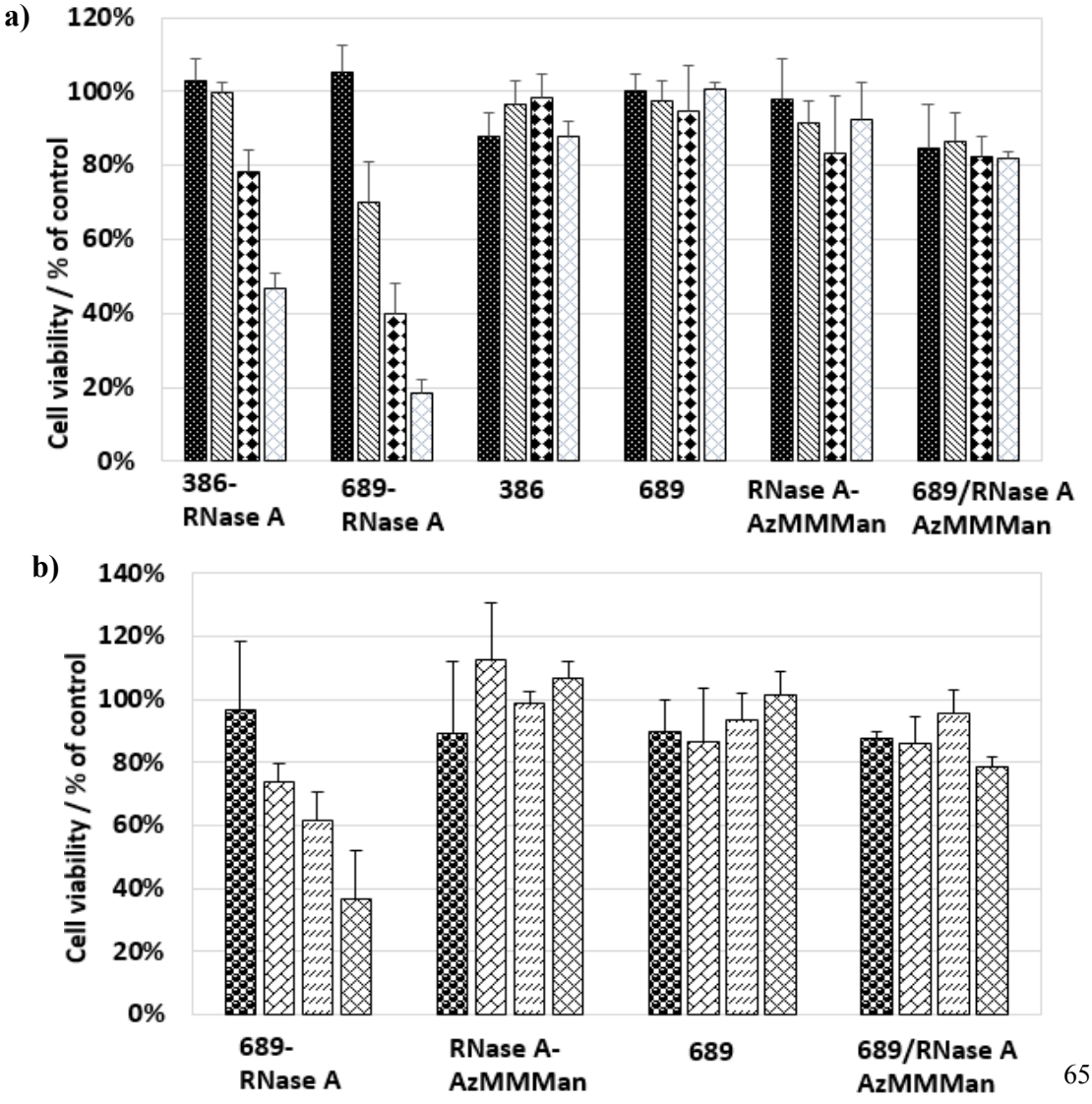

Figure 4.1-15. Cytotoxic potency of RNase A conjugates a) Viability of HeLa cells (MTT) after treatment with 386-RNase A, 689-RNase A conjugates (molar ratio 6) and control groups (bare 386, bare 689, RNase-AzMMMan, mixture of 689 and RNase A-AzMMMan) at various concentrations. Concentration of RNase A conjugates, RNase A-AzMMMan, and oligomer/RNase A control mixtures (from left to right): 0.5 μM, 1.0 μM, 2 μM, 4 μM. Concentration of bare oligomers 386 and 689: 3.0 μM, 6.0 μM, 12 μM, 24 μM. b) Viability of N2A cells (MTT) after treatment with 689 modified RNAse A conjugates (molar ratio 6) under the same conditions as described in c). Experiments were carried out by Peng Zhang (PhD study, Department of Pharmacy, LMU).

Interestingly, when cells were treated with the same concentration of 386- and 689- modified RNase A, 689-modified RNase A always showed higher cytotoxicity than 386-modified RNase A (viability 40% compared to 78% at 2 μM, 19% compared to 49% at 4 μM. We hypothesize that both protein conjugates have the same intracellular delivery ability as a result of same protonation degree at extracellular pH, which is provided by the Figure 4.1-8 and Figure 4.1-14b. However, after cellular uptake and entering into endosomes, as the pH drops from 7.4 to 6.0, the histidines of 689 could promote the proton sponge effect and endosomal escape resulting in more efficient protein delivery into the cytoplasm. The potency of the 689 modified RNase A to kill cancer cells is not restricted to HeLa is also further demonstrated. MTT assays of murine neuroblastoma N2A cells incubated with the most potent RNase A conjugate also showed dose dependent tumor cell killing (Figure 4.1-15b).

4.2 Intracellular delivery of EGFP by combination of targeting ligand and endosomal escape lytic peptide

In the last section work, a polymer was utilized to function as the carrier for protein delivery which exhibits very high delivery efficiency, as well as demonstrated successfully to restore its biological activity during modification and then release its full biological function after traceless cleavage in the endosomal acidic environment. But this system employed the cationic units as the intracellular part, this is not stable in the bloody conditions of the organic, which in rich of all kinds enzymatic degradation and salts. In this section, a multifunctional delivery system, combining a targeting ligand and an endosomal escape lytic peptide, is designed. No polymer is used in this strategy to avoid the electrostatic of the polymer carriers with the abundant macromolecular environment in the organics. EGFP first reacted with AzMMMan linker, and then DBCO coupled folate and INF7 were used to modify with the linker modified EGFP, as showed in Figure 4.2-1.

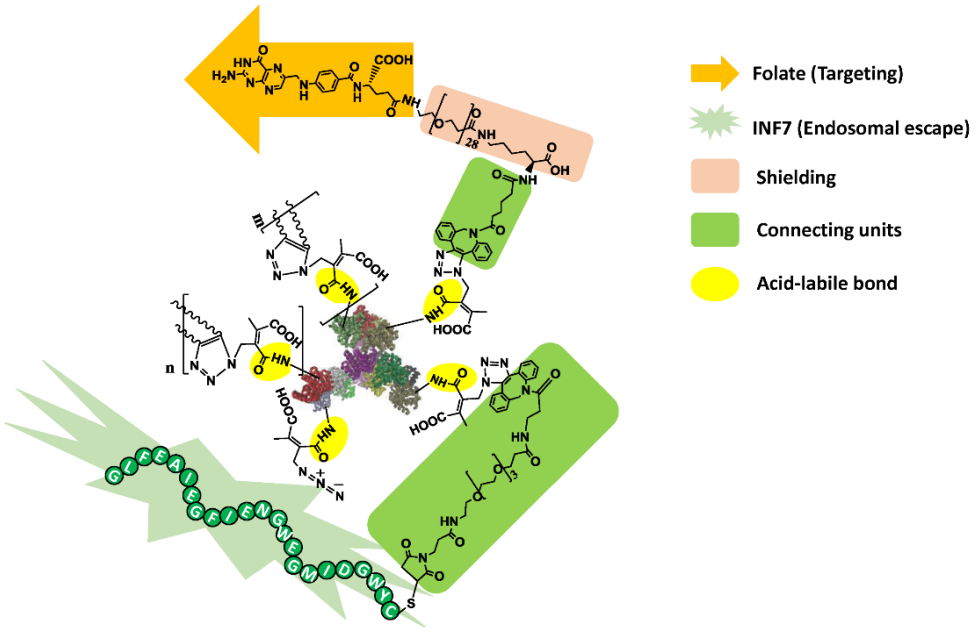

Figure 4.2-1. Schematic illustration of synthesis of target-protein-endosomal escape peptide conjugates. Proteins modified by acidic traceless linker AzMMMan and coupled with target ligand folate and endosomal disruptive peptide INF7 by copper free click chemistry. m, n represents the repeat units of folate and INF7 ligand respectively.

Based on this strategy, a series of further EGFP conjugates were synthesized as displayed in Table 1.

EGFP-AM: DBCO-lysine-PEG_{28}-folate	1:1 (1)	1:5 (2)	1:10 (3)	1:20 (4)	
EGFP-AM: INF7-Mal-PEG_4-DBCO	1:1 (5)	1:5 (6)	1:10 (7)	1:20 (8)	
EGFP-AM: folate-PEG_{28}-lysine-DBCO: INF7-Mal-PEG_4-DBCO	1:10:1 (9)	1:10:5 (10)	1:10:10 (11)	1:10:15 (12)	1:20:5 (13)

4.2.1 Cellular association of EGFP-folate conjugates

Flow cytometry was used to investigate the interaction between EGFP conjugates and target cells and to evaluate the impact of contained folate ligand on the cellular association (Figure 4.2-1). Folic acid receptor positive KB cells were incubated with the four different EGFP conjugates (0.5 μM) and original EGFP (1.5 μM). In a control experiment, preincubation with free folic acid (100 μM) was carried out to inhibit receptor interaction by excessive competition. As expected, unmodified EGFP could not bind to or be internalized into KB cells, similar to folate containing EGFP conjugates after the receptor block by free folic acid. In contrast to the control groups, the cells incubated with folate conjugates show distinct increase of fluorescence indicating the association with EGFP, and the effect increases with the ratio of folate ligand to EGFP. As expected, conjugate 4 shows the highest cellular binding ability compared to conjugates 1, 2, 3 with lower ratio of contained folate. The results demonstrated that the amount of folate ligand connected to the protein, determined the binding ability of the final protein conjugates.

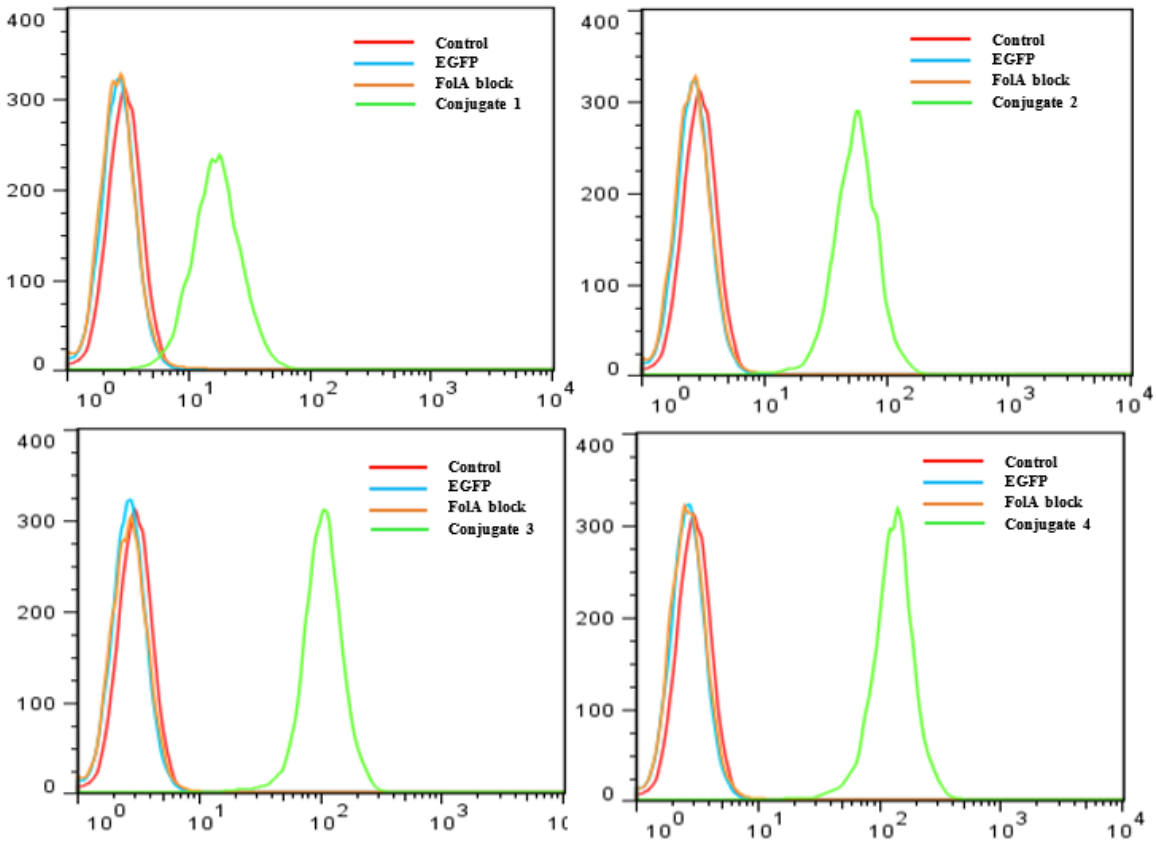

Figure 4.2-1. Cellular association of EGFP conjugates. Red: Blank control without EGFP; Blue: 1.5 µM EGFP was added; Brown: Folate blocked for 30 min before EGFP conjugates were added; Green: 0.5 µM Conjugates. Incubation for 45 min. Experiments were carried out by Peng Zhang (PhD study, Department of Pharmacy, LMU).

4.2.2 Cellular uptake of EGFP-folate conjugates

The investigation of cellular uptake by flow cytometry resulted in similar findings as the cellular association experiments. KB cells pretreated with free folic acid did not show increased fluorescence intensity after incubation with EGFP conjugates, and conjugate 4 achieved highest cellular internalization among all four EGFP conjugates. In general, the levels of cellular uptake were much lower than association which is reasonable since receptor binding is a mandatory prerequisite for the receptor-mediated endocytosis of this kind of protein vectors.

In additional, considering from the structure point of conjugates, spacer PEG_{28} anchoring between protein and folate ligand increased the distance from target sites of cells to protein resulting in a weakening interaction between folate and protein. In addition, the relative dimensions of EGFP compared to low molecular weight folic acid as the native substrate for endocytotic uptake via folic acid receptor could be responsible for restricted internalization despite successful receptor binding.

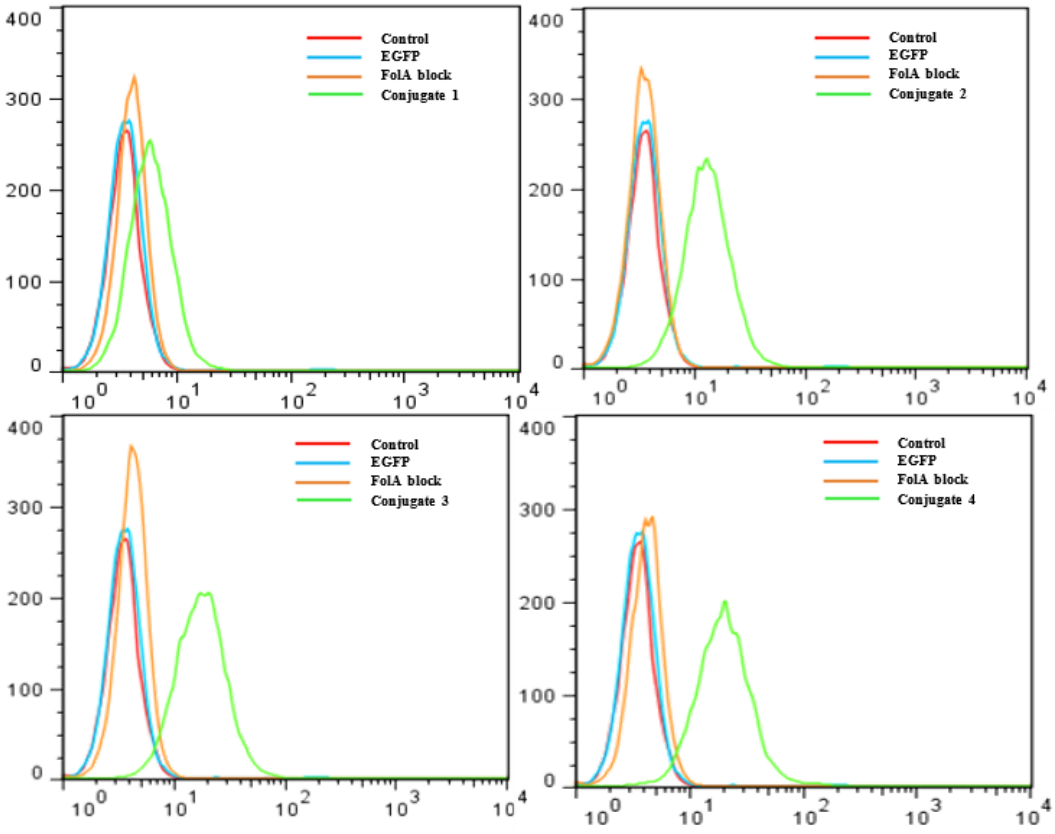

Figure 4.2-2. Cellular uptake of EGFP-folate conjugates. Red: Blank control without EGFP; Blue: 1.5 µM EGFP was added; Brown: Blockade of folate receptor by free folate added for 30 min before EGFP conjugates were added; Green: 0.5 µM conjugates. Experiments were carried out by Peng Zhang (PhD study, Department of Pharmacy, LMU).

4.2.3 EGFP modification with INF7-DBCO

Four different EGFP-INF7 conjugates at different ratios (conjugate 5, 6, 7, 8; DBCO-PEG$_4$-Mal-INF7: EGFP-AzMMMan=1, 5, 10, 20, Table 1) were synthesized, the conjugates were analyzed by SDS polyacrylamide gel electrophoresis (SDS-PAGE) to verify successfully coupling. SDS-PAGE (Figure 4.2-3, left) revealed a gradual blurry shadow of the protein conjugates band in contrast to the band of unmodified EGFP. This could be explained by more INF7 being attached to EGFP with increasing ratio of INF7 to EGFP. In addition, four kinds of INF7-EGFP-folate conjugates were synthesized (conjugate 9, 10, 11, 12; EGFP: folate: INF7=1:10:1, 1:10:5, 1:10:10, 1:10:15, Table 1). Here, SDS-PAGE (Figure 4.2-3, right) showed similar results as for conjugates 5, 6, 7 and 8. Briefly, the migration distance of the conjugates (9, 10, 11, 12) decreased with the ratio of INF7 to EGFP (INF7: EGFP=1, 5, 10, 15), which indicates more INF7 were attached to EGFP when higher ratios of INF7 were used during synthesis.

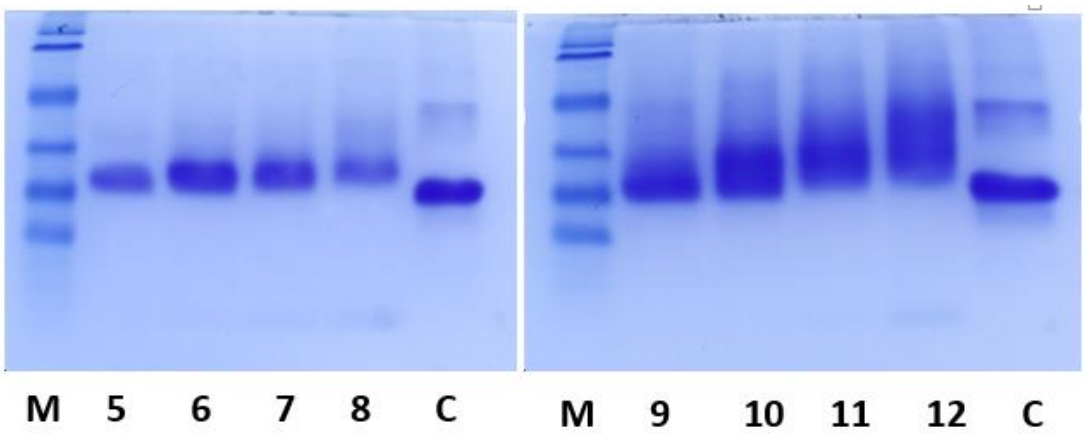

Figure 4.2-3. SDS-PAGE of EGFP-INF7 and folate-EGFP-INF7 conjugates. 5 μg of EGFP were loaded respectively. M, protein mark, C, EGFP control, 5-12 conjugates respond to conjugates in Table 1.

4.2.4 Cellular internalization of EGFP-INF7 and folate-EGFP-INF7

Then the interaction of cell membrane and INF7, a kind of endosomal escape peptide is studied. The pH-dependent lytic peptide is derived from the amino terminal sequence of influenza hemagglutinin HA2 and is able to disrupt liposomes, erythrocytes and endosomal membranes of cells in the acidic environment[109]. The intracellular transduction of EGFP-INF7 (5, 6, 7, 8) and folate-EGFP-INF7 (9, 10, 11, 12) conjugates were analyzed by flow cytometry. EGFP-INF7 conjugates showed moderate internalization into KB cells (Figure 4.2-4) and a slightly positive correlation with increasing degree of INF7 peptide modification could be observed. Conjugate 8 mediated the highest intracellular EGFP fluorescence though still at very low level. This could be explained by the pH-dependance of INF7 peptide which does not reach its full membrane interactive potential at pH 7.4 in the extracellular culture medium. In contrast to the mere INF7 modified protein conjugates, EGFP modified with both folate ligand and INF7 showed much higher uptake quantified by flow cytometry, and all four conjugates (9, 10, 11, 12) mediated similar intracellular EGFP fluorescence levels consistent with the same amount of folate targeting ligand. Taking these together (flow cytometry of conjugates 1-12), the folate ligand could successfully be coupled to EGFP and mediated internalization of the EGFP into folic acid receptor positive KB cells. Meanwhile, INF7 in normal pH (7.4) shows an only slightly disruptive ability of cell membrane.

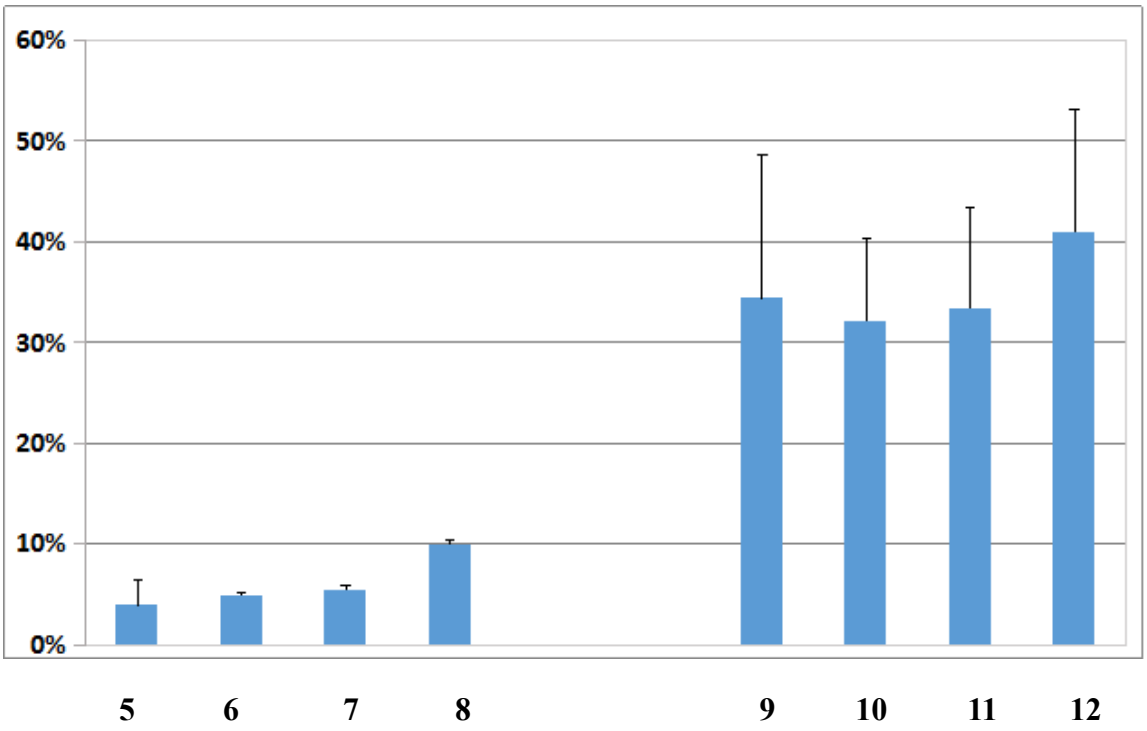

Figure 4.2-4. Cellular internalization of EGFP-INF7 and folate-EGFP-INF7 conjugates measured by flow cytometry. Conjugate 5-8, EGFP-INF7 conjugates, conjugate 9-12, folate-EGFP-INF7 conjugates. Experiments were carried out by Peng Zhang (PhD study, Department of Pharmacy, LMU).

4.2.5 Traceless modification of EGFP conjugate

Since conjugate 4 showed the highest binding and internalization, it was chosen to be further modified with DBCO-PEG_4-Mal-INF7, which results in conjugate 13 (table 1). The shift distance from SDS-PAGE gel indicates the EGFP-AzMMMan (Figure 4.2-5, band 2) was successfully coupled with DBCO-lysine-PEG_{28}-folate (band 3), and then modified by DBCO-PEG_4-Mal-INF7 (conjugate 13, band 4). To investigate the pH-responsive cleavage, conjugate 13 was incubated at neutral or acidic pH and the release of EGFP was monitored by SDS-PAGE (Figure 4.2-5). The gel demonstrated that incubation for 24 hours at pH 5 resulted in significant protein release but not at the point of unmodified EGFP, in

contrast to incubation in PBS buffer at pH 7.4 where almost no cleavage of trait could be observed.

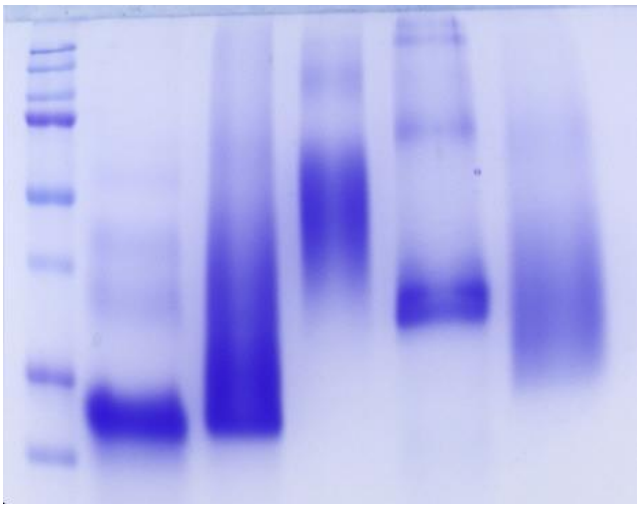

Figure 4.2-5. 1: Mark; 2: EGFP-AM; 3: EGFP-AM-folate; 4: EGFP-AM-folate(INF7) 1:20:5; 5: EGFP-AM-folate(INF7) 1:20:5 incubated in pH 5.0 buffer at 37 ºC for 24 h 6: EGFP-AM-folate(INF7) 1:20:5 incubated in PBS (pH 7,4) buffer at 37 ºC for 24 h.

To find if some irreversible reaction happened between the uncoupled $–NH_2$ group from EGFP-AzMMMan and uncouple -maleimide group from DBCO-PEG_4-Mal with INF7, a higher ratio of INF7 was used to avoid reaction of maleimide group with $-NH_2$ (Figure 4.2-6, band 4), as well as 2-mercaptoethanol was applied to quench the reactive group maleimide group (Figure 4.2-7, band 6) shows similar trend as Figure 4.2-5 (INF7: DBCO-PEG_4-Mal=1:1, band 4). All these demonstrated the high reactive efficiency of click chemistry between DBCO group and $–N_3$ from linker, and no obvious irreversible reaction between $–NH_2$ and maleimide group.

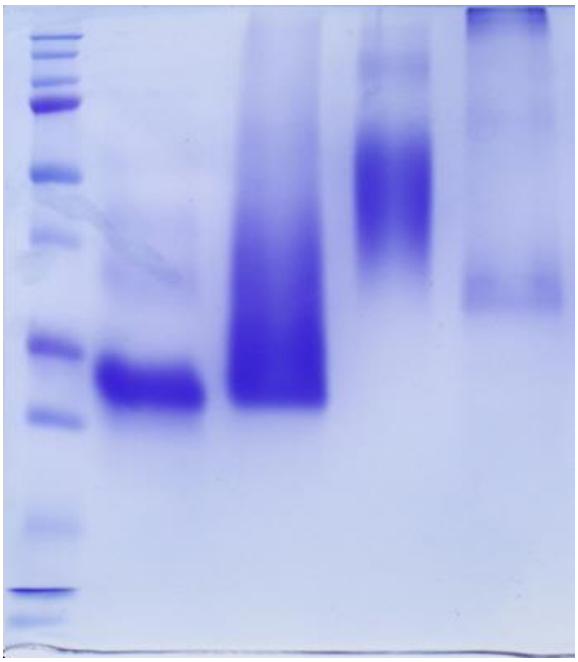

Figure 4.2-6. 1: Mark; 2: EGFP-AM; 3: EGFP-AM: folate-DBCO=1:20 4: EGFP-AM: folate-DBCO:INF7-Mal-PEG$_4$-DBCO=1:20:5, standard steps as usual, except for using 1.1 eq of INF7 to DBCO-PEG$_4$-Mal; 5: EGFP-AzMMMan: folate-DBCO: INF7-Mal-PEG$_4$-DBCO=1:20:5 incubated in pH 5.0 buffer at 37 ^{o}C for 24 h.

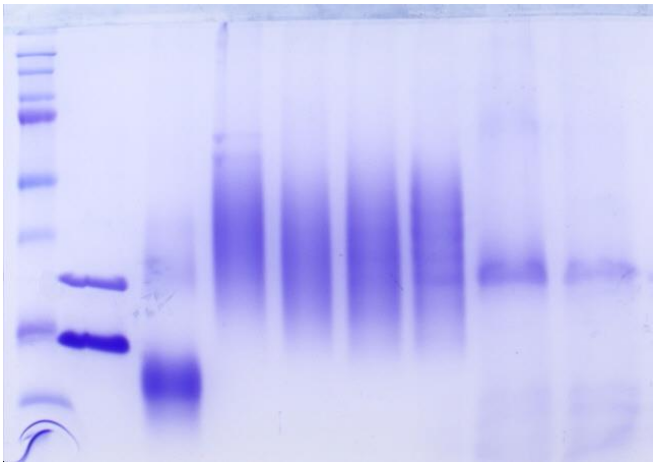

Figure 4.2-7. 1: Mark; 2: EGFP; 3: EGFP-AzMMMan; 4: conjugate EGFP-AM: folate: INF7=1:20:5, standard steps as usual, purified by dialysis (dialysis membrane MWCO 14000); 5: same conjugate as 1, but no purification; 6: conjugate: EGFP-AM: folate: INF7=1:20:5, standard steps as usual, except for after the reaction of INF7 with DBCO-PEG$_4$-Mal, 20eq of 2-mercaptoethanol was added to quench Mal-PEG$_4$-DBCO, and purified by dialysis (dialysis membrane MWCO 14000). 7: same conjugate as 13, but no purification; 8: conjugate 13 incubated in buffer (pH 4.0); 9: conjugate 13 incubated in buffer (pH 4.0).

A mixture of EGFP, DBCO-folate, DBCO-INF7 was prepared, both the mixture

and original EGFP were loaded on the SDS-PAGE (Figure 4.2-8). The gel shows almost no difference. This also indicates AzMMMan linker could bridge the EGFP and DBCO-folate (INF7) by click chemistry with a covalent bond.

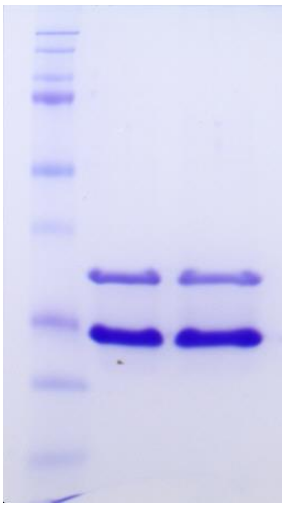

M EGFP Mix

Figure 4.2-8. M, mark; Mix, EGFP mix with folate-DBCO for 1 hour and then mix with DBCO-PEG$_4$-Mal-INF7 for another 3 hours, the same steps as for EGFP-AM-folate (INF7) conjugates.

4.2.6 Intracellular distribution of EGFP

Then conjugate 13 was chosen as a candidate (conjugate 13, EGFP: folate: INF7=1:20:5, Table 1) for visualization of EGFP transduction into cells by fluorescence microscopy (Figure 4.2-9). In an experiment where KB cells were pretreated with free folic acid for 30min and then incubated with the protein conjugate 13, no intracellular transduction could be observed (Column 1, Figure 4.2-9). As a result of pre-incubation with folic acid, the receptor has been blocked and the interaction of conjugate 13 with KB cells could be competitively inhibited. Folic acid receptor negative N2A cells incubated with conjugate 13 also did not

show intracellular fluorescence, since the uptake mechanism is a receptor mediated endocytosis (Column 4, Figure 4.2-9). In contrast, KB cells incubated with conjugate 13 and washed with PBS (pH 4.0) to quench fluorescence of EGFP conjugates attached to the outer cell surface showed significant intracellular EGFP levels (Column 3, Figure 4.2-9). The homogenous distribution EGFP in the whole cells, indicates successful internalization and some kind of endosomal escape of conjugate 13.

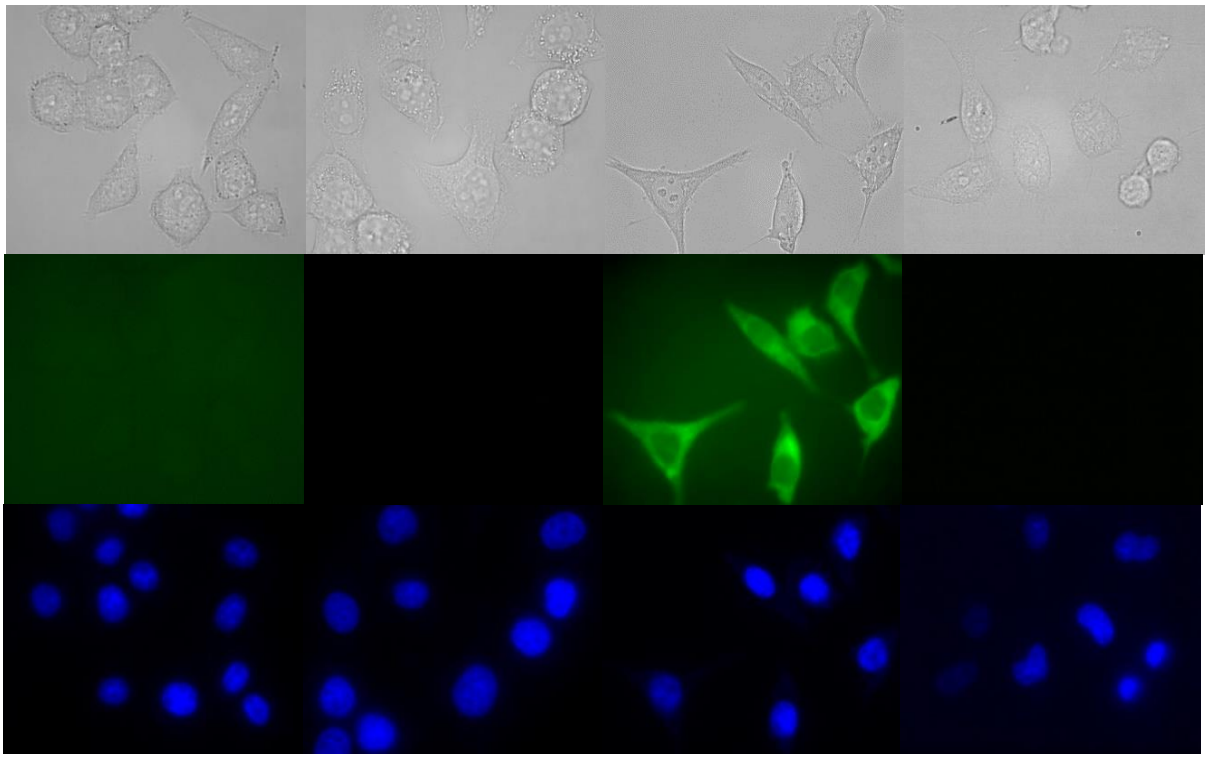

Figure 4.2-9. Microscopy images of cells treated with conjugate 13 (EGFP: folate: INF7=1:20:5) at different conditions. Column 1: KB cell blocked by 100 μM folate for 30min and then incubated with 0.5 μM EGFP conjugate; Column 2: KB cell incubated with 0.5 μM EGFP; Column 3: KB cell incubated with 0.5 μM EGFP conjugate and then incubated by PBS (pH 4) to quench the extracellular fluorescence of EGFP conjugates; Column 4: N2A cells incubated with 0.5 μM EGFP conjugate. Experiments were carried out by Peng Zhang (PhD study, Department of Pharmacy, LMU).

4.3 Traceless bioreversible RNase A conjugates with PEG shielding, folate receptor targeting and endosomal escape domains for intracellular delivery

The chapter has been partly adapted from:

Liu X, Zhang P, Rödl W, Maier K, Lächelt U, Wagner E. Towards artificial immunotoxins: traceless reversible conjugation of RNase A with receptor targeting and endosomal escape domains. Submitted.

In the last section, EGFP covalently modified by folate targeting ligand and INF7 lytic peptide and showed successfully intracellular delivery. Herein, this strategy is applied for the delivery of a cytotoxic protein RNase A for cancer cell killing.

4.3.1 Traceless conjugation strategy

In this work, a multifunctional delivery strategy (Figure 1) to achieve receptor-specific intracellular delivery of antitumoral RNase A is developed, by a pH-responsive traceless and combined functionalization with targeting ligands (folate) and endosomal escape peptides (INF7). The amino group of the targeting ligand reagent (lysine-PEG_{28}-folate) was coupled with succinoyl azadibenzocyclooctyne-N-hydroxysuccinimidyl ester (DBCO-NHS ester) by amidation, and the cysteine thiol group of the endosomolytic INF7 peptide was

conjugated with the maleimide group of DBCO-PEG_4-Mal. Both DBCO coupled functional units were used to react with azidomethyl-methylmaleic anhydride (AzMMMan) modified RNase A protein by strain-promoted azide alkyne cycloaddition.

In the presented delivery strategy, the AzMMMan linker[90] serves two different purposes. First, it should connect the protein and the two functional units, targeting ligand and endosomolytic peptide, by efficient click chemistry to form a soluble single-protein conjugate with cytotoxin-like properties (Figure 4.3-1a); second, after successful folate receptor-mediated cellular internalization, a traceless cleavage of the amide bonds between the AzMMMan-linkers and protein should take place in the acidic endosomal environment, releasing the original RNase A protein from without functional impairment[91]. Facilitated by a pH-triggered endosomal escape activity of released INF7, cytosolic RNA degradation by RNase A is supposed to result in tumor cell killing (Figure 4.3-1b).

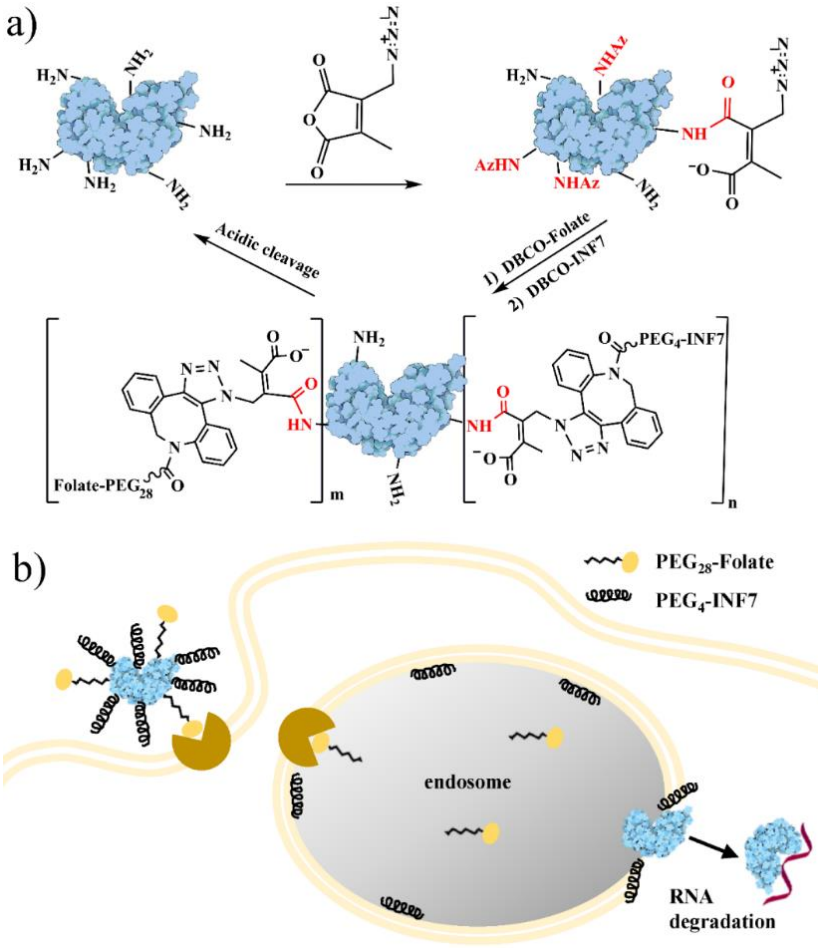

Figure 4.3-1. a) Synthesis of RNase A conjugates by extensive modification with acidic traceless linker AzMMMan ('Az'), followed by copper free click chemistry coupling with the targeting ligand folate and the endosomal disruptive peptide INF7. b) Intracellular delivery of conjugates and traceless release of RNase after endocytosis. The RNase A structure adapted from PDB-101. (D. Goodsell, doi:10.2210/rcsb_pdb/mom_2008_9).

4.3.2 Syntheses of RNase A conjugates

The amino groups of RNase A were reacted with an excessive (8-fold molar) amount of the bifunctional AzMMMan linker, followed by removal of free AzMMMan, as reported in our former work.[97] To quantify the numbers of RNase A amines which reacted with AzMMMan linker, residual free primary amines were determined by a biochemical TNBS assay. According to this assay, at least 9 out of the 11 primary amines of RNase A (10 lysines plus one terminal amino

group)[89] were modified with AzMMMan (Figure 4.3-2).

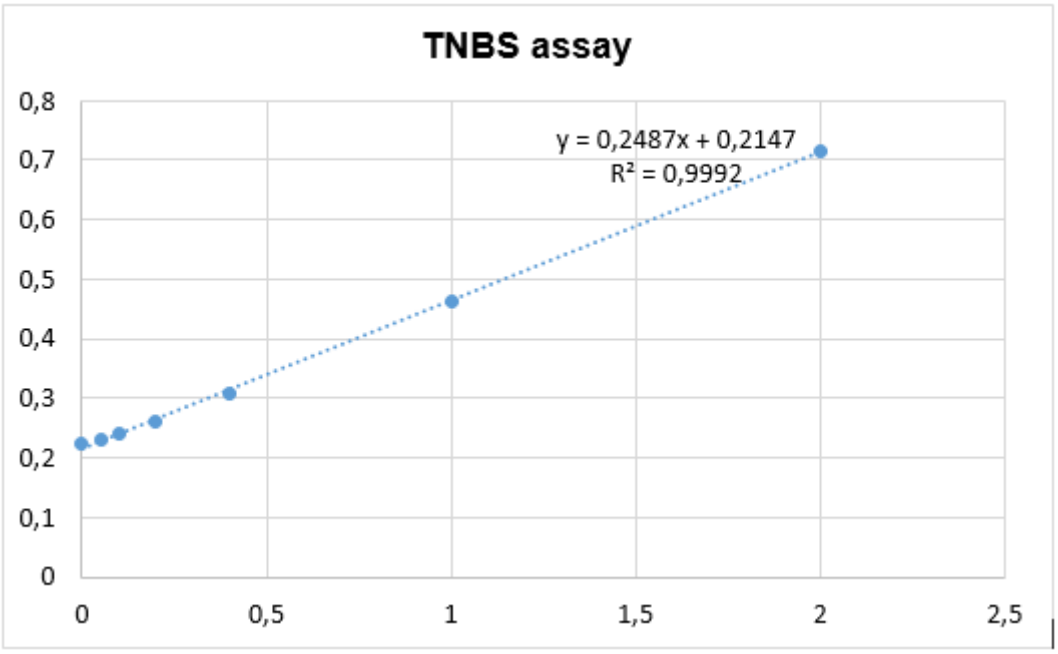

Number of attached AzMMMAn:	11-0,0574/0,0323*11=9,04

Figure 4.3-2. TNBS assay for determination of the number of coupled AzMMMAn linkers.

Next, to study the efficiency of copper free click chemistry, AzMMMan-modified RNase A was reacted with 11 eq of folate-PEG_{28}-lysine-DBCO to generate folate-PEG RNase A conjugate **1**. HPLC was applied to monitor the reaction progress at different time points, by observing the decrease of the folate-PEG_{28}-lysine-DBCO peak (Figure 4.3-3). After 40 min reaction time, 46% of folate-PEG_{28}-lysine-DBCO had coupled with RNase-AzMMMan; after 4 hours, almost 98% folate-PEG_{28}-lysine-DBCO had reacted with RNase A, indicating a high efficiency of RNase A modification with AzMMMan followed by click coupling with DBCO (Figure 4.3-3).

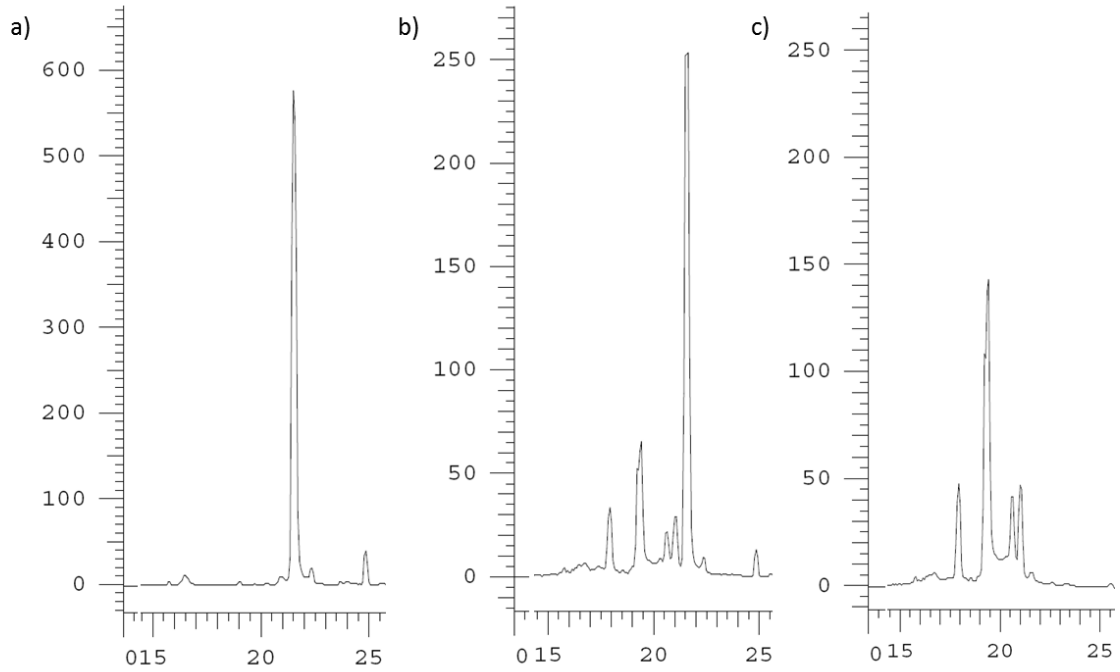

Figure 4.3-3. Reverse Phase HPLC to monitor the reaction process of folate-PEG$_{28}$-lysine-DBCO with RNase A-AzMMMAn to yield conjugate 1 (Waters Xbridge C18 column 5 µm, 4.6 x 150 mm; Hitachi Chromaster 5160 pump module, 5260 auto sampler, 5310 column oven, 5430 diode array detector, detect wavelength 280 nm, 0.1M TEAA buffer / acetonitrile). a) HPLC of folate-PEG$_{28}$-lysine-DBCO; b) HPLC of folate-PEG$_{28}$-lysine-DBCO (11 equivalents) reacted with RNase A-AzMMMAn (one equivalent) for 40 min; c) HPLC of folate-PEG$_{28}$-lysine-DBCO reacted with RNase A-AzMMMAn for 4 hours. Under the latter conditions, folate-PEG$_{28}$-lysine-DBCO without AzMMMan remains unchanged (not shown).

Based on this successful coupling, a series of further RNase A conjugates was synthesized as displayed in Table 2.

Table 2. Synthesized RNase A conjugates.

RNase A conjugate	Molar equivalents of	
	FolA-PEG$_{28}$	INF7-Mal-PEG$_4$
1	11	-
2	3	-
FITC-folate-1	1	-
FITC-folate-3	3	-
3	3	2
4	3	4
5	3	6
6	3	8
7	-	8

4.3.3 Receptor targeting of folate-PEG RNase A conjugates

For cell binding and uptake studies, RNase A was first labeled with FITC and subsequently modified with AzMMMan linker as described above. Afterwards, two different RNase A conjugates (**FITC-folate-1** or **FITC-folate-3**) were generated by copper free click reaction with 1 or 3 equiv of folate-PEG$_{28}$-lysine-DBCO, respectively (Table 2). Flow cytometry was used to evaluate the impact of folate-PEG conjugation on the cellular association (Figure 4.3-4a) and uptake of RNase A (Figure 4.3-5). Folic acid receptor positive KB cells were incubated with the two different RNase A conjugates (2 μM) and FITC-RNase A-AzMMMan (2 μM). In a control experiment, cells were pre-incubated with free folic acid (400 μM) to competitively block receptor interaction.

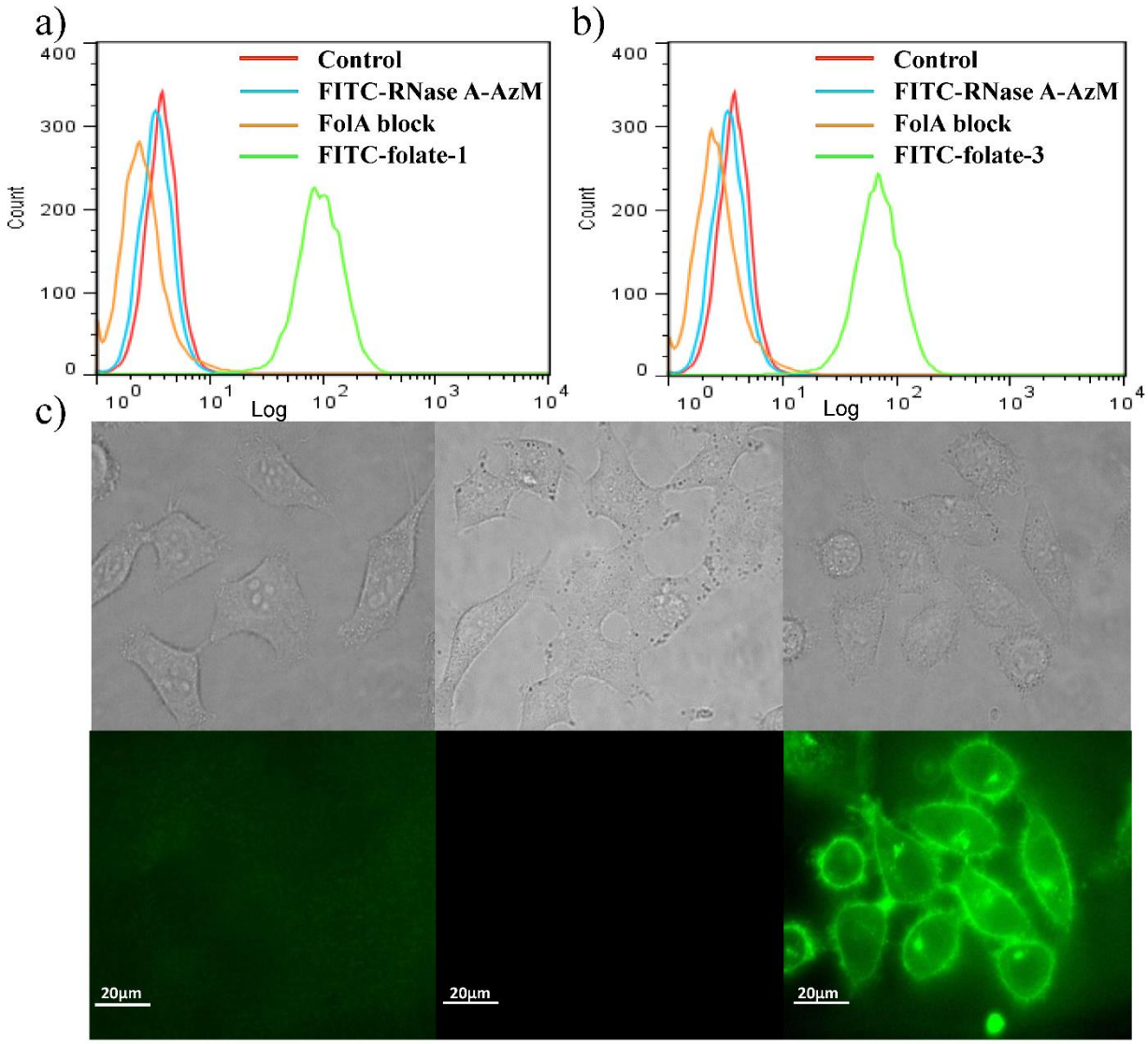

Figure 4.3-4. a) Cellular association of **FITC-folate-1** conjugates. b) Cellular association of **FITC-folate-3** conjugates. Red, blank control without FITC-RNase A conjugates; blue, 2 µM FITC-RNase A-AzMMMan was added; brown, 400 µM free folate block for 30 min on ice before FITC-RNase A-folate conjugates were added; green, 2 µM conjugates. Incubation for 45 min on ice. c) Microscopy images of cells in fresh media (pH 7.4) (Top: Bright-field images of the treated cells; Bottom: FITC fluorescence of the treated cells) treated with RNase A conjugate **FITC-folate-3** at different conditions for 2 h followed by 2 h incubation in fresh medium at 37 °C. *Left*, KB cell incubated with 2 µM FITC-RNase A-AzMMMan; *center*, 400 µM free folate block for 30 min on ice and then incubated with 2 µM RNase A conjugate **FITC-folate-3**; *right*, KB cell incubated with 2 µM RNase A conjugate **FITC-folate-3**. A 63x magnification DIC oil immersion objective was used for image acquisition. Scale bar = 20 µm.Experiments were carried out by Peng Zhang (PhD study, Department of Pharmacy, LMU).

As expected, FITC-RNase A-AzMMMan without conjugated folate ligand could

neither bind to nor be internalized into KB cells, similar to folate-PEG RNase A conjugates after the receptor blockade by free folic acid. In contrast, cells incubated with folate conjugates (**FITC-folate-1** or **FITC-folate-3**) showed distinct fluorescence indicating high cell binding ability. Cellular uptake studies (Figure 4.3-5) gave similar results as the association experiments, though the levels of cellular uptake were lower than cell association. KB cells pretreated with free folic acid did not show uptake of folate-PEG RNase A conjugates. As conjugation of RNase A-AzMMMan with one or three equivalent folate-PEG_{28} did not result in any significant biological difference, all subsequent studies were made with a folate-PEG to RNase A ratio of 3:1.

Fluorescence microscopy of KB cells incubated with **FITC-folate-3** conjugate for 2 hours at 37 ^{o}C followed by medium change and further 2 hours incubation (Figure 4.3-4b) confirmed intracellular uptake of RNase A conjugate **FITC-folate-3**. Cells treated with FITC-RNase A-AzMMMAn control, or cells pretreated with free folic acid for receptor blockade before incubation with FITC-folate-3 did not display intracellular delivery (Figure 4.3-4b).

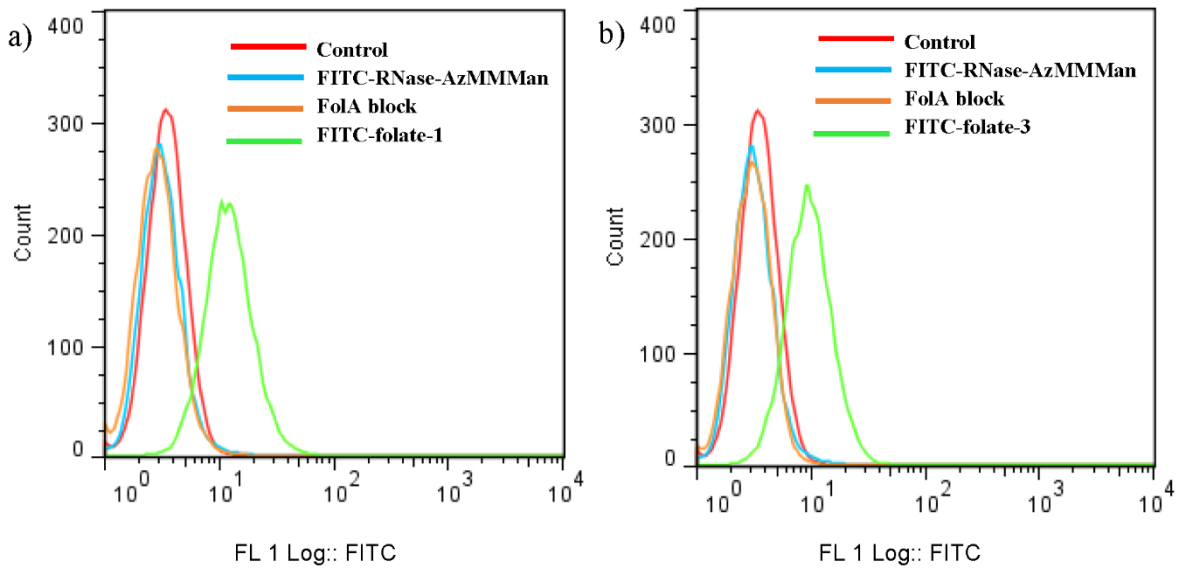

Figure 4.3-5. Cellular internalization of FITC-RNase A-folate conjugates. Red, blank control without FITC-RNase A-folate conjugates; blue, 2 µM FITC-RNase A-AzMMMan was added; brown, free folate block for 30 min on ice before FITC-RNase A-folate conjugates were added; green, 2 µM conjugates. Incubation for 45 min at 37 °C. a) RNase A conjugate FITC-folate-1. b) RNase A conjugate FITC-folate-3. Experiments were carried out by Peng Zhang (PhD study, Department of Pharmacy, LMU).

4.3.4 INF7 conjugates and traceless release of RNase A

Next, four RNase A conjugates **3** to **6** containing both targeting folate-PEG_{28} and the endosomolytic INF7-PEG_4 were synthesized, and two control conjugates, the corresponding folate-PEG_{28} RNase A conjugate **2**, and INF7-PEG_4 RNase A conjugate **7** (Table 2). SDS-PAGE of conjugates is displayed in Figure 4.3-6a. Gel migrations are different from unmodified RNase A but similar to AzMMMan-modified RNase A (Figure 4.3-6d). The different conjugates **2** to **6** show the same gel migration, which probably is attributed to the same content of hydrophilic PEG_{28} chains; conjugate **7** lacking PEG_{28} chains but containing anionic, amphiphilic INF7 displays slightly more migration. For full enzymatic activity of RNase A, the removal of the chemical modifications is necessary. Our former

work demonstrated that RNase A modified with an irreversible SMCC linker or with the reversible AzMMMan linker but without acid treatment had insignificant activity. The RNase A activity of AzMMMan-modified protein however could be recovered by incubation in acidic buffer.[97] To verify whether the AzMMMan-based RNase A conjugation is also a reversible process for the current folate-PEG INF7 RNase A conjugates under the mild acidic conditions of endosomes, we incubated conjugates **3** to **6** in pH 6.0 buffer for 24 hours at 37 °C. The comparison of the SDS PAGE profile of conjugates (Figure 4.3-6a) with pH 6.0 treated conjugates (Figure 4.3-6b) clearly demonstrates the release of RNase A from conjugates. To further demonstrate that the release of the RNase A from the conjugate is a traceless process, MALDI-TOF MS of conjugate **6** after acidic incubation (pH 6.0, 24 hours at 37°C) was performed and the mass peak of free RNase A was detectable, in contrast to the conjugate without acidic treatment (Supporting Figure 4.3-6e). SDS-PAGE of RNase A incubated with PBS and acidic buffer (pH 6.0) did not show any alteration (Figure 4.3-6c), which indicates the stability of RNase A under the treatment conditions.

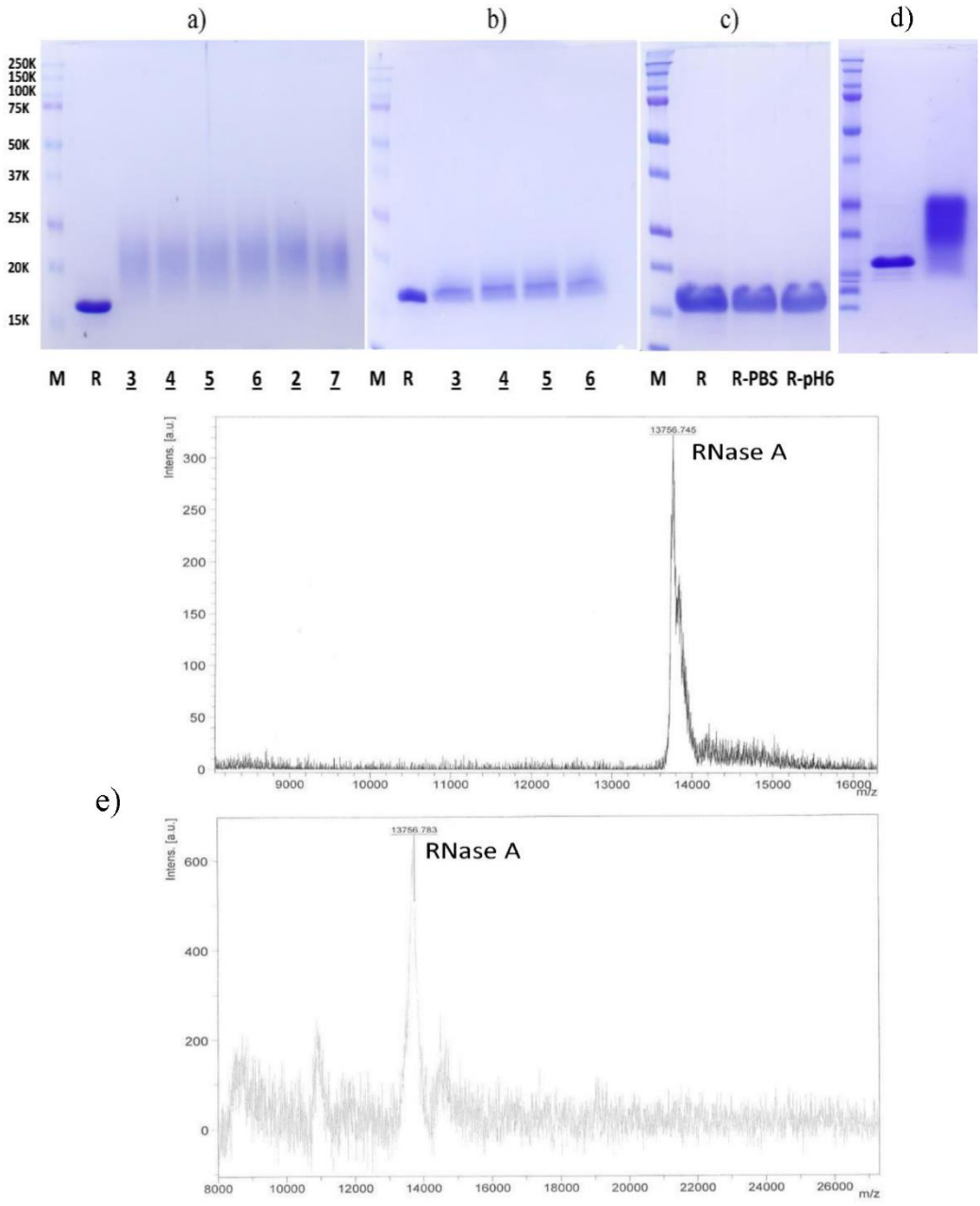

Figure 4.3-6. SDS-PAGE of (a) RNase A conjugates and (b) acidic cleavage of RNase A conjugates after incubation for 24 hours at 37 ºC in acidic pH 6.0 buffer. M, marker protein ladder; R, RNase A control; 3 to 6, folate-PEG_{28} INF7-PEG_4 RNase A conjugates; 2, folate-PEG_{28} RNase conjugate; 7, INF7-PEG_4 RNase A conjugate. (c) R-PBS, RNase A incubation for 24 hours at 37 ºC in PBS (pH 7.4); R-pH6, RNase A incubation for 24 hours at 37 ºC in acidic pH 6.0 buffer. (d) SDS-PAGE of RNase A (middle) and RNase A-AzMMMan (right). 10 µg RNase A samples were loaded in each lane. (e) MALDI-TOF MS of conjugate 6 after acidic cleavage. Above: Fresh RNase A (13756.75). Under these conditions, conjugate 6 did not show any measurable mass peak. Below: After acidic cleavage (conjugate 6 pre-incubated in pH=6.0 buffer for 24 hours at 37 °C), RNase A was found (13756.78).

4.3.5 RNase A conjugates activity at various pH values

The enzymatic activity of RNase A and its conjugate incubated under various pH values were monitored using an ethidium bromide (EtBr) fluorescence assay (Figure 4.3-7). The fluorescence intensity of solutions containing 0.5 ng EtBr and 20 μg RNA in 1 mL of PBS (pH = 7.4) was first monitored during an equilibration time of 5 min. Then RNase A samples were added, and decrease of fluorescence intensity was monitored for another 5 min. The enzymatic activity was the same when RNase A was incubated in PBS (pH 7.4) or acidic buffer (pH 6.0) as compared to fresh RNase A, indicating the stability of RNase after incubation under different conditions. Fresh RNase A conjugates without incubation and RNase A conjugates incubated in PBS (pH 7.4) for 24 hours show the same low bioactivity. Apparently the release of free bioactive RNase from RNase A conjugates is negligible when treated at pH 7.4. In contrast, when RNase A conjugate was incubated in acidic buffer (pH 6.0), the EtBr fluorescence shows significant decrease, which implies that RNase A was released from the conjugate and regained its bioactivity.

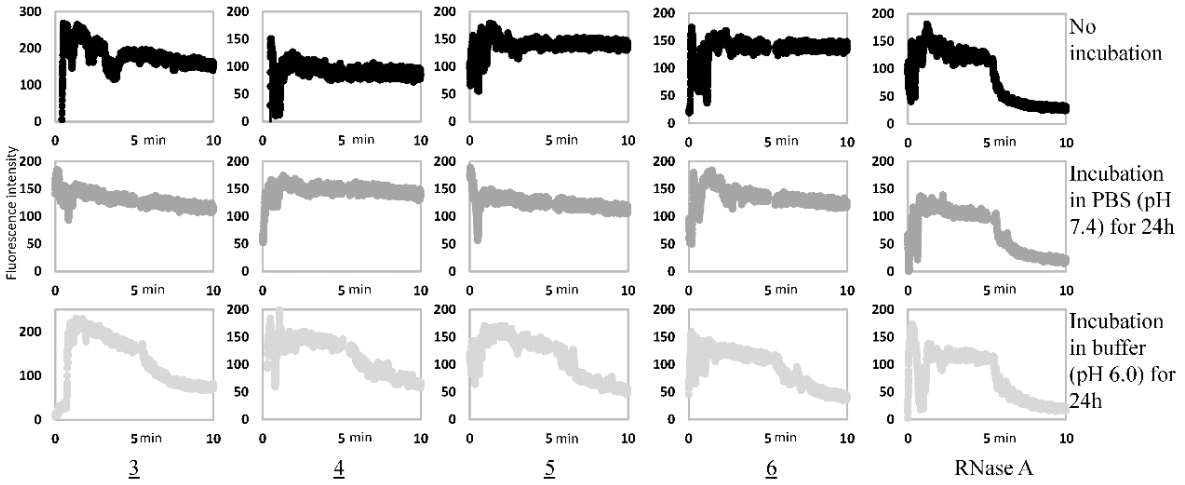

Figure 4.3-7. Enzymatic activity of RNase A conjugates (**3**, **4**, **5**, **6**) and RNase A measured by an ethidium bromide assay. First row, fresh RNase A conjugates and RNase A without pre-incubation. Second row, RNase A conjugates and RNase A after pre-incubation in PBS at 37 °C for 24 hours. Third row, RNase A conjugates and RNase A after pre-incubation in acidic buffer (pH 6.0) at 37 °C for 24 hours. The first five minutes represent the incubation of RNA with EtBr; after five minutes, RNase A samples were added and the decay of RNA-based EtBr fluorescence was measured for five minutes.

4.3.6 RNase A conjugates with pH-dependent lytic activity

INF7 is a negatively charged amphiphilic peptide derived from the N-terminus of the influenza virus hemagglutinin HA 2 subunit; due to sequence variations with glutamic acids it has endosomal pH-specific lytic activity.[109-110, 123] To evaluate the lytic activity of the INF7 containing RNase A conjugates, an erythrocyte leakage assay (Figure 4) was performed. Different concentrations (1 μM, 2 μM, 4 μM) of unmodified RNase A and its conjugates **2** to **6** were incubated with human erythrocytes at various pH conditions (pH 7.4, 6.5, and 5.5), and the degree of hemoglobin release was measured (Figure 4). No significant lytic activity was found for RNase A and folate conjugate **2**. For INF7 containing RNase A

conjugates **3** to **6**, concentration and pH-dependent lytic activities were found, which were highest at pH 5.5, consistent with the known pH-specific leakage profile of unmodified INF7.[109-110, 123] Taking conjugate **3** at the lowest tested 1 μM concentration as an example, the percentage of release hemoglobin was 87% at pH 5.5 compared to 19% at pH 7.4 and 73% at pH 6.5. Conjugates **4** to **6** also showed a similar trend. Not surprisingly, conjugate **6** with highest degree of INF7 conjugation also revealed the highest lytic activity amongst all conjugates. The same concentration of free INF7 and INF7-PEG as contained within conjugate 6 performed a higher lytic ability in comparison with the conjugate (Figure 4.3-8). This might be explained by a higher steric hindrance within the conjugate, reducing the lytic ability of INF7. The AzMMMan-triggered endosomal acidic cleavage from the conjugate would result in favorably increased INF7 activity in the endosome.

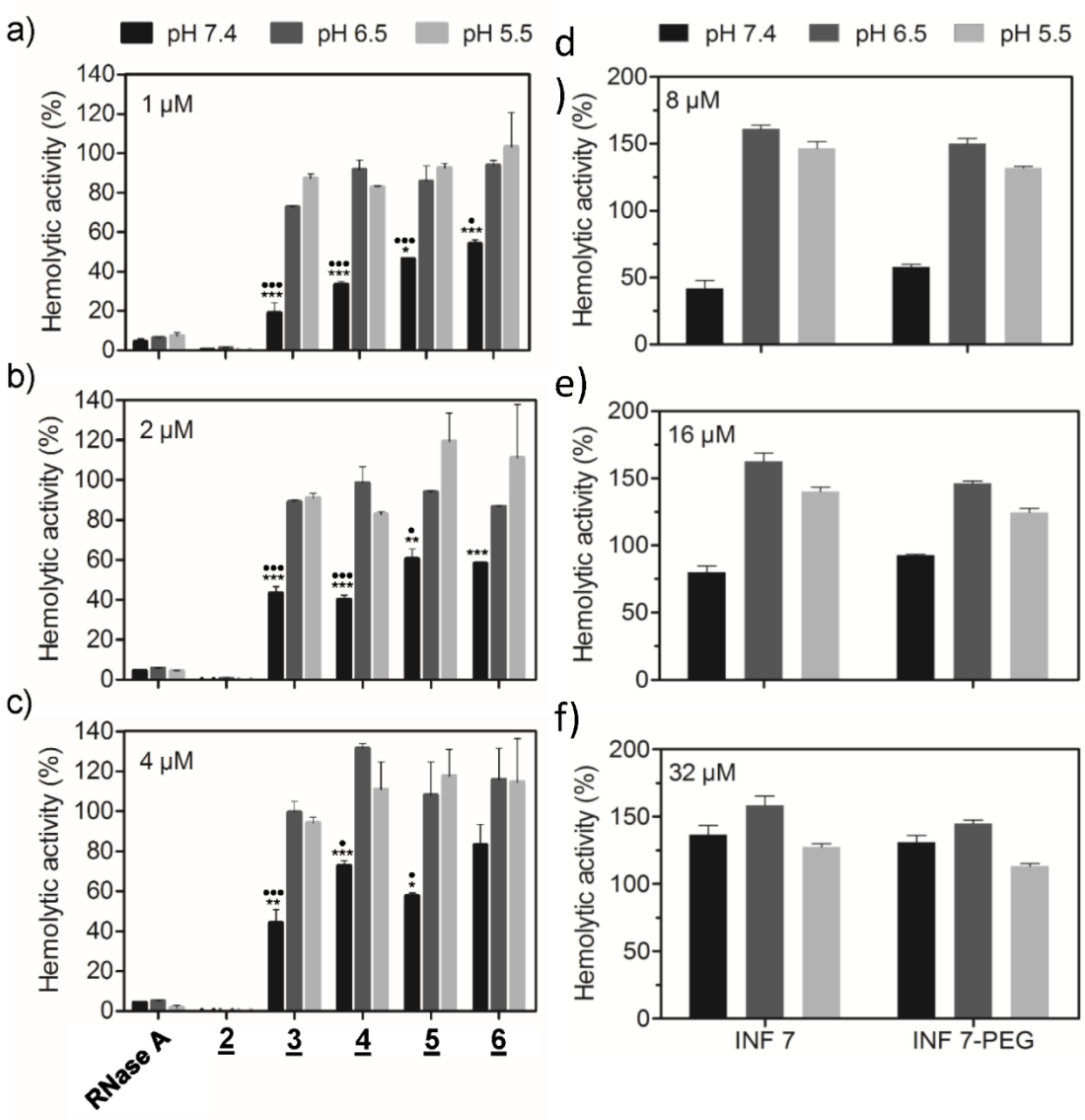

Figure 4.3-8. Leakage activity of INF7 measured by erythrocytes leakage assay. a),b),c) RNase A, RNase A-PEG-folate conjugate 2, and RNase A-PEG-folate-INF7 conjugates 3 to 6; were incubated at indicated concentrations with erythrocytes at indicated pH values. d),e),f) INF7 and INF7-PEG was tested at various concentrations corresponding to the amounts of INF7 using conjugate **6**, **7**. *: compared with pH 6.5; •: compared with pH 5.5. *$p < 0.05$, **$p < 0.01$, ***$p < 0.001$, •$p < 0.05$, •••$p < 0.001$. Experiments d), e), f) were carried out by Peng Zhang (PhD study, Department of Pharmacy, LMU).

4.3.7 Cytotoxicity of RNase A conjugates

In the following, to assess the intracellular transduction and cytotoxicity of the RNase A conjugates, cell viability assays (MTT) were performed. The remaining

biological activity of KB tumor cells after treatment with various concentrations of RNase A conjugates was analyzed after 48 hours (Figure 4.3-9a). Cells treated with RNase A conjugate **7** (INF7-modified only) did not display any significant reduction in cell viability, similarly as free RNase A[43 91]. Conjugate **7** is most likely not sufficiently internalized for successful transduction. Also conjugate **2** (folate-modified only) and conjugate **3** (with the lowest degree of INF7 incorporation) showed an only ~40% reduced metabolic cell viability at the highest dose. The slightly higher potency of these conjugates over **7** can be attributed to the efficient folate receptor mediated cellular uptake, however insufficient endosomal escape (no or insufficient INF7) apparently hampers the cytotoxic activity. RNase A conjugates **4** to **6** showed the desired high cytotoxicity (Figure 4.3-9a) correlating with the degree of INF7-modification and RNase A conjugate concentration. For each conjugate, KB cells treated with 8 μM exhibited the lowest cell viabilities, 7% vs. 2% vs. 1% for conjugates **4** to **6**, respectively. Based on the intracellular delivery analyzed for the RNase A-FITC-folate conjugates (Figure 4.3-4a) and the leakage assays (Figure 4.3-8), it is hypothesize that the RNase A conjugates with the same degree of PEG-folate modification undergo a similar intracellular uptake. However, after endocytosis, the endosome-disruptive ability of INF7 in a pH- and concentration-dependent manner (compare Figure 4.3-8), would well explain why conjugate **6** with highest INF7 content and lytic activity also exhibits the strongest tumor cell killing effect.

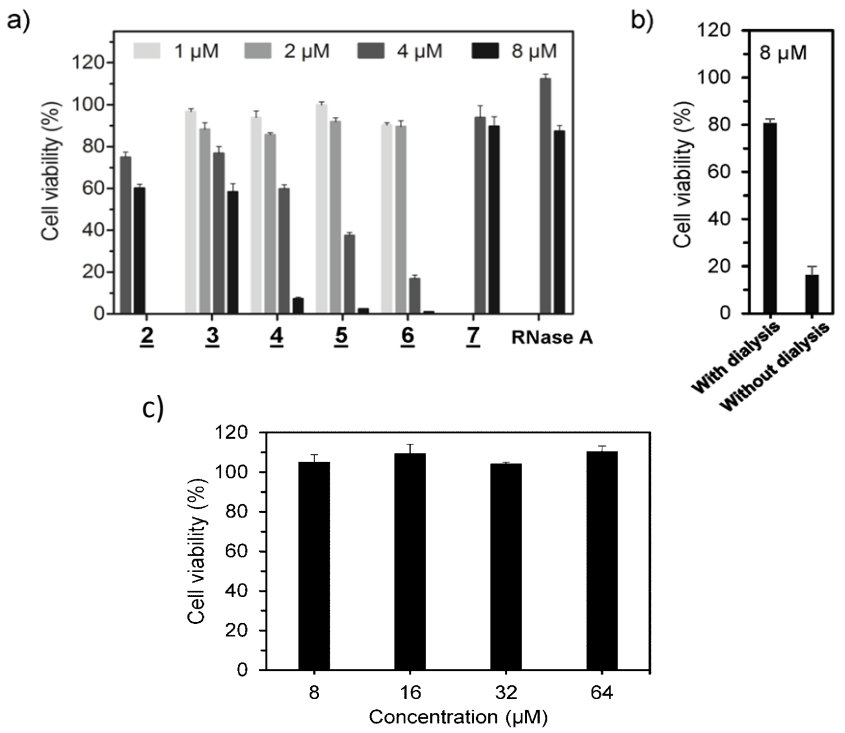

Figure 4.3-9. Cytotoxic potency of RNase A conjugates and free INF7. a) Viability of KB cells (MTT) after treatment with RNase A-PEG-folate conjugate **2**, RNase A-PEG-folate-INF7 conjugates **3** to **6**, or RNase A-PEG-INF7 conjugate **7** at different concentrations for 48 hours. b) A noncovalent mixture of conjugate **2** with 8 equiv of INF7 was prepared and tested in KB cell killing with or without dialysis against PBS buffer (for removal of INF7). c) KB cells treated with indicated concentrations of free INF7. Experiments were carried out by Peng Zhang (PhD study, Department of Pharmacy, LMU).

To evaluate whether free INF7 may enhance the cytotoxic activity of the folate-RNase A conjugate **2**, the conjugate was mixed with 8 equivalents of INF7. As shown in Figure 4.3-9b, this resulted in significantly enhanced cytotoxicity (16% metabolic activity as compared with 60% for **2**) at the 8 µM high RNase A concentration, however by far not as high as for the corresponding covalent INF7 conjugate **6**. Free INF 7 is a small amphipathic peptide which has been found to bind to the surface of lipid membranes at pH 7.4 without lytic insertion, and thus may be simultaneously internalized with the protein conjugate and promote endosomal escape, though less effectively as via AzMMMan linkage.

Furthermore, dialyzing the **2**/INF7 mixture according due the standard conjugate purification process, which should remove non-bound INF7, abolished most of the cytotoxic activity (Figure 4.3-9b). Meanwhile, INF7 and RNase A alone did not trigger any significant cytotoxicity (Figure 4.3-9c, a).

5 DISCUSSION

5.1 Histidine rich-cationic modified RNase A conjugates for enhanced cellular delivery and tumor cell killing

Intracellularly-acting therapeutic proteins are considered promising alternatives for the treatment of various diseases. Major limitations of their application are low efficiency of intracellular delivery and possible reduction of protein activity during derivatization. Herein, a pH reversible linker AzMMMan was first applied to modify with nlsEGFP, a moderate size protein which could be revealed as a standard example for delivery of other kinds of protein, and RNase A, a cytotoxicity protein to degrade the RNA in the cytosol then result in the death of the RNase A intracellular cells. Successful AzMMMan modification of EGFP could be confirmed by UV spectroscopy, since AzMMMan and EGFP-AzMMMan have an intensive absorbance around 240 nm comparing to non-modified EGFP (Figure 4.1-4). The sequence-defined oligoamino amides 689 and 386 were synthesized by solid phase synthesis, and the three contained cysteines were modified with DBCO-PEG_4-Maleimide. The DBCO coupled oligomer were then used to modify with AzMMMan linker-proteins by strain promoted azide alkyne cycloaddition.

Different ratios of oligomers (386, 689) to protein conjugates were synthesized, SDS-PAGE of the conjugates shows a gradual shift of the protein band toward

lower migration distance with increasing 689/386 to protein ratio (Figure 4.1-5), demonstrated the high reactive efficiency of the click chemistry between –N3 from modified protein and DBCO from oligomer. Meanwhile, fluorescence correlation spectroscopy (FCS) also indicates the different coupled ratios by detecting hydrodynamic radii of fluorescent molecules, higher ratios oligomer modified EGFP shows larger hydrodynamic radii (Figure 4.1-6).

Then flow cytometry was used to test the intracellular efficiency of EGFP conjugates modified by a series ratios of oligomer 689 (Figure 4.1.7). Uptake of content EGFP conjugate is increasing with the modified degree of oligomer , which could explained by higher intracellular efficiency because of higher protonatable ability with more oligomer conjugation. And a comparison study between the two similar cationic oligomers 386 and 689 has been carried out. Oligomer 386 is also a three-arm cationic STP-based oligomer, having been successfully used for siRNA, DNA, and protein delivery before, but 689 additionally contains histidines after each STP unit to enhance endosomal buffering. The flow cytometry results show 386 and 689 oligomer modified EGFP being internalized into cells to comparable extent (Figure 4.1.7). In the extracellular environment, the pH is about 7.4, and the additional histidines in 689 are not protonated. Therefore, these two oligomers mediate similar uptake of modified EGFP. The visible of various ratios of oligomer modified nls EGFP was detected by florescence microscopy, all degrees of oligomer modified nlsEGFP reveals successfully intracellular (Figure 4.1-10), though at the ratio of 16

oligomer to EGFP has very high intracellular efficiency, but only optimization ratios of oligomer to nlsEGFP shows some extend of nuclei delivery (Figure 4.1-9). This highlights the importance of modification degree when designing a covalent carrier for $–NH_2$ rich protein.

Then RNase A conjugates treated at different pH values and then performed by SDS-PAGE demonstrated the high stable ability of the conjugate when incubated at extracellular pH 7.4, but traceless cleavage when incubated in acidic buffer pH 5 (Figure 4.1-11). This is very important for designing a protein vector, first, to form a stable formation between the protein and delivery units in extracellular environment has always been a main aim for protein therapeutics, and many electrostatic method is not strong enough for this application. Second, when the protein formation arrives in the target place, the formation should release protein content without any dysfunction of the protein, thus requires the stable formation of the first step is a reversible process, which means could be traceless release of functional protein. Ethidium bromide assay was performed to test the enzymatic activity of RNase A and its conjugates also verify the same result as SDS-PAGE gel (Figure 4.1-12). The RNase A conjugates connected by AzMMMan linker incubated in alkaline buffer shows very low activity, due to the unsuccessful release of RNase A in high pH values, also similar trend when RNase A modified with an irreversible linker SMCC (Figure 4.1-13). Meanwhile, when RNase A conjugates bridged by AzMMMan linker incubated in acidic buffer, RNase A shows regain its enzymatic activity because of the covalent bond traceless

breakage between RNase A and AzMMMan.

To verify that the covalently modified therapeutic protein can be successfully delivered into the cytoplasm and then perform its enzymatic lytic activity for traceless release of RNase A, cell viability assays (MTT) were performed with the two series of oligomer (689 and 386) modified RNase A to investigate the biological activity and effect on tumor cell viability after 48 h treatment (Figure 4.1-14, Figure 4.1-15). For the same series of oligomer (689 or 386) modified RNase A conjugate at the same concentration, the toxicity increased with the degree of conjugation (386/689: RNase A=0.75, 1.5, 3, 6), which means higher degree oligomer performed higher intracellular ability, and thus result in higher cytotoxicity. From the perspective of oligomer structure, 689 modified RNase A conjugates exhibit higher activity than 386 modified RNase A conjugates, this could be explained by 689 equipping with one more histidine after each STP than 386, histidine could be protonatable in endosomal environment, enhancing endosomal escape efficiency and resulting in higher cytotoxicity. The cytotoxicity of RNase A conjugates modified by oligomer 689 is increasing with the treated concentrations, which could be explained by a dose independence of the therapeutics RNase A.

5.2 Traceless reversible conjugation of proteins with receptor targeting and endosomal escape domains

Multifunctional single-protein conjugates as a novel cytotoxin-like intracellular transduction platform were investigated, utilizing receptor-mediated internalization, pH-dependent lytic activity and intracellular release of functional proteins into the cytosol. The chemical strategy to assemble the multifunctional protein conjugates is based on the pH-labile bifunctional AzMMMan linker, which provides a connectivity between the protein cargo and functional units with pH-dependent cleavage.

EGFP performs as a visible protein modified with DBCO-folate and DBCO-INF7, DBCO-folate exhibits targeting function units to the receptor of KB cells and DBCO-INF7 works as endosomal escape to make EGFP release into the cytoplasm, binding and uptake of EGFP conjugates show correlation with degree of coupled folate, and show successful intracellular delivery (Figure 4.2-9), but no obvious nuclear delivery was observed. Possible reason could be the nuclear localization signal (NLS) was also modified and the traceless efficiency was not enough, because EGFP contains 27 amino groups, it requires time and acidic environment to break these modified $–NH_2$ groups.

RNase A was used as the bioactive component which was intended to degrade cytosolic RNA and induce cell death after intracellular delivery.[104] In contrast to nanoparticle-based cationic polymer based delivery systems which can cover

several delivery steps at once, however at the expense of generally less defined nanoparticulate charged complexes, here - similar to natural protein toxins comprising separate subunits for specific purposes - an artificial small protein conjugate containing different defined components was assembled. RNase A was covalently modified with a PEG-folate targeting unit and an endosomal disruptive peptide INF7 unit at different ratios based on the pH-labile AzMMMan linker and copper free click chemistry. The efficiencies of the separate modification steps, amidation and subsequent click reaction, were evaluated by the quantification of free amines after AzMMMan modification by TNBS assay (Figure 4.3-2) and monitoring the depletion of free folate-PEG_{28}-lysine-DBCO during click reaction by RP-HPLC (Figure 4.3-3). According to the results, both steps showed high efficiency with at least 9 out of 11 AzMMMan modified primary amines and almost 98 % conversion of a stoichiometric amount of folate-PEG_{28}-lysine-DBCO after 4 h. The biological effect of each functional unit of the RNase A conjugates was assessed in separate experimental settings. Flow cytometry and fluorescence microscopy with FITC-labeled RNase A variants demonstrated that binding and uptake of RNase A-folate conjugates depended on PEG-folate attachment and pre-incubation with free folate could block the cellular interactions which both confirmed the receptor specificity of the conjugates (Figure 4.3-4, Figure 4.3-5). The biological effect of additional INF7 functionalization was assessed in an erythrocyte leakage assay (Figure 4.3-8) as model for pH-dependent membrane disturbing and potential endosomolytic activity after cellular uptake. The

concentration and pH-dependent lytic activities of INF7 containing RNase A conjugates confirmed the potency of the endosomolytic component for the intended purpose. INF7 within the conjugate showed a significant but lower lytic activity as compared to the unmodified INF7, presumably due to a higher steric hindrance when protein-bound. Consistent with the requirement to overcome both critical limitations, cellular uptake and endosomal escape, for RNase A triggered cell death, only conjugates modified with both PEG-folate ligand and INF7 peptide showed killing of KB tumor cells, with a clear correlation of endosomolytic INF7 content and cytotoxic antitumoral activity. The results of the separate evaluations confirm the functionality and requirement of each of the units which are assembled to the multifunctional RNase A conjugate complexes. Importantly, the traceless AzMMMan linker strategy which provides programmed connectivity for the functional units, also ensures recovery of the enzymatic activity after acidic exposition, which could not be guaranteed in case of irreversible modification techniques.[97] The use of pH-sensitive INF7 as the endosomolytic entity is an additional dynamic element, which changes its properties in a changing environment. These kinds of bioresponsive dynamics are required to fulfill the specific tasks within the intracellular delivery pathway of biomacromolecules efficiently and therefore are also inherent part of several natural delivery complexes, e.g. protein toxins or viruses. Analog to the highly specific natural counterparts, in the design of these artificial immunotoxins, the sequential function and activation of subunits (folate for receptor-specific binding

extracellularly, activation of INF7 in endosomes, reactivation of RNase A after acidic exposition intracellularly) is intended to balance the opposing factors of high cytotoxic activity and safety. Taking all together, this work suggests that a synthetic traceless reversible conjugation of therapeutic cargo proteins such as RNase A with cytotoxin-like delivery domains for receptor targeting and endosomal escape might be an effective delivery strategy for intracellularly acting antitumoral proteins. For further translation toward in vivo administration in animal tumor models or even clinics, a series of aspects have to be considered with great care. Firstly, the residual lytic activity of the pH -sensitive peptide INF7 observed in the standard erythrocyte leakage assay requires attention. The assays however were performed under artificial serum-free conditions, which are not predictable for the in vivo conditions in blood. Secondly, the pharmacokinetic properties with regard to tumor targeting will strongly depend on the size and surface of the formulation[115 124 125]. Small soluble protein conjugates probably strongly differ from commonly used nanoparticle formulations, with regard to accessibility of tumors from the systemic circulation and better intratumoral distribution on the one hand, and the increased kidney clearance and reduced circulation-time of the small soluble protein conjugates on the other hand. Size and density of the PEG shielding domain and proper targeting ligands will be important factors for optimization.

6 SUMMARY

The specific transport of bioactive proteins into designated target cells is an interesting and challenging perspective for the generation of innovative biopharmaceuticals. In this thesis two strategies were applied for intratumoral delivery of proteins followed by traceless intracellular release in bioactive form.

In the first part, covalent protein conjugates based on pH sensitive components were developed as intracellular delivery platform. Cationic three-arm oligoamino amide oligomer 386 or its histidinylated analog 689 were conjugated with proteins (EGFP or RNase A) at different molar ratios using the pH-labile AzMMMan linker and copper-free click chemistry. Fluorescence correlation spectroscopy measurements of 689-EGFP conjugates revealed that the formation of crosslinked protein clusters strongly depends on the conjugation degree. The conjugation degree had also effects both on the amount of protein conjugate taken up by cells and the extent of nuclear delivery after endosomal escape. All four kinds of cationic oligomer modified EGFP (689: EGFP = 2, 4, 8, 16) have efficient internalization capability, but only EGFP conjugates (689: EGFP = 4, 8) showed nuclear delivery. Furthermore, therapeutic protein RNase A conjugates were investigated as cancer cell killing agents. The cationic oligomer 689 modified RNase A showed pH dependent bioactive release in in vitro experiments and high ability to kill cancer cells. Consistent with the known higher endosomal escape

efficacy due to incorporated histidine residues, conjugates of 689 demonstrated higher delivery efficacy than 386 conjugates. Taking together, this study suggests that fine-tuning of pH reversible conjugation of therapeutic proteins with potent intracellular transfection oligomers opens a new window for future medical applications.

The second and third part reports multifunctional single-protein conjugates as a novel cytotoxin-like intracellular transduction platform, utilizing receptor-mediated internalization, pH-dependent lytic activity and intracellular release of functional proteins into the cytosol. RNase A was covalently modified with a PEG-folate targeting unit and an endosomal disruptive peptide INF7 unit at different ratios based on the pH-labile AzMMMan linker and copper free click chemistry. TNBS assays and HPLC showed RNase A successfully coupling with AzMMMan and then modification with DBCO-folate/INF7, flow cytometry demonstrated the intracellular uptake of RNase A-folate conjugates. Only RNase A conjugates modified with both PEG-folate ligand and INF7 peptide showed effective killing of KB tumor cells (by MTT assay), with a clear correlation of degree of INF7 incorporation and cytotoxic antitumoral activity. Taking all together, this work suggests that a synthetic traceless reversible conjugation of a therapeutic cargo protein (RNase A) with cytotoxin-like delivery domains for receptor targeting and endosomal escape can be an effective delivery platform for protein therapeutics.

7 ABBREVIATIONS

μM: Micromolar

μmol: Micromole

ACN: Acetonitrile

AzMMMan: 3-(Azidomethyl)-4-methyl-2, 5-furandione

BCA: Bicinchoninic acid assay

BrMMMan: 3-(bromomethyl)-4-methyl-2, 5-furandione

BOC: Tert-butoxycarbonyl

Boc_2O: Di-tert-butyl dicarbonate

BSA: Bovine serum albumin

cm: centimeter

CPP: Cell-penetrating peptide

Da: Dalton

DBU: 1,8-diazabicyc [5.4.0] undec-7-ene

DBCO: Azadibenzylcyclooctyne

DCM: Dichloromethane

DCVC: Dry column vacuum chromatography

DMF: Dimethylformamide

DMSO: Dimethyl sulfoxide

DNA: Deoxyribonucleic acid

DIPEA: N,N-diisopropylethylamine

DODT: 3,6-dioxa-1,8-octanedithiol

EDTA: Ethylenediamine tetraacetic acid

Et_2O: Diethyl ether

FBS: Fetal bovine serum

EGFP: Enhanced Green fluorescent protein

FDA: Food and Drug Administration

FITC: Fluorescein isothiocyanate

Fmoc: Fluorenylmethyloxycarbonyl

FR: Folic acid receptor

g: Gram

Hepps, 4-(2-hydroxyethyl)-1-piperazinepropanesulfonic acid

HOBt: 1-Hydroxy-benzotriazole

HPLC, high performance liquid chromatography

INF7: Influenza hemagglutinin HA-2 terminal peptide derivative 7

IPTG: Isopropyl-β-D-thiogalactopyran oside

IU: International Units

mg: Milligramm

mL: Milliliter

mM: Millimolar

mmol: Millimole

Mal: Maleimide

MeOH: Methanol

MTT: 1-(4,5-Dimethylthiazol-2-yl)-3,5-diphenylformazan

NHS: N-Hydroxysuccinimide

nm: nanometer

NLS: Nuclear localization signal

nlsEGFP: Nuclear localization signal tagged EGFP

kDa: kilo Dalton

PAGE: Poly Acrylamide Gel Electrophoresis

PBS: Phosphate buffered saline

PD-1: Programmed cell death protein 1

PEG: Poly(ethylene glycol)

pH: Potentia Hydrogenii

PTD: Protein-transduction domain

RNA: Ribonucleic acid

RNase A: Ribonuclease A

SA: Streptavidin

SDS: Sodium dodecyl sulfate

SEC: Size exclusion chromatography

SMCC: N-Succinimidyl 4-(maleimidomethyl)cyclohexanecarboxylate

SPAAC: Strain-promoted alkyne-azide cycloaddition

Stp: Succinoyl-tetraethylenpentamine

SWNT: Single-walled carbon nanotube TCEP: Tris(2-carboxyethyl) phosphine

TEPA: Tetraethylenepentamine

TFA: Trifluoroacetic acid

THF: Tetrahydrofuran

TIS: Triisopropylsilane

TLC: Thin layer chromatography

TNBS: 2,4,6-Trinitrobenzenesulfonic

Tris: Tris(hydroxymethyl)aminomethane

TSE: Transmissible spongiform encephalopathies

UV: Ultraviolett

Vis: Visible

8 PUBLICATIONS

Original papers

Liu X, Zhang P, He D, Rödl W, Preiß T, Rädler JO, Wagner E, Lächelt U. *pH-Reversible Cationic RNase A Conjugates for Enhanced Cellular Delivery and Tumor Cell Killing.* Biomacromolecules. 2016 Jan 11;17(1):173-82. doi: 10.1021/acs.biomac.5b01289.

Liu X, Zhang P, Rödl W, Maier K, Lächelt U, Wagner E. *Towards artificial immunotoxins: traceless reversible conjugation of RNase A with receptor targeting and endosomal escape domains.* Submitted.

Zhang P, He D., Klein P, **Liu X**., Röder R, Döblinger M, Wagner E. *Enhanced Intracellular Protein Transduction by Sequence Defined Tetra-Oleoyl Oligoaminoamides Targeted for Cancer Therapy.* Adv. Funct. Materials. 2015 Nov 11; 25:6627–6636. DOI: 10.1002/adfm.201503152

9 REFERENCES

1. Watson, J. D.; Crick, F. H., Molecular structure of nucleic acids. *Nature* **1953,** *171* (4356), 737-738.
2. Watson, J. D.; Crick, F. H., Genetical implications of the structure of deoxyribonucleic acid. *Journal of the American Medical Association* **1993,** *269* (15), 1967-1969.
3. Goffeau, A.; Barrell, B. G.; Bussey, H.; Davis, R., Life with 6000 genes. *Science* **1996,** *274* (5287), 546.
4. Leader, B.; Baca, Q. J.; Golan, D. E., Protein therapeutics: a summary and pharmacological classification. *Nature Reviews Drug Discovery* **2008,** *7* (1), 21-39.
5. Litchfield, D. W., Protein kinase CK2: structure, regulation and role in cellular decisions of life and death. *Biochemical Journal* **2003,** *369* (1), 1-15.
6. Dunker, A. K.; Brown, C. J.; Lawson, J. D.; Iakoucheva, L. M.; Obradovic, Z., Intrinsic disorder and protein function. *Biochemistry* **2002,** *41* (21), 6573-6582.
7. Karplus, M.; Kuriyan, J., Molecular dynamics and protein function. *Proceedings of the National Academy of Sciences of the United States of America* **2005,** *102* (19), 6679-6685.
8. Peri, S.; Navarro, J. D.; Amanchy, R.; Kristiansen, T. Z.; Jonnalagadda, C. K.; Surendranath, V.; Niranjan, V.; Muthusamy, B.; Gandhi, T.; Gronborg, M., Development of human protein reference database as an initial platform for approaching systems biology in humans. *Genome Research* **2003,** *13* (10), 2363-2371.
9. Kim, M.-S.; Pinto, S. M.; Getnet, D.; Nirujogi, R. S.; Manda, S. S.; Chaerkady, R.; Madugundu, A. K.; Kelkar, D. S.; Isserlin, R.; Jain, S., A draft map of the human proteome. *Nature* **2014,** *509* (7502), 575-581.
10. Wilhelm, M.; Schlegl, J.; Hahne, H.; Gholami, A. M.; Lieberenz, M.; Savitski, M. M.; Ziegler, E.; Butzmann, L.; Gessulat, S.; Marx, H., Mass-spectrometry-based draft of the human proteome. *Nature* **2014,** *509* (7502), 582-587.
11. Bairoch, A.; Apweiler, R., The SWISS-PROT protein sequence database and its supplement TrEMBL in 2000. *Nucleic Acids Research* **2000,** *28* (1), 45-48.
12. Wang, S.; Kaufman, R. J., The impact of the unfolded protein response on human disease. *The Journal of Cell Biology* **2012,** *197* (7), 857-867.
13. Peri, S.; Navarro, J. D.; Kristiansen, T. Z.; Amanchy, R.; Surendranath, V.; Muthusamy, B.; Gandhi, T.; Chandrika, K.; Deshpande, N.; Suresh, S., Human protein reference database as a discovery resource for proteomics. *Nucleic Ccids Research* **2004,** *32* (suppl 1), D497-D501.
14. Prasad, T. K.; Goel, R.; Kandasamy, K.; Keerthikumar, S.; Kumar, S.; Mathivanan, S.; Telikicherla, D.; Raju, R.; Shafreen, B.; Venugopal, A., Human protein reference database—2009 update. *Nucleic Acids Research* **2009,** *37* (suppl 1), D767-D772.
15. He, C.; Tang, Z.; Tian, H.; Chen, X., Co-delivery of chemotherapeutics and proteins for synergistic therapy. *Advanced Drug Delivery Reviews* **2016,** *98*, 64-76.
16. Woodcock, J.; Griffin, J.; Behrman, R.; Cherney, B.; Crescenzi, T.; Fraser, B.; Hixon, D.; Joneckis, C.; Kozlowski, S.; Rosenberg, A., The FDA's assessment of follow-on protein products: a historical perspective. *Nature Reviews Drug Discovery* **2007,** *6* (6), 437-442.
17. Clark, A. L.; Knight, G.; Wiles, P.; Keen, H.; Ward, J.; Cauldwell, J.; Adeniyi-Jones, R.; Leiper, J.; Jones, R.; Maccuish, A., Biosynthetic human insulin in the treatment of diabetes: a double-blind crossover trial in established diabetic patients. *The Lancet* **1982,** *320* (8294), 354-357.
18. Dreyer, M.; Prager, R.; Robinson, A.; Busch, K.; Ellis, G.; Souhami, E.; Van Leendert, R., Efficacy and safety of insulin glulisine in patients with type 1 diabetes. *Hormone and Metabolic Research* **2005,** *37* (11), 702-707.

19. Soran, H.; Younis, N., Insulin detemir: a new basal insulin analogue. *Diabetes, Obesity and Metabolism* **2006,** *8* (1), 26-30.

20. Keen, H.; Pickup, J.; Bilous, R.; Glynne, A.; Viberti, G.; Jarrett, R.; Marsden, R., Human insulin produced by recombinant DNA technology: safety and hypoglycaemic potency in healthy men. *The Lancet* **1980,** *316* (8191), 398-401.

21. Abildgaard, C. F.; Simone, J. V.; Corrigan, J. J.; Seeler, R. A.; Edelstein, G.; Vanderheiden, J.; Schulman, I., Treatment of hemophilia with glycine-precipitated Factor VIII. *New England Journal of Medicine* **1966,** *275* (9), 471-475.

22. Bray, G.; Gomperts, E.; Courter, S.; Gruppo, R.; Gordon, E.; Manco-Johnson, M.; Shapiro, A.; Scheibel, E.; Lee, M., A multicenter study of recombinant factor VIII (recombinate): safety, efficacy, and inhibitor risk in previously untreated patients with hemophilia A. The Recombinate Study Group. *Blood* **1994,** *83* (9), 2428-2435.

23. White, G.; Courter, S.; Bray, G.; Lee, M.; Gomperts, E., A multicenter study of recombinant factor VIII (RecombinateTM) in previously treated patients with hemophilia A. *Haemophilia* **1997,** *3* (3), 232-232.

24. Evans, R. W.; Rader, B.; Manninen, D. L., The quality of life of hemodialysis recipients treated with recombinant human erythropoietin. *Journal of the American Medical Association* **1990,** *263* (6), 825-830.

25. Levin, N. W.; Lazarus, J. M.; Nissenson, A. R.; Group, N. C. r. E. S., National cooperative rHu erythropoietin study in patients with chronic renal failure—an interim report. *American Journal of Kidney Diseases* **1993,** *22* (2), 3-12.

26. Corwin, H. L.; Gettinger, A.; Pearl, R. G.; Fink, M. P.; Levy, M. M.; Shapiro, M. J.; Corwin, M. J.; Colton, T.; Group, E. C. C. T., Efficacy of recombinant human erythropoietin in critically ill patients: a randomized controlled trial. *Journal of the American Medical Association* **2002,** *288* (22), 2827-2835.

27. Holle, L. M., Pegaspargase: an alternative? *Annals of Pharmacotherapy* **1997,** *31* (5), 616-624.

28. Clavell, L. A.; Gelber, R. D.; Cohen, H. J.; Hitchcock-Bryan, S.; Cassady, J. R.; Tarbell, N. J.; Blattner, S. R.; Tantravahi, R.; Leavitt, P.; Sallan, S. E., Four-agent induction and intensive asparaginase therapy for treatment of childhood acute lymphoblastic leukemia. *New England Journal of Medicine* **1986,** *315* (11), 657-663.

29. Keane, J.; Gershon, S.; Wise, R. P.; Mirabile-Levens, E.; Kasznica, J.; Schwieterman, W. D.; Siegel, J. N.; Braun, M. M., Tuberculosis associated with infliximab, a tumor necrosis factor α–neutralizing agent. *New England Journal of Medicine* **2001,** *345* (15), 1098-1104.

30. Klareskog, L.; van der Heijde, D.; de Jager, J. P.; Gough, A.; Kalden, J.; Malaise, M.; Mola, E. M.; Pavelka, K.; Sany, J.; Settas, L., Therapeutic effect of the combination of etanercept and methotrexate compared with each treatment alone in patients with rheumatoid arthritis: double-blind randomised controlled trial. *The Lancet* **2004,** *363* (9410), 675-681.

31. Marchesoni, A.; Zaccara, E.; Gorla, R.; Bazzani, C.; Sarzi‐Puttini, P.; Atzeni, F.; Caporali, R.; Bobbio‐Pallavicini, F.; Favalli, E. G., TNF‐α Antagonist Survival Rate in a Cohort of Rheumatoid Arthritis Patients Observed under Conditions of Standard Clinical Practice. *Annals of the New York Academy of Sciences* **2009,** *1173* (1), 837-846.

32. Topalian, S. L.; Hodi, F. S.; Brahmer, J. R.; Gettinger, S. N.; Smith, D. C.; McDermott, D. F.; Powderly, J. D.; Carvajal, R. D.; Sosman, J. A.; Atkins, M. B., Safety, activity, and immune correlates of anti–PD-1 antibody in cancer. *New England Journal of Medicine* **2012,** *366* (26), 2443-2454.

33. Hamid, O.; Robert, C.; Daud, A.; Hodi, F. S.; Hwu, W.-J.; Kefford, R.; Wolchok, J. D.; Hersey, P.; Joseph, R. W.; Weber, J. S., Safety and tumor responses with lambrolizumab (anti–PD-1) in melanoma. *New England Journal of Medicine* **2013,** *369* (2), 134-144.

34. Rizvi, N. A.; Mazières, J.; Planchard, D.; Stinchcombe, T. E.; Dy, G. K.; Antonia, S. J.; Horn, L.; Lena, H.; Minenza, E.; Mennecier, B., Activity and safety of nivolumab, an anti-PD-1 immune checkpoint inhibitor, for

patients with advanced, refractory squamous non-small-cell lung cancer (CheckMate 063): a phase 2, single-arm trial. *The Lancet Oncology* **2015,** *16* (3), 257-265.

35. Mason, H. S.; Warzecha, H.; Mor, T.; Arntzen, C. J., Edible plant vaccines: applications for prophylactic and therapeutic molecular medicine. *Trends in Molecular Medicine* **2002,** *8* (7), 324-329.

36. Perrin, Y.; Vaquero, C.; Gerrard, I.; Sack, M.; Drossard, J.; Stöger, E.; Christou, P.; Fischer, R., Transgenic pea seeds as bioreactors for the production of a single-chain Fv fragment (scFV) antibody used in cancer diagnosis and therapy. *Molecular Breeding* **2000,** *6* (4), 345-352.

37. Giddings, G.; Allison, G.; Brooks, D.; Carter, A., Transgenic plants as factories for biopharmaceuticals. *Nature Biotechnology* **2000,** *18* (11), 1151-1155.

38. Tarczynski, M. C.; Jensen, R. G.; Bohnert, H. J., Stress protection of transgenic tobacco by production of the osmolyte mannitol. *Science* **1993,** *259*, 508-508.

39. D'Astolfo, D. S.; Pagliero, R. J.; Pras, A.; Karthaus, W. R.; Clevers, H.; Prasad, V.; Lebbink, R. J.; Rehmann, H.; Geijsen, N., Efficient intracellular delivery of native proteins. *Cell* **2015,** *161* (3), 674-690.

40. Erazo-Oliveras, A.; Najjar, K.; Dayani, L.; Wang, T.-Y.; Johnson, G. A.; Pellois, J.-P., Protein delivery into live cells by incubation with an endosomolytic agent. *Nature Methods* **2014,** *11* (8), 861-867.

41. Lu, Y.; Sun, W.; Gu, Z., Stimuli-responsive nanomaterials for therapeutic protein delivery. *Journal of Controlled Release* **2014,** *194*, 1-19.

42. Wu, J.; Kamaly, N.; Shi, J.; Zhao, L.; Xiao, Z.; Hollett, G.; John, R.; Ray, S.; Xu, X.; Zhang, X., Development of multinuclear polymeric nanoparticles as robust protein nanocarriers. *Angewandte Chemie International Edition* **2014,** *53* (34), 8975-8979.

43. Zhang, P.; He, D.; Klein, P. M.; Liu, X.; Röder, R.; Döblinger, M.; Wagner, E., Enhanced Intracellular Protein Transduction by Sequence Defined Tetra‐Oleoyl Oligoaminoamides Targeted for Cancer Therapy. *Advanced Functional Materials* **2015,** *25* (42), 6627-6636.

44. Vermonden, T.; Censi, R.; Hennink, W. E., Hydrogels for protein delivery. *Chemical Reviews* **2012,** *112* (5), 2853-2888.

45. Yan, M.; Du, J.; Gu, Z.; Liang, M.; Hu, Y.; Zhang, W.; Priceman, S.; Wu, L.; Zhou, Z. H.; Liu, Z., A novel intracellular protein delivery platform based on single-protein nanocapsules. *Nature Nanotechnology* **2010,** *5* (1), 48-53.

46. Liguori, L.; Marques, B.; Villegas-Mendez, A.; Rothe, R.; Lenormand, J.-L., Liposomes-mediated delivery of pro-apoptotic therapeutic membrane proteins. *Journal of Controlled Release* **2008,** *126* (3), 217-227.

47. Chatin, B.; Mével, M.; Devallière, J.; Dallet, L.; Haudebourg, T.; Peuziat, P.; Colombani, T.; Berchel, M.; Lambert, O.; Edelman, A., Liposome-based formulation for intracellular delivery of functional proteins. *Molecular Therapy—Nucleic Acids* **2015,** *4* (6), e244.

48. Jo, J.; Hong, S.; Choi, W. Y.; Lee, D. R., Cell-penetrating peptide (CPP)-conjugated proteins is an efficient tool for manipulation of human mesenchymal stromal cells. *Scientific Reports* **2014,** *4*.

49. Lindgren, M.; Hällbrink, M.; Prochiantz, A.; Langel, Ü., Cell-penetrating peptides. *Trends in Pharmacological Sciences* **2000,** *21* (3), 99-103.

50. Schwarze, S. R.; Ho, A.; Vocero-Akbani, A.; Dowdy, S. F., In vivo protein transduction: delivery of a biologically active protein into the mouse. *Science* **1999,** *285* (5433), 1569-1572.

51. Nagahara, H.; Vocero-Akbani, A. M.; Snyder, E. L.; Ho, A.; Latham, D. G.; Lissy, N. A.; Becker-Hapak, M.; Ezhevsky, S. A.; Dowdy, S. F., Transduction of full-length TAT fusion proteins into mammalian cells: TAT-p27Kip1 induces cell migration. *Nature Medicine* **1998,** *4* (12), 1449-1452.

52. Green, M.; Loewenstein, P. M., Autonomous functional domains of chemically synthesized human immunodeficiency virus tat trans-activator protein. *Cell* **1988,** *55* (6), 1179-1188.

53. Lee, Y.; Ishii, T.; Kim, H. J.; Nishiyama, N.; Hayakawa, Y.; Itaka, K.; Kataoka, K., Efficient delivery of bioactive antibodies into the cytoplasm of living cells by charge‐conversional polyion complex micelles. *Angewandte Chemie International Edition* **2010,** *49* (14), 2552-2555.

54. Kim, A.; Miura, Y.; Ishii, T.; Mutaf, O. F.; Nishiyama, N.; Cabral, H.; Kataoka, K., Intracellular Delivery of Charge-Converted Monoclonal Antibodies by Combinatorial Design of Block/Homo Polyion Complex Micelles. *Biomacromolecules* **2016,** *17* (2), 446-453.

55. Shaji, J.; Patole, V., Protein and peptide drug delivery: oral approaches. *Indian Journal of Pharmaceutical Sciences* **2008**.

56. Shah, R. B.; Ahsan, F.; Khan, M. A., Oral delivery of proteins: progress and prognostication. *Critical Reviews™ in Therapeutic Drug Carrier Systems* **2002,** *19* (2).

57. Mahato, R. I.; Narang, A. S.; Thoma, L.; Miller, D. D., Emerging trends in oral delivery of peptide and protein drugs. *Critical Reviews™ in Therapeutic Drug Carrier Systems* **2003,** *20* (2&3).

58. Hamman, J. H.; Enslin, G. M.; Kotzé, A. F., Oral delivery of peptide drugs. *BioDrugs* **2005,** *19* (3), 165-177.

59. Morishita, M.; Peppas, N. A., Is the oral route possible for peptide and protein drug delivery? *Drug Discovery Today* **2006,** *11* (19), 905-910.

60. Renukuntla, J.; Vadlapudi, A. D.; Patel, A.; Boddu, S. H.; Mitra, A. K., Approaches for enhancing oral bioavailability of peptides and proteins. *International Journal of Pharmaceutics* **2013,** *447* (1), 75-93.

61. Mitragotri, S.; Burke, P. A.; Langer, R., Overcoming the challenges in administering biopharmaceuticals: formulation and delivery strategies. *Nature Reviews Drug Discovery* **2014,** *13* (9), 655-672.

62. Privalov, P. L., Stability of proteins small globular proteins. *Advances in Protein Chemistry* **1979,** *33*, 167-241.

63. Keppler, A.; Gendreizig, S.; Gronemeyer, T.; Pick, H.; Vogel, H.; Johnsson, K., A general method for the covalent labeling of fusion proteins with small molecules in vivo. *Nature Biotechnology* **2003,** *21* (1), 86-89.

64. Tjelle, T. E.; Brech, A.; Juvet, L. K.; Griffiths, G.; Berg, T., Isolation and characterization of early endosomes, late endosomes and terminal lysosomes: their role in protein degradation. *Journal of Cell Science* **1996,** *109* (12), 2905-2914.

65. Poteryaev, D.; Datta, S.; Ackema, K.; Zerial, M.; Spang, A., Identification of the switch in early-to-late endosome transition. *Cell* **2010,** *141* (3), 497-508.

66. Varkouhi, A. K.; Scholte, M.; Storm, G.; Haisma, H. J., Endosomal escape pathways for delivery of biologicals. *Journal of Controlled Release* **2011,** *151* (3), 220-228.

67. Mayol, L.; Biondi, M.; Quaglia, F.; Fusco, S.; Borzacchiello, A.; Ambrosio, L.; La Rotonda, M. I., Injectable thermally responsive mucoadhesive gel for sustained protein delivery. *Biomacromolecules* **2010,** *12* (1), 28-33.

68. Zentner, G. M.; Rathi, R.; Shih, C.; McRea, J. C.; Seo, M.-H.; Oh, H.; Rhee, B.; Mestecky, J.; Moldoveanu, Z.; Morgan, M., Biodegradable block copolymers for delivery of proteins and water-insoluble drugs. *Journal of Controlled Release* **2001,** *72* (1), 203-215.

69. Azagarsamy, M. A.; Anseth, K. S., Wavelength‐Controlled Photocleavage for the Orthogonal and Sequential Release of Multiple Proteins. *Angewandte Chemie International Edition* **2013,** *52* (51), 13803-13807.

70. Petersen, S.; Alonso, J. M.; Specht, A.; Duodu, P.; Goeldner, M.; del Campo, A., Phototriggering of cell adhesion by caged cyclic RGD peptides. *Angewandte Chemie International Edition* **2008,** *47* (17), 3192-3195.

71. Wang, M.; Alberti, K.; Sun, S.; Arellano, C. L.; Xu, Q., Combinatorially Designed Lipid‐like Nanoparticles for Intracellular Delivery of Cytotoxic Protein for Cancer Therapy. *Angewandte Chemie* **2014,** *126* (11), 2937-2942.

72. Wang, M.; Sun, S.; Neufeld, C. I.; Perez‐Ramirez, B.; Xu, Q., Reactive Oxygen Species‐Responsive Protein Modification and Its Intracellular Delivery for Targeted Cancer Therapy. *Angewandte Chemie* **2014,** *126* (49), 13662-13666.

73. Lee, J. S.; Feijen, J., Polymersomes for drug delivery: design, formation and characterization. *Journal of Controlled Release* **2012,** *161* (2), 473-483.

74. Kam, N. W. S.; Liu, Z.; Dai, H., Carbon nanotubes as intracellular transporters for proteins and DNA: an investigation of the uptake mechanism and pathway. *Angewandte Chemie* **2006,** *118* (4), 591-595.

75. Chen, R. J.; Zhang, Y.; Wang, D.; Dai, H., Noncovalent sidewall functionalization of single-walled carbon nanotubes for protein immobilization. *Journal of the American Chemical Society* **2001,** *123* (16), 3838-3839.

76. Chithrani, B. D.; Chan, W. C., Elucidating the mechanism of cellular uptake and removal of protein-coated gold nanoparticles of different sizes and shapes. *Nano Letters* **2007,** *7* (6), 1542-1550.

77. Bhumkar, D. R.; Joshi, H. M.; Sastry, M.; Pokharkar, V. B., Chitosan reduced gold nanoparticles as novel carriers for transmucosal delivery of insulin. *Pharmaceutical Research* **2007,** *24* (8), 1415-1426.

78. Slowing, I. I.; Trewyn, B. G.; Lin, V. S.-Y., Mesoporous silica nanoparticles for intracellular delivery of membrane-impermeable proteins. *Journal of the American Chemical Society* **2007,** *129* (28), 8845-8849.

79. Park, H. S.; Kim, C. W.; Lee, H. J.; Choi, J. H.; Lee, S. G.; Yun, Y.-P.; Kwon, I. C.; Lee, S. J.; Jeong, S. Y.; Lee, S. C., A mesoporous silica nanoparticle with charge-convertible pore walls for efficient intracellular protein delivery. *Nanotechnology* **2010,** *21* (22), 225101.

80. Chen, Q.; Wang, C.; Cheng, L.; He, W.; Cheng, Z.; Liu, Z., Protein modified upconversion nanoparticles for imaging-guided combined photothermal and photodynamic therapy. *Biomaterials* **2014,** *35* (9), 2915-2923.

81. Richard, J. P.; Melikov, K.; Vives, E.; Ramos, C.; Verbeure, B.; Gait, M. J.; Chernomordik, L. V.; Lebleu, B., Cell-penetrating peptides A reevaluation of the mechanism of cellular uptake. *Journal of Biological Chemistry* **2003,** *278* (1), 585-590.

82. Deshayes, S.; Morris, M.; Divita, G.; Heitz, F., Cell-penetrating peptides: tools for intracellular delivery of therapeutics. *Cellular and Molecular Life Sciences* **2005,** *62* (16), 1839-1849.

83. Nischan, N.; Herce, H. D.; Natale, F.; Bohlke, N.; Budisa, N.; Cardoso, M. C.; Hackenberger, C. P., Covalent attachment of cyclic TAT peptides to GFP results in protein delivery into live cells with immediate bioavailability. *Angewandte Chemie International Edition* **2015,** *54* (6), 1950-1953.

84. Thompson, D. B.; Villaseñor, R.; Dorr, B. M.; Zerial, M.; Liu, D. R., Cellular uptake mechanisms and endosomal trafficking of supercharged proteins. *Chemistry & Biology* **2012,** *19* (7), 831-843.

85. Pesce, D.; Wu, Y.; Kolbe, A.; Weil, T.; Herrmann, A., Enhancing cellular uptake of GFP via unfolded supercharged protein tags. *Biomaterials* **2013,** *34* (17), 4360-4367.

86. Solaro, R.; Chiellini, F.; Battisti, A., Targeted delivery of protein drugs by nanocarriers. *Materials* **2010,** *3* (3), 1928-1980.

87. Kos, P.; Lächelt, U.; Herrmann, A.; Mickler, F. M.; Döblinger, M.; He, D.; Levačić, A. K.; Morys, S.; Bräuchle, C.; Wagner, E., Histidine-rich stabilized polyplexes for cMet-directed tumor-targeted gene transfer. *Nanoscale* **2015,** *7* (12), 5350-5362.

88. Zhang, G.; Gurtu, V.; Kain, S. R., An enhanced green fluorescent protein allows sensitive detection of gene transfer in mammalian cells. *Biochemical and Biophysical Research Communications* **1996,** *227* (3), 707-711.

89. Raines, R. T., Ribonuclease a. *Chemical Reviews* **1998,** *98* (3), 1045-1066.

90. Maier, K.; Wagner, E., Acid-labile traceless click linker for protein transduction. *Journal of the American Chemical Society* **2012,** *134* (24), 10169-10173.

91. Liu, X.; Zhang, P.; He, D.; Rödl, W.; Preiß, T.; Rädler, J. O.; Wagner, E.; Lächelt, U., pH-reversible

cationic RNase A conjugates for enhanced cellular delivery and tumor cell killing. *Biomacromolecules* **2015,** *17* (1), 173-182.

92. Montecucco, C., Protein toxins and membrane transport. *Current Opinion in Cell Biology* **1998,** *10* (4), 530-536.

93. Sandvig, K.; van Deurs, B., Delivery into cells: lessons learned from plant and bacterial toxins. *Gene Therapy* **2005,** *12* (11), 865-872.

94. Johannes, L.; Decaudin, D., Protein toxins: intracellular trafficking for targeted therapy. *Gene Therapy* **2005,** *12* (18), 1360-1368.

95. Wernick, N. L.; Chinnapen, D. J.-F.; Cho, J. A.; Lencer, W. I., Cholera toxin: an intracellular journey into the cytosol by way of the endoplasmic reticulum. *Toxins* **2010,** *2* (3), 310-325.

96. Oh, K. J.; Senzel, L.; Collier, R. J.; Finkelstein, A., Translocation of the catalytic domain of diphtheria toxin across planar phospholipid bilayers by its own T domain. *Proceedings of the National Academy of Sciences* **1999,** *96* (15), 8467-8470.

97. Ratts, R.; Zeng, H.; Berg, E. A.; Blue, C.; McComb, M. E.; Costello, C. E.; Murphy, J. R., The cytosolic entry of diphtheria toxin catalytic domain requires a host cell cytosolic translocation factor complex. *The Journal of Cell Biology* **2003,** *160* (7), 1139-1150.

98. Gilliland, D. G.; Steplewski, Z.; Collier, R. J.; Mitchell, K. F.; Chang, T. H.; Koprowski, H., Antibody-directed cytotoxic agents: use of monoclonal antibody to direct the action of toxin A chains to colorectal carcinoma cells. *Proceedings of the National Academy of Sciences* **1980,** *77* (8), 4539-4543.

99. Pai, L. H.; Wittes, R.; Setser, A.; Willingham, M. C.; Pastan, I., Treatment of advanced solid tumors with immunotoxin LMB-1: an antibody linked to Pseudomonas exotoxin. *Nature Medicine* **1996,** *2* (3), 350-353.

100. Fidias, P.; Grossbard, M.; Lynch, T. J., A phase II study of the immunotoxin N901-blocked ricin in small-cell lung cancer. *Clinical Lung Cancer* **2002,** *3* (3), 219-222.

101. Schnell, R.; Borchmann, P.; Staak, J.; Schindler, J.; Ghetie, V.; Vitetta, E.; Engert, A., Clinical evaluation of ricin A-chain immunotoxins in patients with Hodgkin's lymphoma. *Annals of Oncology* **2003,** *14* (5), 729-736.

102. Liu, T. F.; Hall, P. D.; Cohen, K. A.; Willingham, M. C.; Cai, J.; Thorburn, A.; Frankel, A. E., Interstitial diphtheria toxin-epidermal growth factor fusion protein therapy produces regressions of subcutaneous human glioblastoma multiforme tumors in athymic nude mice. *Clinical Cancer Research* **2005,** *11* (1), 329-334.

103. Filpula, D.; Yang, K.; Basu, A.; Hassan, R.; Xiang, L.; Zhang, Z.; Wang, M.; Wang, Q.-c.; Ho, M.; Beers, R., Releasable PEGylation of mesothelin targeted immunotoxin SS1P achieves single dosage complete regression of a human carcinoma in mice. *Bioconjugate Chemistry* **2007,** *18* (3), 773-784.

104. Schirrmann, T.; Krauss, J.; Arndt, M. A.; Rybak, S. M.; Dübel, S., Targeted therapeutic RNases (ImmunoRNases). *Expert Opinion on Biological Therapy* **2009,** *9* (1), 79-95.

105. Lee, R. J.; Low, P. S., Delivery of liposomes into cultured KB cells via folate receptor-mediated endocytosis. *Journal of Biological Chemistry* **1994,** *269* (5), 3198-3204.

106. Leamon, C. P.; Low, P. S., Folate-mediated targeting: from diagnostics to drug and gene delivery. *Drug Discovery Today* **2001,** *6* (1), 44-51.

107. Low, P. S.; Henne, W. A.; Doorneweerd, D. D., Discovery and development of folic-acid-based receptor targeting for imaging and therapy of cancer and inflammatory diseases. *Accounts of Chemical Research* **2007,** *41* (1), 120-129.

108. Xia, W.; Low, P. S., Folate-targeted therapies for cancer. *Journal of Medicinal Chemistry* **2010,** *53* (19), 6811-6824.

109. Plank, C.; Oberhauser, B.; Mechtler, K.; Koch, C.; Wagner, E., The influence of endosome-disruptive peptides on gene transfer using synthetic virus-like gene transfer systems. *Journal of Biological Chemistry* **1994,**

269 (17), 12918-12924.

110. Plank, C.; Zauner, W.; Wagner, E., Application of membrane-active peptides for drug and gene delivery across cellular membranes. *Advanced Drug Delivery Reviews* **1998,** *34* (1), 21-35.

111. Schaffert, D.; Troiber, C.; Salcher, E. E.; Fröhlich, T.; Martin, I.; Badgujar, N.; Dohmen, C.; Edinger, D.; Kläger, R.; Maiwald, G., Solid‐Phase Synthesis of Sequence‐Defined T‐, i‐, and U‐Shape Polymers for pDNA and siRNA Delivery. *Angewandte Chemie International Edition* **2011,** *50* (38), 8986-8989.

112. Schaffert, D.; Badgujar, N.; Wagner, E., Novel Fmoc-polyamino acids for solid-phase synthesis of defined polyamidoamines. *Organic Letters* **2011,** *13* (7), 1586-1589.

113. Kaiser, E.; Colescott, R.; Bossinger, C.; Cook, P., Color test for detection of free terminal amino groups in the solid-phase synthesis of peptides. *Analytical Biochemistry* **1970,** *34* (2), 595-598.

114. Dohmen, C.; Fröhlich, T.; Lächelt, U.; Röhl, I.; Vornlocher, H.-P.; Hadwiger, P.; Wagner, E., Defined folate-PEG-siRNA conjugates for receptor-specific gene silencing. *Molecular Therapy—Nucleic Acids* **2012,** *1* (1), e7.

115. Dohmen, C.; Edinger, D.; Fröhlich, T.; Schreiner, L.; Lächelt, U.; Troiber, C.; Rädler, J.; Hadwiger, P.; Vornlocher, H.-P.; Wagner, E., Nanosized multifunctional polyplexes for receptor-mediated siRNA delivery. *ACS Nano* **2012,** *6* (6), 5198-5208.

116. Geisow, M. J.; Evans, W. H., pH in the endosome: measurements during pinocytosis and receptor-mediated endocytosis. *Experimental Cell Research* **1984,** *150* (1), 36-46.

117. Magde, D.; Elson, E.; Webb, W. W., Thermodynamic fluctuations in a reacting system—measurement by fluorescence correlation spectroscopy. *Physical Review Letters* **1972,** *29* (11), 705.

118. Khalil, I. A.; Kogure, K.; Akita, H.; Harashima, H., Uptake pathways and subsequent intracellular trafficking in nonviral gene delivery. *Pharmacological Reviews* **2006,** *58* (1), 32-45.

119. Behr, J.-P., The proton sponge: a trick to enter cells the viruses did not exploit. *CHIMIA International Journal for Chemistry* **1997,** *51* (1-2), 34-36.

120. Maier, K.; Martin, I.; Wagner, E., Sequence defined disulfide-linked shuttle for strongly enhanced intracellular protein delivery. *Molecular Pharmaceutics* **2012,** *9* (12), 3560-3568.

121. Wagner, E., Polymers for siRNA delivery: inspired by viruses to be targeted, dynamic, and precise. *Accounts of Chemical Research* **2011,** *45* (7), 1005-1013.

122. Lächelt, U.; Kos, P.; Mickler, F. M.; Herrmann, A.; Salcher, E. E.; Rödl, W.; Badgujar, N.; Bräuchle, C.; Wagner, E., Fine-tuning of proton sponges by precise diaminoethanes and histidines in pDNA polyplexes. *Nanomedicine: Nanotechnology, Biology and Medicine* **2014,** *10* (1), 35-44.

123. Mechtler, K.; Wagner, E., Gene transfer mediated by influenza virus peptides: the role of peptide sequence. *New Journal of Chemistry* **1997,** *21*, 105-11.

124. Cabral, H.; Matsumoto, Y.; Mizuno, K.; Chen, Q.; Murakami, M.; Kimura, M.; Terada, Y.; Kano, M.; Miyazono, K.; Uesaka, M., Accumulation of sub-100 nm polymeric micelles in poorly permeable tumours depends on size. *Nature Nanotechnology* **2011,** *6* (12), 815-823.

125. Maeda, H., The enhanced permeability and retention (EPR) effect in tumor vasculature: the key role of tumor-selective macromolecular drug targeting. *Advances in Enzyme Regulation* **2001,** *41* (1), 189-207.

10 ACKNOWLEDGEMENTS

Now coming to the end of this exciting moment, the scene of the past four years is still vivid in my mind, there are many people deserve my heartfelt gratitude for their mental or technical contribution to this thesis.

My deepest gratitude goes first and foremost to Prof. Dr. Ernst Wagner, my supervisor, for giving me the opportunity to do my PhD in his great group. I convey my deepest gratitude for his illuminating instruction, professional guidance and scientific support over these four years. I could not forget my supervisor's allowance of my accommodation in his apartment the beginning when I came to Munich.

I would like to express my cordial and sincere thanks to Wolfgang and Dr. Ulrich Lächelt for introducing me into this great group. As a student majoring in material before, I unexpectedly could express and purify protein, this could not imagine without Wolfgang's very warmly and thorough assistance. I have learned so many from our comprehensive Dr. Ulrich Lächelt, many difficulties were solved by means of his critical suggestions. I am grateful to Dr. Martina Rüffer for her unexpected St. Nicholas chocolate, the traditional Weißwurst, and Glühwein every year. Andi also deserves big thanks for his arrangement to this great group. My big thanks also go to the chemical group- Claudia, Linda and Ruth, Ines, Philipp Klein, Sören, Stephan, Benjamin, Dominik, for the discussion of

synthesizing and chemical duty keeping everything in order and clean. I also express my great gratitude to the cell culture group- Phillipp Heissig, Miriam, Melinda, Anna, Jasmin, it is their synergetic and great effort, that the huge kinds of material in our group, including some of mine, could be tested successfully. Thanks to our technical members-Ursula, Olga, Markus, Anna, we could focus on science issues due to their contributions to the group. My big thanks also go to Peng for his effective cooperation in cell experiment and many scientific discussions, my work possible could not come true without his effort. Very special thanks go to the lunch group-Dongsheng, Wei, Peng, Dianjang, Xiudong, for many happy and valuable discussions.

Extraordinary gratitude to the China Scholarship Council for offering me the scholarship to study in LMU.

I would like to express my appreciative thanks to my oversee friends in China, forever friend- Zhuang (master supervisor), Lu, Wende, Cheng, Zhigang, Changtao and many others for their assistance in my life. Finally, I would like to acknowledge my big family, my full heart salute to my grandparents, for their love without any reservation. It is not so easy for my farmer parents to cultivate me, I learnt a lot from their hard working, kindness and generous love to their sons. I also express great thanks to my younger brother, he is the strength that keeps me going.